NOTE TO USERS

PROPAGATION OF THE NEAR-INERTIAL ENERGY AND THE ROLE OF EDDIES IN THE OCEAN

By

XIAOMING ZHAI

SUBMITTED IN PARTIAL FULFILLMENT OF THE
REQUIREMENTS FOR THE DEGREE OF
DOCTOR OF PHILOSOPHY
AT
DALHOUSIE UNIVERSITY
HALIFAX, NOVA SCOTIA
SEPTEMBER 2007

Your file Votre référence
ISBN: 978-0-494-31512-5
Our file Notre référence
ISBN: 978-0-494-31512-5

DALHOUSIE UNIVERSITY

To comply with the Canadian Privacy Act the National Library of Canada has requested that the following pages be removed from this copy of the thesis:

Preliminary Pages
- Examiners Signature Page (pii)
- Dalhousie Library Copyright Agreement (piii)

Appendices
- Copyright Releases (if applicable)

Contents

List of Figures

Abstract

In this thesis, we find that (1) the wind power input is reduced by about 17% when ocean surface currents are included in the wind stress parameterization in a high-resolution model of the northwest Atlantic Ocean; (2) contrary to the traditional view that wind-induced near-inertial energy is redistributed by the beta-dispersion effect, we argue that the bulk of energy input from the wind to the near-inertial frequency band is dissipated, and leads to mixing, locally within mesoscale eddies in the ocean rather than being spread equatorward by β-dispersion. Therefore, strong diapycnal mixing associated with near-inertial wave breaking is expected to occur in the Gulf Stream system and other regions of the world ocean with high levels of eddy kinetic energy; (3) eddy-induced mixing in the surface mixed layer due to interaction with the atmosphere can play an important role in the ocean heat budget. We then estimate the eddy-induced diffusivity for heat in the surface mixed layer in two ways: (i) directly combining satellite-derived geostrophic velocity and sea surface temperature anomalies from the western North Atlantic Ocean and (ii) conducting numerical experiments with a high-resolution model of the northwest Atlantic Ocean. The surface eddy-induced diffusivities estimated from these two methods are broadly consistent with each other and show considerable spatial variability with large values to the south of the Gulf Stream and smaller values within the Gulf Stream itself. Finally, we introduce a new method (the semi-diagnostic method) for use with ocean models, which has the advantage that model drift is effectively prevented, while at the same time the meso-scale eddy field is free to evolve. This new method is then used to probe the importance of the eddy-driven circulation in the northwest Atlantic Ocean, and we find that the eddies strongly reinforce the eastward Gulf Stream jet and the northern recirculation in the slope region, with over

50% of the total transport of this recirculation being directly eddy-driven. The counterpart of the semi-diagnostic method is also used to examine the impact of assimilating eddies on the large-scale circulation.

List of Abbreviation Used

CFC	Chlorofluorocarbons
ECMWF	European Centre for Medium-Range Weather Forecasts
EKE	Eddy Kinetic Energy
GM	Gent and McWilliams (1990)
GVA	Geostrophic Velocity Anomaly
NCEP	National Centers for Environment Prediction
SDM	The Semi-Diagnostic Method
SST	Sea Surface Temperature
TW	Tera Watts
UTC	Universal Coordinated Time

Acknowledgements

It has been a great pleasure and truly rewarding experience to work with my supervisor, Dr. Richard Greatbatch, who is always willing to share his expertise with me in science (and beer drinking). I also appreciate the freedom I was given to explore new ideas during my PhD research.

I thank Drs. John Marshall, Jinyu Sheng, Helmuth Thomas, Tom Duck and Dan Kelley for agreeing to serve in my examining committee and also for their quick response and helpful comments.

I would like to thank my co-authors of the paper we wrote together, Dr. Richard Greatbatch, Dr. Jinyu Sheng, Jun Zhao, Dr. Carsten Eden, and Prof. Dr. Dirk Olbers, from whom I learned a great deal.

I wish to thank Jackie Hurst and people from the main office for their valuable help dealing with the many day to day problems.

I thank all my friends in Halifax, who make my stay in Halifax a really enjoyable memory. I wish you the best.

I thank my parents and my sister for their love and selfless support.

In the end, my special thanks goes to Jie, whose care and encouragement make my life meaningful, and our cat, Jiaojiao. Dalhousie University graduate scholarships are also gratefully acknowledged.

Chapter 1

Introduction

The overturning circulation of the ocean is associated with the spreading of dense water masses from their formation sites in the Nordic and Labrador Seas, and around Antarctica, and upwelling throughout the rest of the global ocean. Mechanical energy input from the wind and tides is thought to be necessary to generate the diapycnal mixing required to maintain the overturning circulation (*Munk and Wunsch* (1998) and *Wunsch* (2002)), analagous to the mixing-driven estuary circulation. *Munk and Wunsch* (1998) estimated that about 2 Tera Watts (TW) power input is needed to generate the required mixing, with half being of tidal origin and the other half being due to wind work on the ocean. This number can be reduced if the role of direct mechanical pumping over the Southern Ocean is considered (e.g., *Toggweiler and Samuels* (1998), *Webb and Suginohara* (2001)); i.e., some deep water can be brought to the surface through Ekman suction, where the water mass transformation can be completed in the surface mixed layer. Recently, *Wunsch* (1998) estimated the wind work on the ocean general circulation (that is, the geostrophic flow) to be about 1 TW using altimetry and the wind stress estimates available from the National Centers for Environmental Prediction (NCEP). However, the estimate made by *Wunsch* (1998) does not consider the effect of including ocean surface currents in the parameterization for wind stress. Using simple scaling arguments plus a quasi-geostrophic (QG) model, *Duhaut and Straub* (2006) argued that accounting for the ocean surface current dependence in the wind stress could reduce the calculation of the mechanical energy input to the ocean by 20% -

35%. It is clearly important that the effect of including the ocean surface current in the wind stress parameterisation be investigated further. In Chapter 2, the wind power input to the northwest Atlantic Ocean is examined using a realistic high-resolution ocean model driven by synoptic wind forcing. Two model runs are conducted with the difference only in the way the wind stress is calculated. The results show that the effect of including ocean surface currents in the wind stress formulation is to reduce the total wind power input integrated over the model domain by about 17%. The reduction is caused mostly by a sink term in the wind power input calculation associated with the presence of ocean currents. In addition, the modelled eddy kinetic energy decreases by about 10%, in response to direct mechanical damping by the surface stress. A simple scaling argument shows that the latter can be expected to be more important than bottom friction in the energy budget.

Wind power input to near-inertial motions at the surface is one of the important energy sources for mixing (e.g., *Alford* (2003b)). The subsequent spreading of near-inertial energy from the surface mixed layer to the deep ocean is necessary for the associated internal-wave-induced mixing to occur, causing water mass transformation and contributing to driving the overturning circulation. Wind-induced near-inertial energy is usually thought to be redistributed by the propagation of inertial-gravity waves to lower latitudes, for example, by the beta-dispersion effect (see *Anderson and Gill* (1979), *Gill* (1984), *Garrett* (2001)). Observational evidence has been found to support this idea (e.g., *Chiswell* (2003); *Alford* (2003a)). However, the real ocean is not homogeneous, and the background mean currents and meso-scale eddy field can strongly influence the propagation of near-inertial waves, and may dominate in some regions. The spreading of inertial oscillations induced by the passage of Hurricane Juan (2003) across the Gulf Stream and the Scotian Shelf is examined in Chapter 3 using a regional model of the northwest Atlantic Ocean. It is found that the near-inertial energy induced by Juan is advected into the ocean interior by the Gulf Stream, suggesting that geostrophic advection could play a role in redistributing near-inertial energy in the ocean. The fact that inertial oscillations can be advected by a background flow raises the question of what happens if inertial oscillations are advected poleward beyond their turning latitude, where they cannot exist by themselves since their frequency will be

less than the local inertial frequency. In Chapter 4, it is shown that inertial oscillations can be advected poleward beyond their turning latitude because of the Doppler shift effect. The inertial oscillations shrink meridionally with latitude during this advection. As the scales become smaller, the near-inertial waves are more vulnerable to nonlinear interactions, which could eventually lead to small-scale dissipation and mixing. Similar to the idea of β-dispersion, the horizontal gradient of the relative vorticity can also influence the propagation of near-inertial waves (e.g., *Kunze* (1985); *Young and ben Jelloul* (1997); *van Meurs* (1998); *Lee and Niiler* (1998); *Klein and llewellyn Smith* (2001); *Zhai et al.* (2005b)). Furthermore, *Zhai et al.* (2005b) recently pointed out that there is a remarkable coincidence between the regions where near-inertial energy is input to the ocean (the atmospheric storm track) and regions of enhanced eddy activity (the oceanic storm track), making it necessary to examine the effect of a mesocale eddy field on the input of the near-inertial energy and its subsequent vertical propagation. The interaction between inertial oscillations generated by a storm and a mesoscale eddy field is studied in Chapter 5 using an idealized eddying channel model mimicing the Southern Ocean. It is found that the near-inertial energy is trapped inside the anticyclonic eddies and several "hot spots" are formed. The near-inertial energy is locally drained from the surface to the deep ocean through the "chimney effect" inside the anticyclonic eddies (*Lee and Niiler* (1998)). However, it is still not clear how significant the chimney effect is in reality in comparison with β-dispersion. In Chapter 6, a first attempt is made to address this issue using a realistic eddy-resolving ($1/12^o$) model of the North Atlantic Ocean driven by synoptically varying wind forcing. It is found that: (1) the horizontal scale of variations in near-inertial energy in the model, both at the surface and subsurface, is strongly influenced by the mesoscale eddy field and, as a result, is much smaller than that of the applied wind forcing; (2) most of the near-inertial energy input at the surface is drained locally to the deep ocean by the mesoscale eddy field, and in particular, by the chimney effect associated with anticyclonic eddies; and (3) the interior of the subtropical gyre is a "desert" for near-inertial energy, contrary to expectations from β-dispersion theory (e.g., *Garrett* (2001), *Nagasawa et al.* (2000)).

Not all the relevant water mass transformation processes have to happen in the deep

ocean. On the contrary, the surface mixed layer is one place where diabatic processes are recognized as being ubiquitous. The eddies generated by baroclinic (or any other) instability process can be strongly modified in the surface mixed layer by interaction with the atmosphere or the surrounding water, leading to irreversible diapycnal mixing (i.e., water mass conversion) associated with eddies. It has been recently proposed that diapycnal eddy fluxes play an important role in the maintenance of the main thermocline (*Marshall et al.* (2002); *Radko and Marshall* (2004)) and in closing the ocean heat budget (*Greatbatch et al.* (2007)). Using an integral constaint (see also *Walin* (1982), *Niiler and Stevenson* (1982), *Garrett et al.* (1995), *McWilliams et al.* (1996)), it is shown in Chapter 7 that mixing is the essential ingredient for balancing the surface heat input to the ocean. In particular, it is argued that eddy-induced mixing in the surface mixed layer due to air-sea interaction processes can play an important role in closing the ocean heat budget. Therefore, it is important to provide estimates of this eddy-induced diffusivity from observed data or eddy-resolving model output, so that the eddy-induced diffusivity can be correctly parameterized in ocean/climate models. A regional diagnosis of the eddy-induced diffusivity for heat is presented in Chapter 8 by directly combining satellite-derived geostrophic velocity and sea surface temperature anomalies from the western North Atlantic Ocean. After a rotational eddy flux is removed, the resulting eddy-induced diffusivity shows considerable spatial variability with a value near 10^4 m^2 s^{-1} just to the south of the Gulf Stream and values in the range 1-2 $\times$ 10^3 m^2 s^{-1} within the Gulf Stream itself. A modeling study of the surface eddy diffusivity is carried out in Chapter 9. The diffusive effect of eddies is illustrated by comparing two model runs, in the second of which the surface heat flux acts only on large spatial scales and interaction with the mesoscale eddies is suppressed. This second run exhibits finer-scale structure and tighter thermal fronts than in the fully interactive run. The surface eddy diffusivity associated with surface thermal damping is then estimated from the fully interactive run. The estimated diffusivity takes large values (more than 10^3 m^2 s^{-1}) south of the Gulf Stream and smaller values elsewhere, which is broadly consistent with the diffusivity diagnosed in Chapter 8.

Apart from eddy-induced mixing, eddies are also known to play an important role in

shaping the large-scale ocean circulation, especially in the western boundary region and in the Southern Ocean (e.g., *Danabasoglu et al.* (1994), *Rintoul et al.* (2001)). In Chapter 10, a new method (the semi-diagnostic method) is presented for use with ocean models, which has the advantage that model drift is effectively prevented, while at the same time the meso-scale eddy field is free to evolve. This new method is then used to probe the importance of the eddy-driven circulation in the northwest Atlantic Ocean. For the particular model used in Chapter 10, it is shown that the eddies strongly reinforce the eastward Gulf Stream jet and the northern recirculation in the slope region, with over 50% of the total transport of this recirculation being directly eddy-driven. The eddies also play a role in setting the temperature and salinity properties of the "northwest corner" southeast of Newfoundland. In Chapter 11, the counterpart of the semi-diagnostic method (SDM) introduced by *Zhai et al.* (2004b) (see Chapter 10) is used to examine the impact of assimilating eddies on the large-scale circulation in a model of the northwest Atlantic Ocean. A novel feature of this study is that while the eddy field is strongly constrained by the assimilation procedure, there is no direct constraint on the large-scale circulation in the model. Assimilation of the eddies (i) drives an anomalous circulation corresponding to the northern recirculation gyre of the Gulf Stream, but of insufficient strength to appear in the mean field and (ii) leads to a much enhanced circulation in the northwest corner, east of Newfoundland. It is argued that the blocking of f/H contours from the east by the mid-Atlantic Ridge is a major influence on the dynamics of the northwest corner, and that the dynamics of the eddy-driven northern recirculation and the northwest corner are fundamentally similar.

Chapter 2

Wind Work in a Model of the Northwest Atlantic Ocean[1]

The work done by the wind over the northwest Atlantic Ocean is examined using a realistic high-resolution ocean model driven by synoptic wind forcing. Two model runs are conducted with the difference only in the way the wind stress is calculated. Our results show that the effect of including ocean surface currents in the wind stress formulation is to reduce the total wind work integrated over the model domain by about 17%. The reduction is caused by a sink term in the wind work calculation associated with the presence of ocean currents. In addition, the modelled eddy kinetic energy decreases by about 10%, in response to direct mechanical damping by the surface stress. A simple scaling argument shows that the latter can be expected to be more important than bottom friction in the energy budget.

[1]**Citation:** Zhai, X., and R. J. Greatbatch, Wind work in a model of the northwest Atlantic Ocean, *Geophys. Res. Lett.*, *34*, L04606, doi:10.1029/2006GL028907, 2007.

2.1 Introduction

Following *Duhaut and Straub* (2006), the formula for computing surface wind stress exerted by the atmosphere on the ocean can be expressed as:

$$\tau_1 = \rho_a c_d |\mathbf{U}_a - \mathbf{U}_o|(\mathbf{U}_a - \mathbf{U}_o) \tag{2.1}$$

where τ is the wind stress, ρ_a the density of air at sea level, c_d the drag coefficient as a function of wind speed and air-sea temperature difference (in this paper, we use *Large and Pond* (1981)), $\mathbf{U}_a$ the 10-m wind speed, and $\mathbf{U}_o$ the surface ocean velocity. Equation (2.1) states that the wind stress depends on the relative motion between the 10-m wind and the ocean surface current. However, since over most of the ocean the speed of the ocean surface current is at least one order of magnitude smaller than that of the 10-m wind, the wind stress is often computed using the 10-m wind alone, i.e.,

$$\tau_0 = \rho_a c_d |\mathbf{U}_a| \mathbf{U}_a, \tag{2.2}$$

neglecting the contribution from the surface ocean currents. The use of (2.2) rather than (2.1) has been questioned by a number of authors. For example, *Pacanowski* (1987) noted that in equatorial regions, surface currents approach 1 $m\ s^{-1}$ while surface wind speeds are around 6 $m\ s^{-1}$, and including ocean surface currents in the wind stress calculation leads to a considerable improvement in simulations of the tropical Atlantic in comparison with observed data. *Luo et al.* (2005) found a similar improvement in simulating the cold tongue in the tropical Pacific in coupled models when using (2.1) rather than (2.2). Scatterometers, on the other hand, measure wind stress relative to the moving ocean surface, instead of relative to the earth, and ocean surface currents can be recovered from scatterometer measurements in energetic regions, e.g., the western boundary currents and the tropics (*Cornillon and Park* (2001), *Kelly et al.* (2001), *Chelton et al.* (2004)), lending credance to (2.1). For example, *Cornillon and Park* (2001) inferred the presence of a warm core ring from NSCAT data.

The work done by the wind on the ocean can be computed as

$$P = \tau \cdot \mathbf{U}_o, \tag{2.3}$$

and it is conventional to compute τ using (2.2) instead of (2.1). Using (2.3), one can calculate the wind energy input to the near-inertial motion (*Alford* (2003b)) or the geostrophic circulation (*Wunsch* (1998)). For example, *Wunsch* (1998) recently estimated the wind work on the oceanic general circulation to be about 1 TW (1 TW = 10^{12} Watts) using altimetry and wind stress depending on the 10-m wind alone. However, using simple scaling arguments plus a quasi-geostrophic (QG) model, *Duhaut and Straub* (2006) argued that accounting for the ocean surface current dependence in the wind stress could reduce the calculation of the mechanical energy input to the ocean by 20% - 35%. Indeed, *Dawe and Thompson* (2006) found a decrease of 27% in the wind energy input using a $1/5^o$ horizontal resolution model of the North Pacific Ocean. Given the importance of the mechanical energy input from the wind for driving the meridional overturning circulation (*Munk and Wunsch* (1998)), it is clearly important that the effect of including the ocean surface current in the wind stress parameterisation be investigated further. In this study, we examine the work done by the wind over the northwest Atlantic Ocean using a realistic high-resolution ocean circulation model.

2.2 Ocean Model

2.2.1 Model Description

The model is the same as the northwest Atlantic Ocean model described in *Greatbatch and Zhai* (2006). The model domain spans the area between 30°W and 76°W and 35°N and 66°N with a horizontal resolution at each latitude of $1/5^o$ in longitude. There are 31 unevenly spaced z levels. The model is initialized with January mean temperature and salinity fields and forced by monthly mean surface heat flux from *da Silva et al.* (1994) and 12-hourly NCEP 10-m wind starting at the beginning of January 1990 (see below). The sea

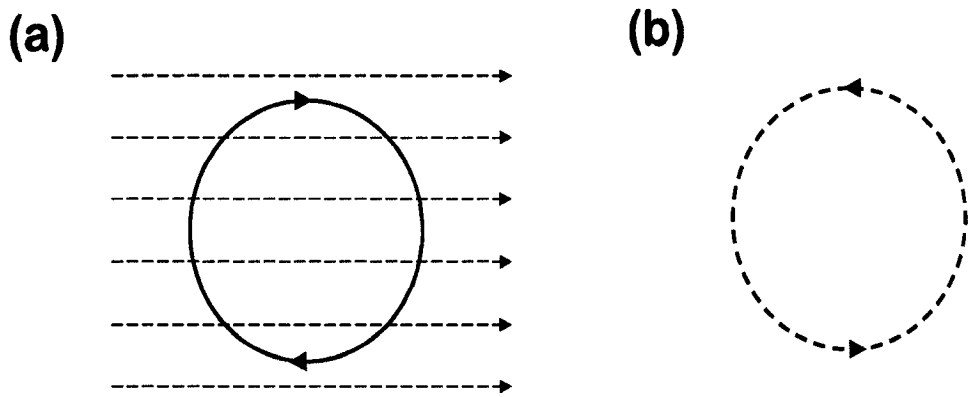

Figure 2.1: Schematic illustrating the damping effect on a warm core ring. The dashed lines in (a) represent the surface wind and the solid circle the surface current (northern hemisphere) associated with the eddy. Since the wind stress depends on the relative motion between the atmosphere and ocean, the stress exerted by the wind is smaller on the northern side of the warm eddy, where the current flows in the same direction as the wind, and larger on the southern side where it against the wind. This arises partly from the stress that is exerted on the overlying atmosphere by the ocean surface currents (the first term on the right hand side of (2.6) and illustrated schematically in (b) for the case $\mathbf{U_a} = 0$) and partly because the magnitude of the relative motion between the atmosphere and the ocean is larger on the southern side of the eddy than on the northern side (the second term on the right hand side of (2.6)). In (b), the dashed circle represents the drag exerted on the ocean when the atmosphere is at rest.

surface salinity in the model is restored to the monthly mean climatology on a time scale of 15 days. Along the model's open boundaries, temperature and salinity are restored to climatology and the transport is specified as described by *Sheng et al.* (2001).

2.2.2 The Semi-Diagnostic Method (SDM)

The model runs in this study use the SDM introduced in *Zhai et al.* (2004b). The SDM is a special case of the semi-prognostic method (*Greatbatch et al.* (2004)). In the version used here, the density variable in the model's hydrostatic equation is computed on large spatial scales from the climatological data of *Geshelin et al.* (1999), whereas on the mesoscale, the corresponding density variable is the model density. In this way, the large scale flow in the model is strongly constrained, while the mesoscale is completely free, ensuring a rich eddy

field. Readers are referred to *Zhai et al.* (2004b) for details. Use of the SDM eliminates the common problems of Gulf Stream overshooting and the disappearance of the northwest corner in models (*Willebrand et al.* (2001)).

2.2.3 Experiment Design

Two model runs are conducted with the difference only in the way of computing the surface wind stress. The control run (CONTROL) is forced by the wind stress calculated from NCEP 10-m wind using equation (2.2), as is the common practice in ocean circulation models. Correspondingly, the wind work in CONTROL is

$$\begin{aligned} P_0 &= \tau_0 \cdot \mathbf{U}_o \\ &= \rho_a c_d |\mathbf{U}_a| \mathbf{U}_a \cdot \mathbf{U}_o. \end{aligned} \tag{2.4}$$

An additional model run (DS) is conducted for comparison, where the wind stress is calculated from NCEP 10-m wind using equation (2.1). In DS, the wind stress depends on the relative motion between the atmosphere and the ocean. The wind work is then computed using

$$\begin{aligned} P_1 &= \tau_1 \cdot \mathbf{U}_o \\ &= \rho_a c_d |\mathbf{U}_a - \mathbf{U}_o| (\mathbf{U}_a - \mathbf{U}_o) \cdot \mathbf{U}_o \\ &= \rho_a c_d |\mathbf{U}_a - \mathbf{U}_o| \mathbf{U}_a \cdot \mathbf{U}_o - \rho_a c_d |\mathbf{U}_a - \mathbf{U}_o| \mathbf{U}_o \cdot \mathbf{U}_o. \end{aligned} \tag{2.5}$$

Assuming for now that the ocean surface velocity, $\mathbf{U}_o$, is same in both simulations, the difference ($P_0 - P_1$) between the wind work in the two models can be expressed as

$$\begin{aligned} P_0 - P_1 &= \rho_a c_d |\mathbf{U}_a - \mathbf{U}_o| \mathbf{U}_o \cdot \mathbf{U}_o \\ &\quad - \rho_a c_d (|\mathbf{U}_a - \mathbf{U}_o| - |\mathbf{U}_a|) \mathbf{U}_a \cdot \mathbf{U}_o. \end{aligned} \tag{2.6}$$

The first term on the right hand side of (2.6) is sign definite and is a sink term associated with the presence of surface ocean currents in P_1 and is believed to dominate the wind work difference. It should be noted that the sink term exists even when the wind velocity is zero and is associated with the stress that the ocean surface currents exert on the overlying atmosphere. The second term, on the other hand, operates only when the wind velocity is non-zero and arises from the dependence of the wind stress on the magnitude of the relative velocity, $\mathbf{U}_a - \mathbf{U}_o$. Both these effects are illustrated in Figure 2.1 for the case of a uniform wind blowing over a warm ocean eddy. The second term is also sign definite and is a sink term. This is because $|\mathbf{U}_a| < |\mathbf{U}_o - \mathbf{U}_a|$ for $\mathbf{U}_a \cdot \mathbf{U}_o < 0$, and vice versa. However, the instantaneous $\mathbf{U}_o$ in the two model runs turns out (not surprisingly) to be different and the wind work difference between CONTROL and DS associated with the second term on the right hand side of (2.6) has locally both positive and negative values (shown later) when computed using the ocean surface velocity, $\mathbf{U}_o$, taken from DS.

2.3 Results

Figure 2.2a shows the work done by the wind in the second year of CONTROL. The wind acts primarily as a mechanical source in the model domain, especially along the Gulf Stream and near the northwest corner. The most noticable regions where the wind blows, on average, against the ocean surface currents are the slope region to the south of the Canadian shelf, where the shelf break current flows southwestward, and to the south of Greenland, where the West Greenland Current moves northwestward along the shelf. The magnitude and pattern of the wind work in CONTROL compares reasonably well with the estimate for the same region made by *Wunsch* (1998) (see his Figure 2.2a), except that we resolve more detailed structure (e.g. the shelf break current) because of the higher horizontal resolution used here, and our estimate also includes a contribution from the near-inertial frequency band (*Alford* (2003b)). Integrating over the whole model domain, the total wind power input in CONTROL is slightly more than 2×10^{10} W. We note that there is no accounting for the ocean surface current dependence of the wind stress in the estimates of

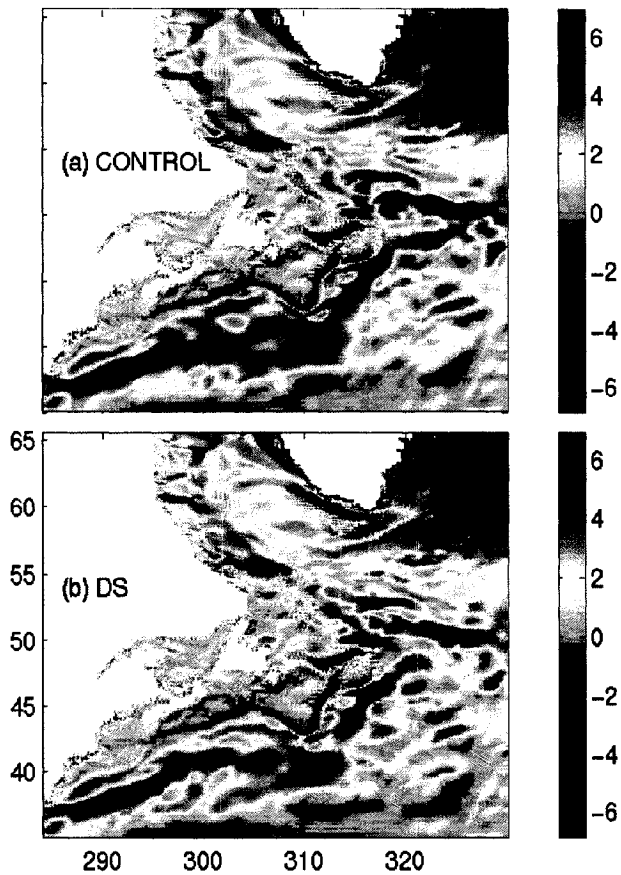

Figure 2.2: The work done by the wind in the second year in (a) CONTROL and (b) DS. Unit: 10^{-3} W m^{-2}.

Wunsch (1998) and *Alford* (2003b).

Figure 2.2b shows the work done by the wind in DS, and takes account of the ocean surface velocity dependence in the wind stress. Comparison with Figure 2.2a (see Figure 2.3a) shows that the wind work is reduced in most parts of the model domain, especially over the Gulf Stream system. The total wind power input integrates over the whole model domain to 1.7×10^{10} W, a reduction of about 17% compared to CONTROL, with locally a reduction of more than 20% over the Gulf Stream system. The reduction in the total wind power input is broadly consistent with the estimate of *Duhaut and Straub* (2006), but rather less than that of *Dawe and Thompson* (2006) perhaps because their calculation extends to lower latitudes. The first term on the right hand side of (2.6) is diagnosed using the ocean surface velocity from DS and is shown in Figure 2.3b. It is positive everywhere in the model domain, as we expect, with large values in the energetic regions (e.g., the Gulf Stream, the North Atlantic Current, the West Greenland Current and the Labrador Sea Current). The reduction of the wind power input associated with this term integrates to 4.4×10^9 W, about 22% of the total wind power in CONTROL. This is a larger reduction than the total wind power difference between DS and CONTROL of 3.4×10^9 W, indicating that the second term in (2.6) makes a negative contribution to the wind power difference between the two model runs when computed using the ocean surface velocity from DS. This is because the ocean surface velocity $\mathbf{U}_o$ is different in the two model runs.

If the surface stress systematically damps the mesoscale eddies as illustrated in Figure 2.1, we should observe a noticable decrease of eddy kinetic energy (EKE) in DS compared to CONTROL due to mechanical damping by the wind stress. Figure 2.4 shows the surface EKE distribution in the two model runs. (Note that the magnitude of the EKE in the model is comparable to that computed from altimeter data by *Stammer and Wunsch* (1999)). The spatial patterns are similar, but the EKE level in DS is now lower than that in CONTROL. The EKE integrated over the domain is about 8.0×10^{10} m^4 s^{-2} in DS, in comparison with about 9.0×10^{10} m^4 s^{-2} in CONTROL, a decrease of over 10%. In particular, the EKE along the Gulf Stream and in the northwest corner (high EKE regions) has been most noticably reduced.

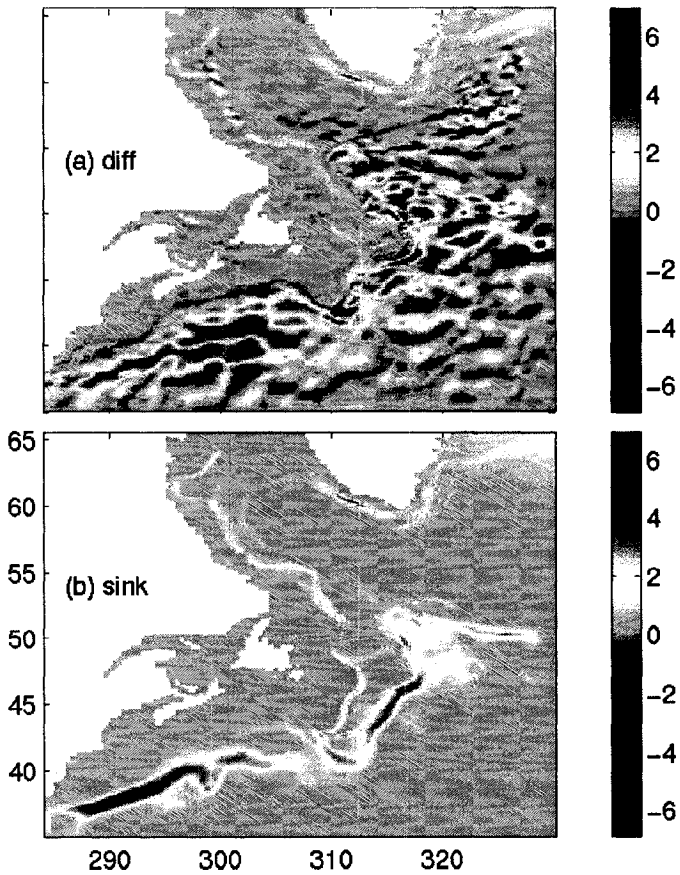

Figure 2.3: (a) The wind work difference, CONTROL minus DS. (b) The wind work associated with the sink term. Unit: 10^{-3} W m^{-2}.

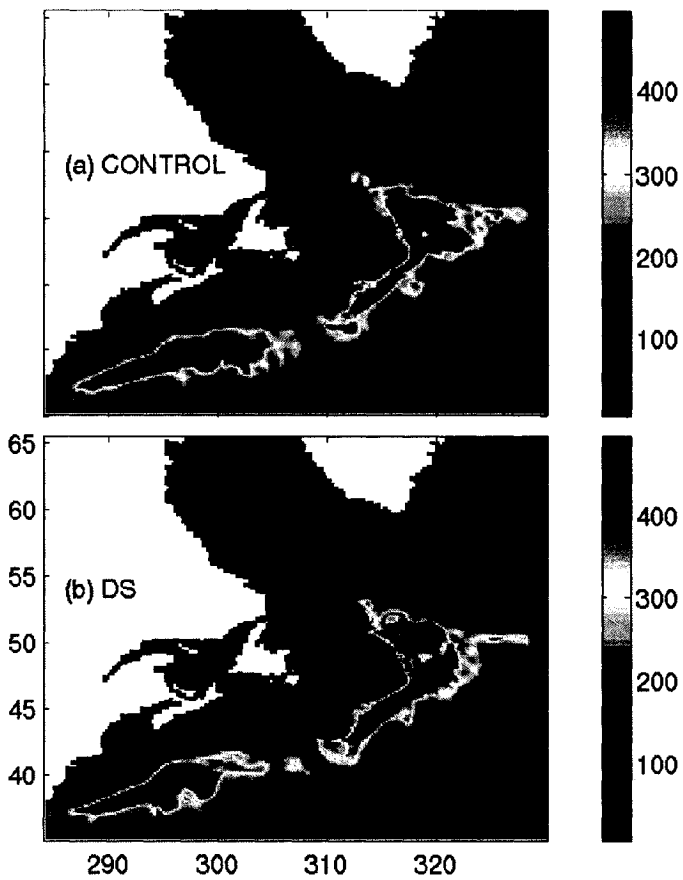

Figure 2.4: The eddy kinetic energy at the surface in the second year in (a) CONTROL and (b) DS. Unit: $cm^2\ s^{-2}$.

2.4 Summary and Discussion

The overturning circulation is thought to be driven by mechanical energy input from the wind and tides (see *Munk and Wunsch* (1998), *Wunsch* (2002)). *Munk and Wunsch* (1998) estimated that about 2 terawatts (TW) of energy input is required, with half being of tidal origin and half due to the wind. (Note that this number can be reduced if the direct role of the Southern Ocean wind forcing is considered; see *Toggweiler and Samuels* (1998), *Webb and Suginohara* (2001)). Recently, *Wunsch* (1998) estimated the wind work on the ocean general circulation to be about 1 TW. However, the estimate made by *Wunsch* (1998) does not consider the effect of including ocean surface currents in the wind stress. Here, we have described two model runs, in one of which we include ocean surface velocity dependence in the wind stress calculation, and in the other we do not. Our results show that accounting for the surface ocean velocity dependence has a noticable impact. In particular, using a model of the northwest Atlantic Ocean, we find that the total wind work is reduced by about 17% when the ocean surface currents are accounted for in the wind stress, supporting the claim by *Duhaut and Straub* (2006). The reduction of the wind work comes mostly from a sink term associated with the surface ocean velocity dependence of the wind stress. The sink term has large values in the energetic regions, where the damping of eddies by the surface stress is important. We also found a decrease of the EKE level by over 10% when integrated over the model domain, due to the damping mechanism illustrated in Figure 2.1. While our results are broadly consistent with previous studies (e.g. *Duhaut and Straub* (2006), *Dawe and Thompson* (2006)), it should be noted that our model has only been run for 2 years, the second year being used for the analysis, and that model is not fully eddy-resolving. Clearly future work should involve using models of much higher resolution, longer multi-year simulations, and wind forcing with higher time and spatial resolution.

It is of interest to compare the magnitude of the first term on the right hand side of (2.6), given by $\rho_a c_d |\mathbf{U}_a - \mathbf{U}_o| \mathbf{U}_o \cdot \mathbf{U}_o$ (the sink term), with the energy extracted by the bottom stress given by $\rho_o c_d |\mathbf{U}_b| |\mathbf{U}_b \cdot \mathbf{U}_b$, where ρ_o is a characteristic density for sea water and $\mathbf{U}_b$ is the bottom velocity. Taking $|\mathbf{U}_a - \mathbf{U}_o|$ to be 10 m s^{-1}, $\mathbf{U}_o$ to be 0.1 m s^{-1} and $\mathbf{U}_b$ to be 0.02 m s^{-1}, then the sink term is found to be one order of magnitude larger than the

energy dissipation associated with bottom friction. This result stresses the importance of taking account of the ocean velocity dependence in the specification of surface stress if the energetics of the ocean circulation are to be properly represented in models.

The Southern Ocean is one place that is expected to be important for the wind energy input (see *Wunsch* (1998)), since the Antarctic Circumpolar Current (ACC) moves in the same direction as the circumpolar wind. However, the Southern Ocean is also rich in eddies and, hence, we should expect to see a noticable reduction in estimates of the wind power input over the Southern Ocean when the ocean surface velocity dependence of the wind stress is taken into account, a topic for future research.

Acknowledgments

This work has been funded by NSERC and CFCAS in support of the Canadian CLIVAR Research Network. We wish to thank Dr. David Straub for bringing our attention to the issue of ocean surface velocity dependence in the calculation of the surface wind stress and two anonymous reviewers for their constructive comments on an earlier version of the manuscript.

Bibliography

Alford, M.H. (2003), Improved global maps and 54-year history of wind work on ocean inertial motions, *Geophys. Res. Lett.*, *30*, 1424, doi:10.1029/2002GL016614.

Chelton, D.B., M.G. Schlax, M.H. Freilich, and R.F. Milliff (2004), Satellite measurements reveal persistent small-scale features in ocean winds, *Science*, *303*, 978-983.

Cornillon, P., and K.-A. Park (2001), Warm core ring velocity inferred from NSCAT, *Geophys. Res. Lett.*, *28*, 575-578.

da Silva, A.M., C.C. Young, and S. Levitus (1994), *Atlas of Surface Marine Data 1994*, vol. 3, *Anomalies of Heat and Momentum Fluxes, NOAA Atlas NESDIS 8*, 413 pp., NOAA, Silver Spring, Md.

Dawe, J.T., and L. Thompson (2006), Effect of ocean surface currents on wind stress, heat flux, and wind power input to the ocean, *Geophys. Res. Lett.*, *33*, L09604, doi:10.1029/2006GL025784.

Duhaut, T.H., and D.N. Straub (2006), Wind stress dependence on ocean surface velocity: Implications for mechanical energy input to ocean circulation, *J. Phys. Oceanogr.*, *36*, 202-211.

Geshelin, Y., J. Sheng, and R.J. Greatbatch (1999), Monthly mean climatologies of temperature and salinity in the western North Atlantic, Canadian Data Report of Hydrography and Ocean Sciences, 153pp.

Greatbatch, R.J., and X. Zhai (2006), Influence of assimilated eddies on the large-scale circulation in a model of the northwest Atlantic Ocean, *Geophys. Res. Lett.*, *33*, L02614, doi:10.1029/2005GL025139.

Greatbatch, R.J., et al. (2004), The semi-prognostic method, *Cont. Shelf Res.*, *24/18*, 2149-2165.

Kelly, K.A., S. Dickinson, M.J. McPhaden, and G.C. Johnson (2001), Ocean currents evident in satellite wind data, *Geophys. Res. Lett.*, *28*, 2469-2472.

Large, W.G., and S. Pond (1981), Open-ocean momentum flux measurements in moderate to strong winds, *J. Phys. Oceanogr.*, *11*, 324-336.

Luo, J.J., S. Masson, E. Roeckner, G. Madec, and T. Yamagata (2005), Reducing climatology bias in an ocean-atmosphere CGCM with improved coupling physics, *J. Climate*, *18*, 2344-2360.

Munk, W., and C. Wunsch (1998), Abyssal recipes II, Energetics of tidal and wind mixing, *Deep Sea Res. Part I*, *45*, 1977-2010.

Pacanowski, R.C. (1987), Effect of equatorial currents on surface stress, *J. Phys. Oceanogr.*, *17*, 833-838.

Sheng, J., R.J. Greatbatch, and D.G. Wright (2001), Improving the utility of ocean circulation models through adjustment of the momentum balance, *J. Geophys. Res.*, *106*, 16,711-16,728.

Stammer, D., and C. Wunsch (1999), Temporal changes in eddy energy of the oceans,

Deep-Sea Res., II,, 46, 77-108.

Toggweiler, J.R., and B. Samuels (1998), On the ocean's large scale circulation near the limit of no vertical mixing, *J. Phys. Oceanogr.*, *28*, 1832-1852.

Webb, D.J., and N. Suginohara (2001), Vertical mixing in the ocean, *Nature*, *409*, 37-37.

Willebrand, J., et al. (2001), Circulation characteristics in three eddy-permitting models of the North Atlantic, *Prog. Oceanogr.*, *48*, 123-161.

Wunsch, C. (1998), The work done by the wind on the oceanic general circulation, *J. Phys. Oceanogr.*, *28*, 2332-2340.

Wunsch, C. (2002), What is the thermohaline circulation? *Science*, *298*, 1179-1181.

Zhai, X., R.J. Greatbatch, and J. Sheng (2004), Diagnosing the role of eddies in driving the circulation of the northwest Atlantic Ocean, *Geophys. Res. Lett.*, *31*, L23304, doi:10.1029/2004GL021146.

Chapter 3

Advective Spreading of Storm-Induced Inertial Oscillations in a Model of the Northwest Atlantic Ocean[1]

The spreading of inertial oscillations induced by the passage of Hurricane Juan (2003) across the Gulf Stream and the Scotian Shelf is examined using a regional model of the northwest Atlantic Ocean. It is found that surface-intensified inertial oscillations develop at locations remote from the storm track after a period of 5-10 days. A diagnostic technique reveals the importance of advection by the background geostrophic flow for explaining this effect. The results suggest that advection by mean circulation can play a role in redistributing near-inertial energy in the ocean. We argue that advective redistribution could have important consequences for understanding diapycnal mixing in the ocean.

[1]**Citation:** Zhai. X., R.J. Greatbatch, and J. Sheng (2004), Advective spreading of storm-induced inertial oscillations in a model of the northwest Atlantic Ocean, *Geophys. Res. Lett.*, *31*, L14315, doi:10.1029/2004GL020084.

3.1 Introduction

The upper ocean response to a moving storm has been studied observationally (e.g., *Leipper* (1967), *Brink* (1989) and *Dickey et al.* (1998)) and numerically (e.g., *Chang and Anthes* (1978), *Price* (1981), *Greatbatch* (1983), *Bender and Ginis* (2000)). The response is characterized by sea surface temperature (SST) cooling, and inertial oscillations that are most energetic to the right of the storm track. *Greatbatch* (1983) showed that on a time scale of a few inertial periods, the horizontal pressure gradients are small compared with the Coriolis terms for "large", "fast" storms (that is "large" in the sense that the scale of the storm is large compared to the internal Rossby radius of deformation, and "fast" in the sense that the translation speed of the storm is large compared to the baroclinic gravity wave speed). The dominant balance is then between the acceleration terms and the Coriolis terms, resulting in inertial oscillations. The horizontal pressure gradient terms are crucial, however, to the dispersion of energy by inertial-gravity waves away from the storm track in the geostrophic adjustment process, and can not be neglected on time scales characteristic of that process (*Greatbatch* (1983)). *Gill* (1984) showed that the inertial energy propagates both horizontally and vertically as different vertical modes separate out from the storm track. On a β-plane, inertial oscillations generated at a particular latitude can propagate equatorward due to beta-dispersion (*Anderson and Gill* (1979); *Garrett* (2001)). Data from moorings agree to some extent with the idea of the deep equatorward propagation of inertial oscillations (see *Chiswell* (2003) and *Alford* (2003a)). However, most previous studies do not consider the interaction between the inertial oscillations and the background flow. *Kunze* (1985) showed that for near-inertial waves propagating in geostrophic shear, the horizontally nonuniform relative vorticity has the same effect as the β-effect on the near-inertial waves. As a consequence, these waves can be trapped in regions of negative vorticity (see also *D'Asaro* (1995)). *Davies and Xing* (2002) showed that the existence of the coast and the presence of density fronts influences the distribution of inertial energy and the propagation of near-inertial internal waves. *Xing and Davies* (2002) examined the non-linear interaction between inertial oscillations and internal tides and argued that non-linear interaction represents an important contribution to the energy cascade into higher frequency

waves and eventually mixing. In this letter, we show the importance of geostrophic advection, rather than wave processes, for carrying inertial energy away from the storm track to remote regions in a model of the northwest Atlantic Ocean.

3.2 The Model

We use the northwest Atlantic Ocean model developed by *Sheng et al.* (2001), which covers the area between 30°W and 76°W and between 35°N and 66°N with a horizontal resolution of one third degree in longitude. There are 31 unevenly spaced z levels with the centers of the top five levels located at 5, 16, 29, 44 and 61 m, respectively. A spin-up of 600 days using seasonally varying climatological forcing is used to allow the model to reach a quasi-equilibrium state before the storm forcing is introduced. The semi-prognostic method introduced by *Sheng et al.* (2001) is used to adjust the model momentum equations to correct for systematic errors during the spin-up period (see *Greatbatch et al.* (2004) for an overview). The end of the spin-up corresponds to early September.

To specify the storm forcing, we use Hurricane Juan from September 2003. Juan formed near Bermuda and then tracked northward across the Gulf Stream and the Scotian Shelf, making landfall at Halifax, Nova Scotia, as a category 2 hurricane on the Saffir-Simpson Hurricane Scale (that is, winds ranging from 154-177 km/hr). The wind stress for the storm is specified following *Chang and Anthes* (1978) as

$$\tau = \tau_{max} \times \begin{cases} r/r_{min} & 0 \le r \le r_{min} \\ (r_{max} - r)/(r_{max} - r_{min}) & r_{min} \le r \le r_{max} \\ 0 & r \ge r_{max} \end{cases} \tag{3.1}$$

where τ is the amplitude of tangential wind stress with respect to the storm center, and r is the radial distance from the center (the radial wind stress is put to zero). Here, we put $r_{min} = 30$ km, $r_{max} = 300$ km, and $\tau_{max} = 3$ N m^{-2}. The realistic storm track of Juan compiled by the National Hurricane Center is used in this study. Only wind stress forcing

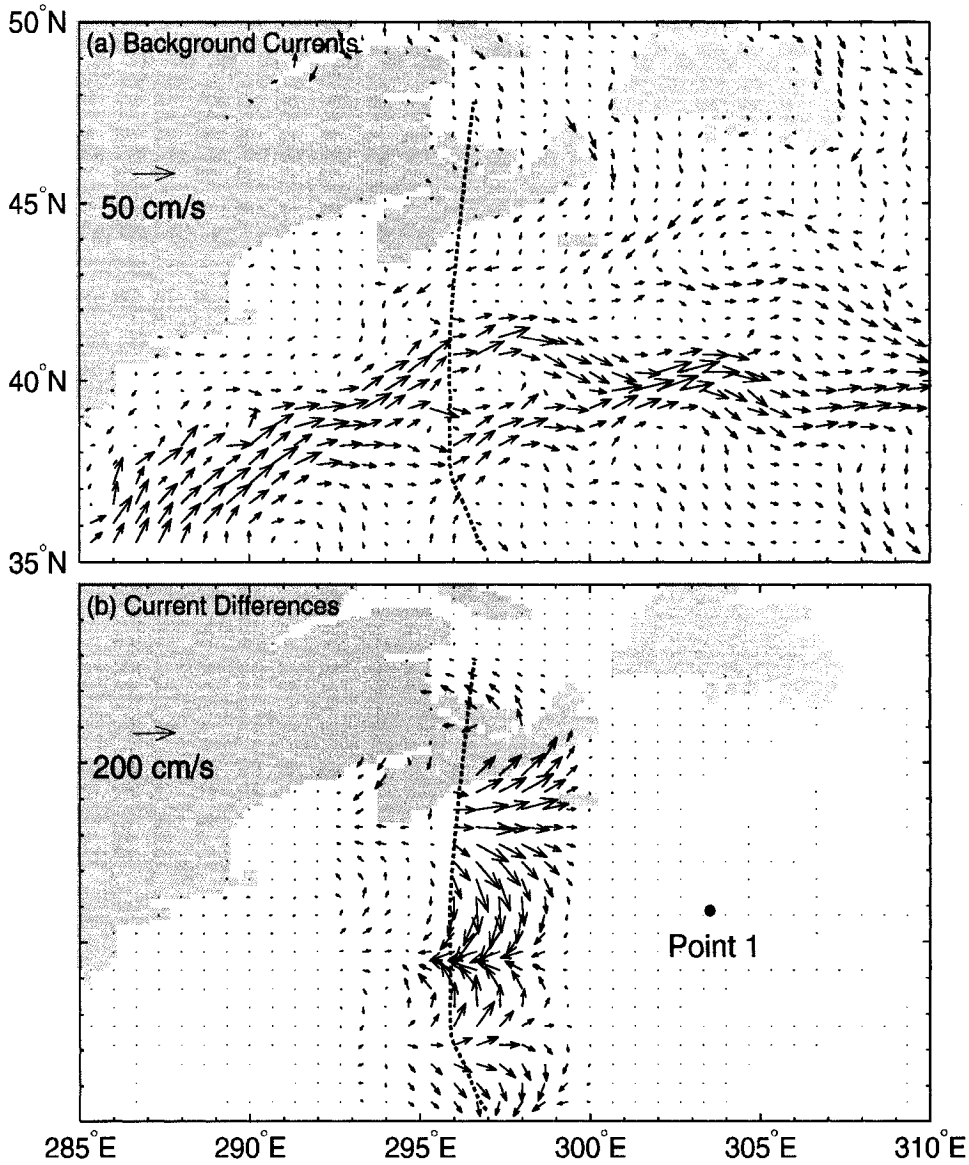

Figure 3.1: (a) The surface flow field at day 0 immediately before Hurricane Juan arrives; (b) the surface velocity differences between the model runs with and without Juan (Run 1 minus Run 2) at day 6. The storm track is represented by the dotted line. The bullet indicates the position of Point 1.

due to the storm is used to force the model; the surface buoyancy forcing due to the storm is not considered and has been shown elsewhere (e.g., *Price* (1981)) to be small in its effect. During the period of storm forcing, the vertical mixing scheme is modified from that used by *Sheng et al.* (2001) to include entrainment at the base of the mixed layer due to shear instability based on a bulk Richardson number formulation following *Price et al.* (1986) (see *Zhai* (2004), for details). Two model runs are conducted using the end of the spin-up as the initial condition. The first (Run 1) has the storm forcing added to the climatological forcing, the second (Run 2) uses climatological forcing only. In addition, both these model runs are repeated, including the spin-up, with the density field specified from climatology (Runs 3 and 4, respectively). The difference between Runs 1 and 2, and between Runs 3 and 4, is used to represent the ocean response to the wind stress associated with the storm.

3.3 Model Results

Run 1 yields a reasonable oceanic response to the hurricane, including the rightward bias of the SST cooling, inertial oscillations in the wake and the generation of shelf waves on the eastern Canadian shelf (see Figure 3.1; details can be found in *Zhai* (2004)). In this letter, we focus on the onset of inertial oscillations (Figures 3.2a,b) after day 10 at Point 1 shown in Figure 3.1, a location far from the storm track and beyond the influence of the direct forcing by the storm. The horizontal velocity differences at this point are almost zero during the first 10 days (Figure 3.2a). After day 10, significant oscillations set in at the local inertial frequency with an amplitude of about 5 cm s^{-1}. There are two competing hypotheses concerning the mechanism for the onset of the inertial oscillations at Point 1: linear wave dispersion of inertial-gravity waves from the storm track (e.g. *Gill* (1984)) and advective processes (as noted by *D'Asaro* (1995)).

We use Runs 3 and 4 to determine the main process responsible for the appearance of the inertial oscillations at Point 1. Since the density field is specified from climatology in these runs, the horizontal pressure gradients are independent of the model-calculated temperature and salinity fields so that the baroclinic dispersion of inertial-gravity waves is

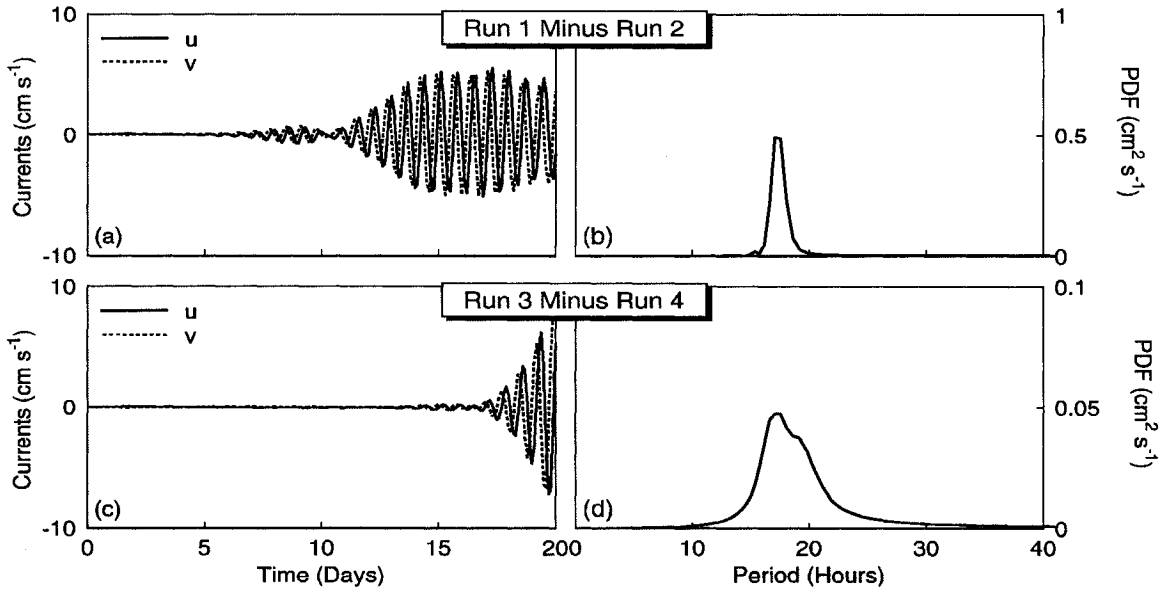

Figure 3.2: (a) Time series of the horizontal velocity differences between Run 1 and Run 2 at Point 1 ; (b) spectrum of the horizontal velocity differences between Run 1 and Run 2 at Point 1; (c) time series of the horizontal velocity differences between Run 3 and Run 4 at Point 1; (d) spectrum of the horizontal velocity differences between Run 3 and Run 4 at Point 1. Note the spectral peak near the local inertial period of about 18 hours.

excluded. Advection by the geostrophic flow associated with the climatology is nevertheless retained. (*Eden and Greatbatch* (2003) use a similar approach to diagnose the role of advection in the dynamics of a decadal oscillation in a model of the North Atlantic). Inertial oscillations now appear after day 17 (Figures 3.2c,d) and can only have been transported to Point 1 by geostrophic advection. The appearance of the inertial signal in the diagnostic run (Run 3) several days later than in Figure 3.2a can be explained by the different background (or advective) currents in Runs 1 and 2 compared with Runs 3 and 4. It is also shown by scale analysis (*Zhai et al.* (2005a)) that advective processes are 5 to 6 times more important than dispersive processes for the spreading of inertial energy along the Gulf Stream path in Run 1.

In order to extract energy at the near-inertial frequency, a bandpass filter centered at the local (41^oN) inertial frequency is used. The kinetic energy of the surface currents (Run 1 minus Run 2), given by $(u^2 + v^2)/2$ (where u and v are the horizontal velocities) is

computed after the bandpass filter is applied. The temporal and spatial evolution of the near-inertial energy at the sea surface is shown in Figure 3.3. The near-inertial energy is biased to the right of the storm track at day 6, due to the rightward bias in the storm-generated currents (e.g. *Price* (1981)). The near-inertial energy is then advected gradually by the Gulf Stream to the east at the latitude around 41°N (Figures 3.3b,c,d). The near-inertial energy decays as it is advected horizontally, due to dissipation and the vertical propagation of the energy. The time scale of the horizontal advection is consistent with the velocity scale for the Gulf Stream in the model. The shelf-break jet also advects the near-inertial energy to the southwest along the shelf-break as seen in Figure 3.3.

The near-inertial energy generated by the storm is initially confined in the mixed layer. It gradually propagates downward in the following ten days mainly on the right side of the storm track, where there exists a larger energy source in the mixed layer (Figures 3.4a,b,c). The vertical propagation of the near-inertial energy can be interpreted using the concept of modal interference and separation as described in *Gill* (1984) and *Zervakis and Levine* (1995). The total near-inertial energy decreases with time due to dissipation and only a small amount is left at day 18, which is advected eastward by the Gulf Stream from its source region on the right side of the storm track (Figure 3.4d).

3.4 Discussion

The thermohaline circulation of the ocean results primarily from deep water formation at sites in the Nordic and Labrador Seas, and around Antarctica, and upwelling throughout the rest of the global ocean. Mechanical energy input from the wind and tides is thought to be necessary to generate the diapycnal mixing required to support the upwelling branch of the thermohaline circulation (*Munk and Wunsch* (1998), *Wunsch* (2002)). A large part of the wind-induced energy flux goes to generate near-inertial oscillations in the mixed layer. Global maps of the wind-induced energy flux to inertial motions have been drawn by *Watanabe and Hibiya* (2002) and *Alford* (2003b). Wind-induced inertial energy is believed to be redistributed by the propagation of inertial-gravity waves to lower latitudes, for

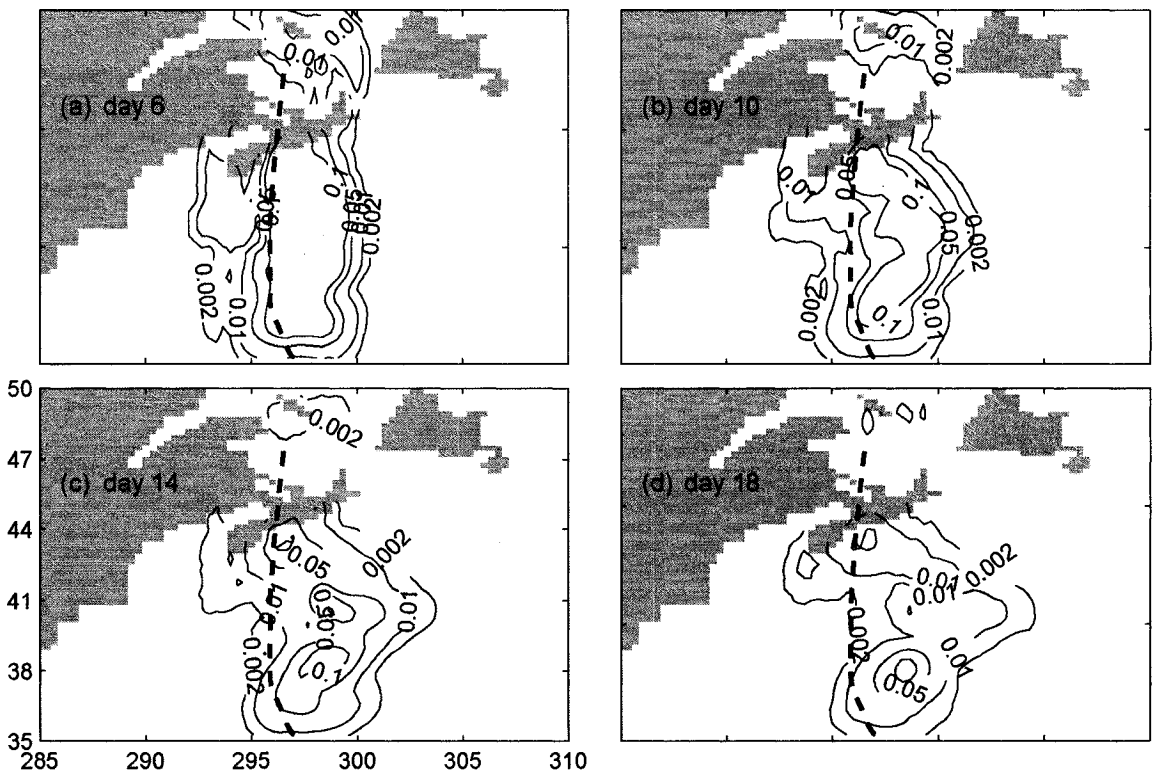

Figure 3.3: Temporal evolution of the near-inertial energy at the sea surface (unit: $m^2 s^{-2}$). The dashed line represents the storm track. The 0.1, 0.05, 0.01, 0.002 contours are drawn.

example by the beta-dispersion effect (see *Alford* (2003a)). Our model results suggest that geostrophic advection could also play a role in redistributing inertial energy in the ocean. Furthermore, geostrophic advection could carry inertial energy to higher, rather than lower latitudes, where we speculate significant mixing could take place. (For example, near-inertial oscillations could be transported poleward of their turning latitude, see *Zhai et al.* (2005a)). Since a given energy level at higher latitudes causes much more mixing than at lower latitudes (*Gregg et al.* (2003), *Garrett* (2003)), mechanisms for transporting inertial energy to higher latitudes could be important for understanding mixing in the ocean.

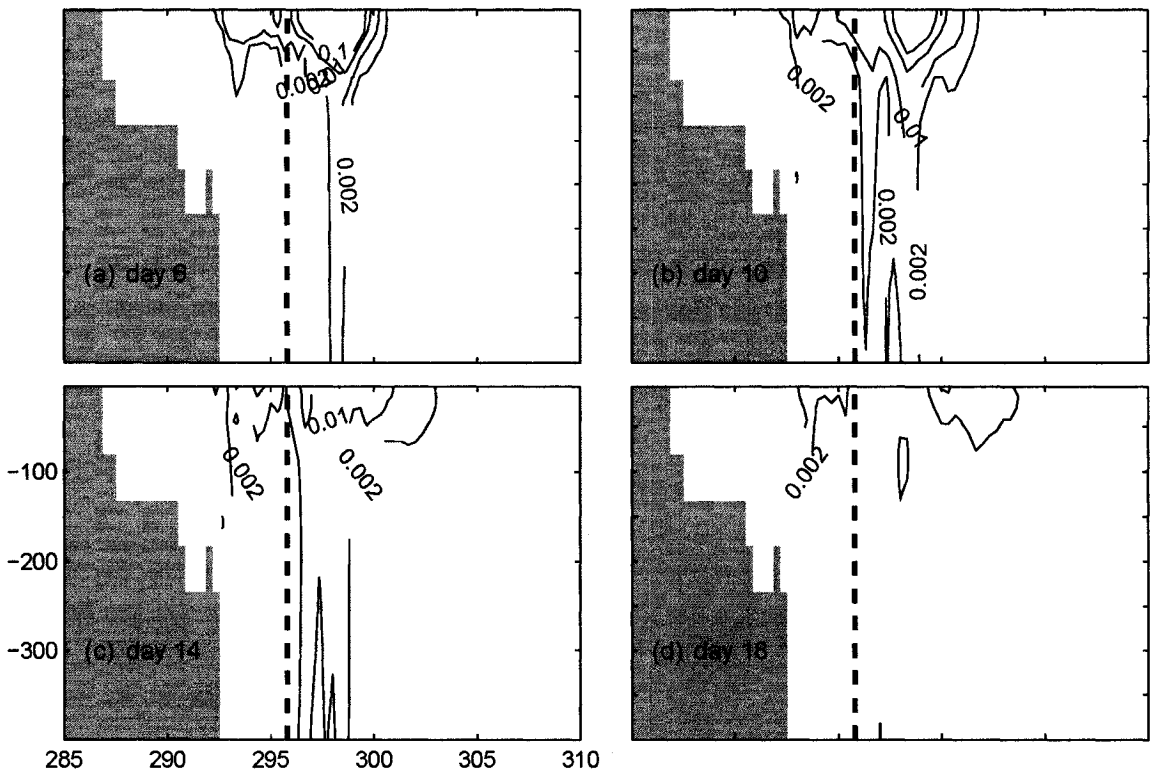

Figure 3.4: Vertical transect showing the temporal evolution of the near-inertial energy (unit: $m^2\ s^{-2}$) in the upper 400 m. The dashed line shows where the storm center intersects the transect. The same contours are drawn as in Figure 3.3.

3.5 Summary

We have reported on the spreading of storm-induced inertial oscillations in a model of the northwest Atlantic Ocean. Forcing mimicing the passage of Hurricane Juan in September 2003, as Juan crossed the Gulf Stream and the Scotian Shelf, was used to drive the model. We noted the onset, about 10 days after the storm, of inertial oscillations in regions far away from the storm track. A diagnostic technique, following *Eden and Greatbatch* (2003), was used to show the importance of geostrophic advection for carrying the inertial energy to regions remote from the storm track. The temporal evolution of the near-inertial energy isolated by a bandpass filter shows that the near-inertial energy spreads horizontally and vertically away from the storm track. It is advected mainly by two currents, the Gulf Stream and the shelf-break jet. This advective process, together with the long-range propagation of internal gravity waves, could be important for the global redistribution of wind-induced inertial energy in the ocean, and subsequently for the determining the global distribution of diapycnal mixing.

Acknowledgments

We wish to thank Jian Lu (GFDL), Youyu Lu (BIO) and Chris Fogarty (MSC) for helpful discussions. This project is supported by funding from CFCAS.

Bibliography

Alford, M.H., Redistribution of energy available for ocean mixing by long-range propagation of internal waves, *Nature*, *423*, 159-162, 2003a.

Alford, M.H., Improved global maps and 54-years history of wind-work on ocean inertial motions, *Geophys. Res. Lett.*, *30(8)*, 1424, doi:10.1029/2002GL016614, 2003b.

Anderson, D.L.T., and A.E. Gill, Beta dispersion of inertial waves, *J. Geophys. Res.*, *84*, 1836-1842, 1979.

Bender, M.A., and I. Ginis, Real-case simulations of hurricane-ocean interaction using a high-resolution coupled model: effects on hurricane intensity, *Monthly Weather Review*, *128*, 917-946, 2000.

Brink, K.H., Observations of the response of thermocline currents to a hurricane, *J. Phys. Oceanogr.*, *19*, 1017-1022, 1989.

Chang, S.W., and R.A. Anthes, Numerical simulations of the ocean's nonlinear baroclinic response to translating hurricanes, *J. Phys. Oceanogr.*, *8*, 468-480, 1978.

Chiswell, S.M., Deep equatorward propagation of inertial oscillations, *Geophys. Res. Lett.*, *30*, 1533-1536, 2003.

Davies, A.M., and J. Xing, Influence of coastal fronts on near-inertial internal waves, *Geophys. Res. Lett.*, *29*, 2114-2117, 2002.

D'Asaro, E.A., Upper-ocean inertial currents forced by a strong storm. Part III: Interaction of inertial currents and mesoscale eddies, *J. Phys. Oceanogr.*, *25*, 2953-2958, 1995.

Dickey, T., D. Frye, J. McNeil, D. Manov, N. Nelson, D. Sigurdson, H. Jannasch, D. Siegel, T. Michaels and R. Johnson, Upper-ocean temperature response to hurricane Felix as measured by the Bermuda tested mooring, *Mon. Wea. Rev.*, *126*, 1195-1201, 1998.

Eden, C., and R.J. Greatbatch, A damped decadal oscillation in the North Atlantic climate system, *J. Climate*, *16*, 4043-4060, 2003.

Garrett, C., What is the "Near-Inertial" band and why is it different from the rest of the internal wave spectrum, *J. Phys. Oceanogr.*, *31*, 962-971, 2001.

Garrett, C., Mixing with latitude, *Nature*, *422*, 477-478, 2003.

Gill, A.E., On the behavior of internal waves in the wake of storms, *J. Phys. Oceanogr.*, *14*, 1129-1151, 1984.

Greatbatch, R.J., On the response of the ocean to a moving storm: The nonlinear dynamics, *J. Phys. Oceanogr.*, *13*, 357-367, 1983.

Greatbatch, R.J., J. Sheng, C. Eden, L. Tang, X. Zhai, and J. Zhao, The semi-prognostic method, *Cont. Shelf Res.*, *24*, 2149-2165, 2004.

Gregg, M.C., T.B. Sanford, and D.P. Winkel, Reduced mixing from the breaking of internal

waves in equatorial waters, *Nature*, *422*, 513-515, 2003.

Kunze, E., Near-inertial propagation in geostrophic shear, *J. Phys. Oceanogr.*, *15*, 544-565, 1985.

Leipper, D.F., Observed ocean conditions and hurricane Hilda (1964), *J. Atmos. Sci.*, *24*, 182-196, 1967.

Munk, W., and C. Wunsch, Abyssal recipes II, Energetics of tidal and wind mixing, *Deep Sea Res., Part I, 45*, 1977-2010, 1998.

Price, J.F., Upper ocean response to a hurricane, *J. Phys. Oceanogr.*, *11*, 153-175, 1981.

Price, J.F., R.A. Weller, and R. Pinkel, Diurnal cycling: Observations and models of the upper ocean response to diurnal heating, cooling, and wind mixing, *J. Geophys. Res.*, *91*, 8411-8427, 1986.

Sheng, J., R. J. Greatbatch, and D. G. Wright, Improving the utility of ocean circulation models through adjustment of the momentum balance, *J. Geophys. Res.*, *106*, 16,711-16,728, 2001.

Watanabe, M., and T. Hibiya, Global estimates of the wind-induced energy flux to inertial motions in the surface mixed layer, *Geophys. Res. Lett.*, *29(8)*, doi:10.1029/2001GL014422, 2002.

Wunsch, C., What is the thermohaline circulation? *Science*, *298*, 1179-1181, 2002.

Xing, J., and A.M. Davies, Processes influencing the non-linear interaction between inertial oscillations, near inertial internal waves and internal tides, *Geophys. Res. Lett.*, *29*, 1067-1070, 2002.

Zervakis, V., and M.D. Levine, Near-inertial energy propagation from the mixed layer: Theoretical consideration, *J. Phys. Oceanogr.*, *25*, 2872-2889, 1995.

Zhai, X., Studying storm-induced circulation on the Scotian Shelf and slope using a two-way nested-grid model, M.Sc. thesis, Dalhousie University, 2004.

Zhai, X., R.J. Greatbatch, and J. Sheng, Doppler-shifted inertial oscillations on a β-plane, *J. Phys. Oceanogr.*, *35*, 1480-1488, 2005.

Chapter 4

Doppler Shifted Inertial Oscillations on a β-Plane[1]

On the spherical earth, and in the absence of a background flow, the poleward propagation of near-inertial oscillations is restricted by the turning latitude. A background flow, on the other hand, provides a way to increase the apparent frequency of near-inertial waves through Doppler shifting. In this note, we show that near-inertial oscillations can be advected to latitudes higher than their turning latitude. Associated with the poleward advection there is a squeezing of the meridional wavelength. We use a numerical model to verify this result. The squeezed inertial oscillations are vulnerable to nonlinear interactions, which could eventually lead to small-scale dissipation and mixing.

4.1 Introduction

It is well known that there is an asymmetry in the meridional propagation of near-inertial waves, since waves that propagate poleward soon reach their turning latitude and are reflected back toward the equator (*Geisler and Dickinson* (1972); *Anderson and Gill* (1979);

[1]**Citation:** Zhai. X., R.J. Greatbatch, and J. Sheng (2005), Doppler-shifted inertial oscillations on a beta-plane, *J. Phys. Oceanogr., 35*, 1480-1488, 2005.

Gill (1984); *Garrett* (2001)). The theory is supported by observations (e.g., *Fu* (1981); *Chiswell* (2003); *Alford* (2003a)). Furthermore, the equatorward propagation of near-inertial waves is important for the redistribution of the energy available for ocean mixing (*Alford* (2003a)). Near-inertial waves can also interact with background currents and meso-scale eddies during their propagation (*Olbers* (1981); *D'Asaro* (1995); *Lee and Eriksen* (1997)). *Kunze* (1985) showed that for near-inertial waves propagating in geostrophic shear, horizontally non-uniform relative vorticity has the same effect as the variation of the Coriolis parameter with latitude. As a consequence, near-inertial energy can be trapped in regions of anticyclonic relative vorticity. In addition, *White* (1972) found evidence from mooring data that a uniform background current can cause a Doppler shift of the inertial frequency. Further evidence of this effect has been provided by a case study of Doppler-shifted inertial oscillations in the Norwegian Coastal Current (*Orvik and Mork* (1995)).

Zhai et al. (2004a) recently studied the zonal advective spreading of storm-induced inertial oscillations in a model of the northwest Atlantic Ocean. The fact that inertial oscillations can be advected by a background flow raises the question of what happens if inertial oscillations are advected poleward beyond their turning latitude, where they cannot exist by themselves since these waves are strictly subinertial. Doppler shifting, on the other hand, provides a way to increase the apparent wave frequency. In this note we show that it is possible for near-inertial energy to be carried poleward due to Doppler shifting and we provide a simple theory to predict the change of shape of the inertial waves as they are advected poleward on a β-plane.

4.2 Analytic Model

We start from the reduced-gravity model and then extend the theory to a continuously stratified ocean. The equations governing linear wave motion on an f-plane in the presence of a barotropic, uniform poleward flow are

$$u_t + Vu_y - fv = -g'\eta_x \tag{4.1}$$

$$v_t + Vv_y + fu = -g'\eta_y \tag{4.2}$$

$$\eta_t + V\eta_y + H(u_x + v_y) = 0 \tag{4.3}$$

where (u, v) are perturbation velocities in x and y directions respectively, f is the Coriolis parameter, V is the poleward background current, H is the averaged upper layer depth, g' is the reduced gravity (defined as $g(\rho_2 - \rho_1)/\rho_2$, where ρ_1 and ρ_2 are upper and lower layer densities, respectively), and η is the downward displacement of the interface between the two layers.

The divergence and vorticity equations are, respectively,

$$\left(\frac{\partial}{\partial t} + V\frac{\partial}{\partial y}\right)(u_x + v_y) - f(v_x - u_y) = -g'(\eta_{xx} + \eta_{yy}) \tag{4.4}$$

and

$$\left(\frac{\partial}{\partial t} + V\frac{\partial}{\partial y}\right)(v_x - u_y) + f(u_x + v_y) = 0. \tag{4.5}$$

Combining equations (4.3), (4.4) and (4.5), we get the equation for η

$$\left[\left(\frac{\partial}{\partial t} + V\frac{\partial}{\partial y}\right)^2 + f^2\right](\eta_t + V\eta_y) = \left(\frac{\partial}{\partial t} + V\frac{\partial}{\partial y}\right)[g'H(\eta_{xx} + \eta_{yy})]. \tag{4.6}$$

Looking for solutions of the form

$$\eta = \eta_0 e^{i(kx+ly-\omega t)} \tag{4.7}$$

where (k, l) are the horizontal wavenumbers and ω is the frequency, leads to the dispersion relationship

$$(\omega - Vl)^2 = f^2 + g'H(k^2 + l^2) \tag{4.8}$$

plotted in Fig. 4.1. We note that ω can be less than f when there is a poleward flow in the northern hemisphere ($V > 0$ and $l < 0$).

The theory can be easily extended to continuous stratification by noting, following *Gill* (1982), that the equations for a continuously stratified, flat-bottomed ocean can be separated

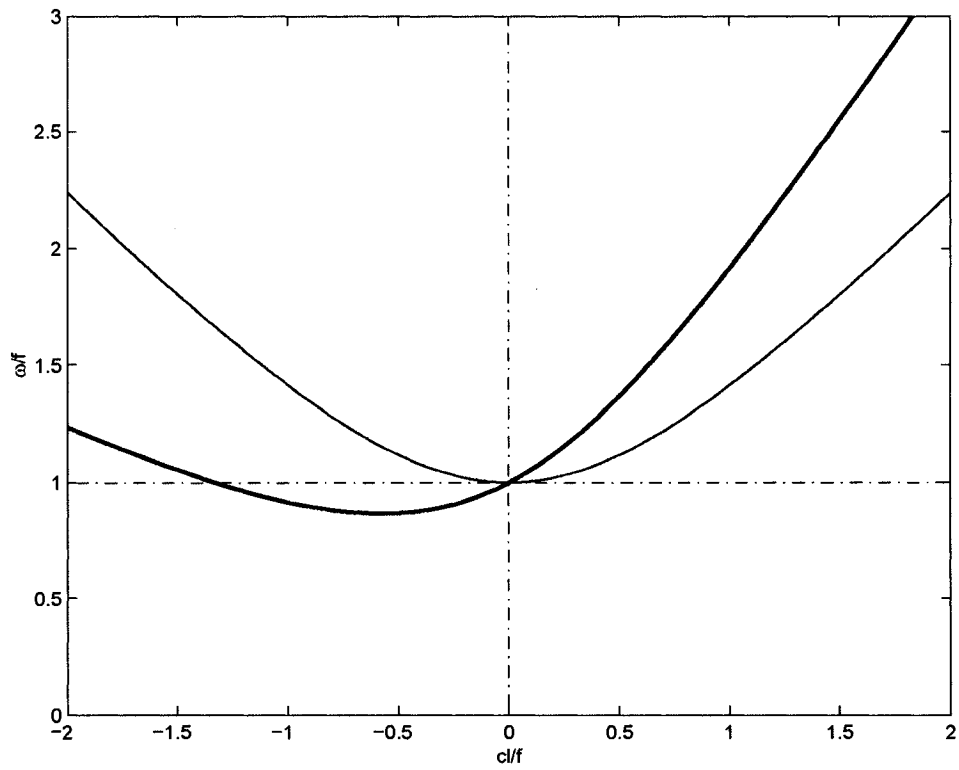

Figure 4.1: The dispersion relationship modified by the Doppler shift due to a uniform poleward flow. The thin line represents wave frequency without background current and the thick line represents wave frequency with background current. Here $V = 0.5\ m\ s^{-1}$, $c = \sqrt{g'H} = 1.0\ m\ s^{-1}$ and the zonal wavenumber $k = 0$.

into an infinite set of vertical normal modes. For each baroclinic mode, the equations are the same as (4.1), (4.2) and (4.3), but with g' replaced by g and a different H (equivalent depth) for each mode. For a uniform stratification (that is, the buoyancy frequency, N, independent of depth) the dispersion relationship corresponding to (4.8) takes the form

$$(\omega - Vl)^2 = f^2 + \frac{N^2(k^2 + l^2)}{m^2} \tag{4.9}$$

where m is the vertical wavenumber (for the n^{th} baroclinic normal mode, $m = \frac{n\pi}{H}$ where $n \geq 1$). When $V = 0$ (no background flow), equation (4.9) reduces to equation (8.4.23) in *Gill* (1982).

4.2.1 On a β-plane

We first investigate this problem in the "diagnostic" case. "Diagnostic" means that the density field is specified and the horizontal pressure gradients are no longer interactive with the flow, so that baroclinic dispersion of inertial-gravity waves is excluded[2]. On an f-plane, the dispersion relation is then the same as in (4.8) or (4.9) but with the terms involving g' and N neglected (that is $(\omega - Vl)^2 = f^2$), and is the same for both the reduced gravity and continuously stratified models. To take account of the variation of the Coriolis parameter with latitude, we make use of the WKBJ approximation (see *Gill* (1982)). The dispersion relationship can then be written as

$$(\omega - Vl)^2 = (f_0 + \beta y)^2 \tag{4.10}$$

where f is replaced by $f_0 + \beta y$ on a β-plane. f_0 is the local inertial frequency at the latitude where the near-inertial waves are generated and β is the variation of f with latitude. The use of the WKBJ approximation to write equation (4.10) assumes that the wavelength implied by the meridional wavenumber, l, is small compared to the scale on which f varies with latitude (that is, the planetary scale). The same approach has been used by *Anderson and*

[2]The diagnostic case is appropriate when the horizontal length scales are large compared to the internal radius of deformation; see *Greatbatch* (1983).

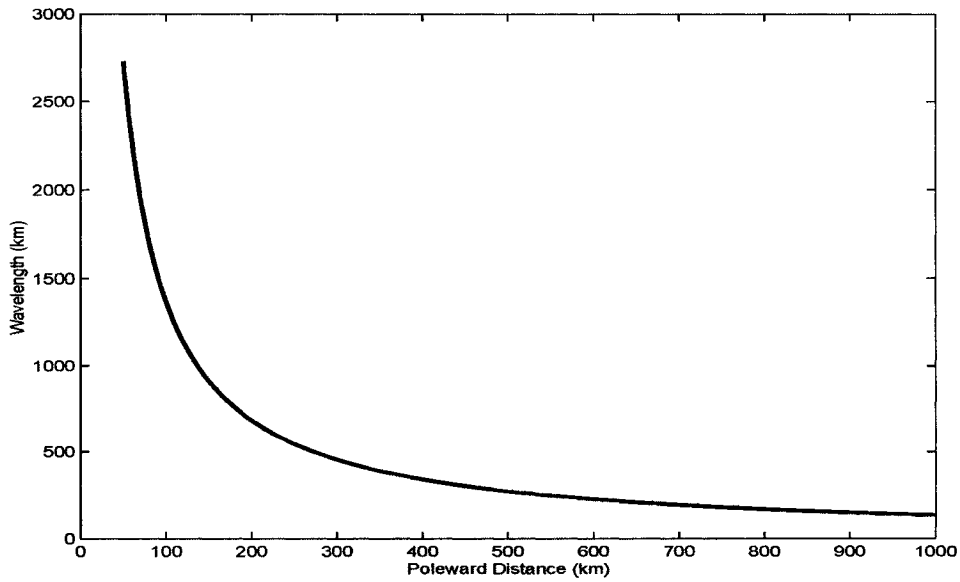

Figure 4.2: Variation of near-inertial wavelength against the poleward distance from the generation latitude in the diagnostic case. For this plot, $\beta = 2.3 \times 10^{-11}\ m^{-1}\ s^{-1}$ and $V = 0.5\ m\ s^{-1}$.

Gill (1979) (compare our equation (4.10) with their equation (4.8)) and *Garrett* (2001) (see his equation (4.7)).

For near-inertial waves, ω is very close to f_0, and (4.10) can be approximated by

$$-Vl = \beta y. \tag{4.11}$$

It follows that the meridional wavenumber is given by $-\beta y/V$, where $y/V = t$ is the advective time scale from the generation latitude $y = 0$. For a poleward background current, V is positive, y is positive and β is positive, so l is negative and its magnitude increases linearly with latitude during the advection. This indicates that the inertial oscillations shrink meridionally when carried poleward (Fig. 4.2). The same is true for inertial oscillations that are carried equatorward, as can be seen from equation (4.11), since this time both V and y are negative, and l is once again negative.

The near-inertial energy is carried by the group velocity. The horizontal group velocity

in the diagnostic case is

$$\frac{\partial \omega}{\partial l} = V \tag{4.12}$$

which means the near-inertial energy is transported poleward solely by the background current at the speed of the background current velocity and the near-inertial waves act as passive tracers. The vertical group velocity is $\partial\omega/\partial m = 0$ in this case, which indicates that the near-inertial energy is trapped in the mixed layer and dissipated there, and this energy is not available for deep ocean mixing.

However, in the real ocean, the density field is free to interact with the flow. In this case, baroclinic dispersion can play a role and the near-inertial waves become active tracers. To illustrate this case, we assume vertically uniform stratification. As before, we use the WKBJ approximation to write (4.9) as

$$(\omega - Vl)^2 = (f_0 + \beta y)^2 + \frac{N^2 l^2}{m^2} \tag{4.13}$$

where, for simplicity, only vertical and meridional propagation are considered. Assuming once again that $\omega \approx f_0$ it follows that $l < -\beta y/V$, which indicates that the inertial oscillations shrink quicker meridionally than in the diagnostic case. The horizontal group velocity is given by

$$\frac{\partial \omega}{\partial l} = V + \frac{N^2 l}{m^2(\omega - Vl)} \tag{4.14}$$

showing that the horizontal group velocity is determined by the sum of the background advective velocity, V, and a modified horizontal wave dispersion term. Since l is negative, near-inertial energy is transported poleward at a speed less than the background current velocity. Similarly, the vertical group velocity is given by

$$\frac{\partial \omega}{\partial m} = -\frac{N^2 l^2}{m^3(\omega - Vl)}. \tag{4.15}$$

The negative sign indicates downward (upward) propagation of the near-inertial energy when phase velocity is upward (downward) as in the case when $V = 0$ (see *Gill* (1982)). Since $\omega - Vl > \omega$, the amplitude of the vertical group velocity is reduced by a factor of

$(\omega - Vl)/\omega$ from the case with $V = 0$. For storm-generated near-inertial waves that are carried poleward by a background current, the downward propagation of the near-inertial energy is therefore reduced and less energy escapes from the mixed layer to the deep ocean.

Zhai et al. (2004a) showed that inertial energy can be carried by a background current (in their case, the Gulf Stream) to remote regions in a model of the northwest Atlantic Ocean. The dominance of advection over wave dispersion in their model can easily be demonstrated using the theory developed here, but modified to take account of advection by a zonal, rather than meridional flow. The zonal component of the horizontal group velocity is then

$$\frac{\partial \omega}{\partial k} = U + \frac{N^2 k}{m^2(\omega - Vk)} \tag{4.16}$$

where U is the zonal background flow. For the size of storm in *Zhai et al.* (2004a), k is about $2\times10^{-5}\ m^{-1}$, ω is about $10^{-4}\ s^{-1}$, we take $N^2/m^2 = 1.0\ m^2\ s^{-2}$ and the background current velocity U is close to $1\ m\ s^{-1}$. Thus

$$\frac{\text{dispersive processes}}{\text{advective processes}} = \frac{N^2 k}{m^2(\omega - Vk)U} = \frac{0.2}{1} \tag{4.17}$$

which indicates that advective processes dominate the near-inertial wave dispersion in their case.

4.2.2 On an f-plane

On the f-plane, the β-effect is excluded. In the diagnostic case, the dispersion relationship reduces to

$$(\omega - Vl)^2 = {f_0}^2 \tag{4.18}$$

which shows that $Vl = constant$. As long as the poleward background current V is spatially uniform, the meridional wavenumber l is constant, which indicates that the inertial oscillations keep their shape during the poleward advection.

When baroclinic wave dispersion plays a role, northward energy propagation is enhanced by the northward advection, while the southward energy propagation is reduced as

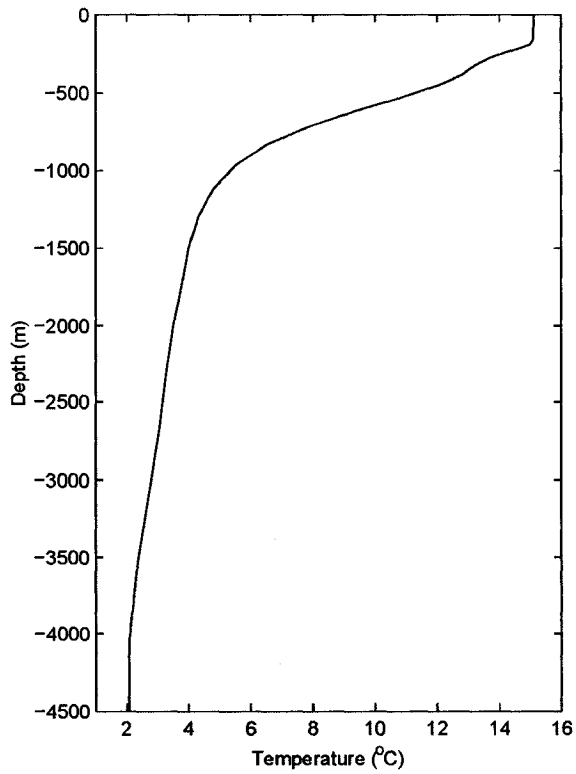

Figure 4.3: Initial vertical temperature profile used in the model. Note that the temperature is initially horizontally uniform.

seen from the dispersion curve (Fig. 4.1). Depending on the strength of the background flow, the first baroclinic mode is the mode that can most easily overcome the poleward advection and propagate equatorward (we shall see evidence of this in the model results presented below). This is because the quadratic dependence on horizontal wavenumber in (4.8) is stronger the larger the gravity wave speed $\sqrt{g'H}$, and for the baroclinic modes, the first mode has the largest wave speed. (Equivalently, amongst the baroclinic modes, the vertical wavenumber m is smallest for the first baroclinic mode, from which it follows that the dispersion term on the right hand side of equation (4.14) is largest for the first mode).

4.3 Numerical Model

The ocean model used here is the same as in *Zhai et al.* (2004a), except that we use an idealized model set-up. The model domain is rectangular and covers the area between 30°W and 60°W and between 30°N and 60°N, with two open boundaries at the south and the north and two solid boundaries at the east and the west. The horizontal resolution is about 20 km and there are 31 unevenly distributed vertical levels with the centers of the top five levels located at 5, 16, 29, 44 and 61 m, respectively. The stratification is horizontally uniform, with a vertical temperature structure representative of the mid-latitude Atlantic Ocean (Fig. 4.3). The salinity is set everywhere uniform. An initial poleward current of 50 $cm\ s^{-1}$ is introduced everywhere in the domain and maintained by the open boundaries throughout the simulation. To prevent western intensification of the barotropic background flow, the bottom relief is designed in such a way as to compensate for the variation of the Coriolis parameter with latitude. The water depth is a function of longitude and latitude and is given by

$$H(x,y) = H(x) \times 2sin(\phi) \tag{4.19}$$

where the zonal dependence $H(x)$ is a linear slope and ϕ is the latitude. In this way,

$$\frac{f}{H} = \frac{2\Omega sin(\phi)}{H(x) \times 2sin(\phi)} = \frac{\Omega}{H(x)} \tag{4.20}$$

where Ω is the Earth's rotation rate, and the f/H contours coincide with lines of longitude. The poleward background flow is then an almost spatially uniform flow throughout the model runs, following the f/H contours rather than forming an intensified western boundary current as happens with a flat bottom. Storm forcing is specified following *Chang and Anthes* (1978) and used to generate the inertial oscillations. The wind stress for the storm is

$$\tau = \tau_{max} \times \begin{cases} r/r_{min} & 0 \le r \le r_{min} \\ (r_{max} - r)/(r_{max} - r_{min}) & r_{min} \le r \le r_{max} \\ 0 & r \ge r_{max} \end{cases} \tag{4.21}$$

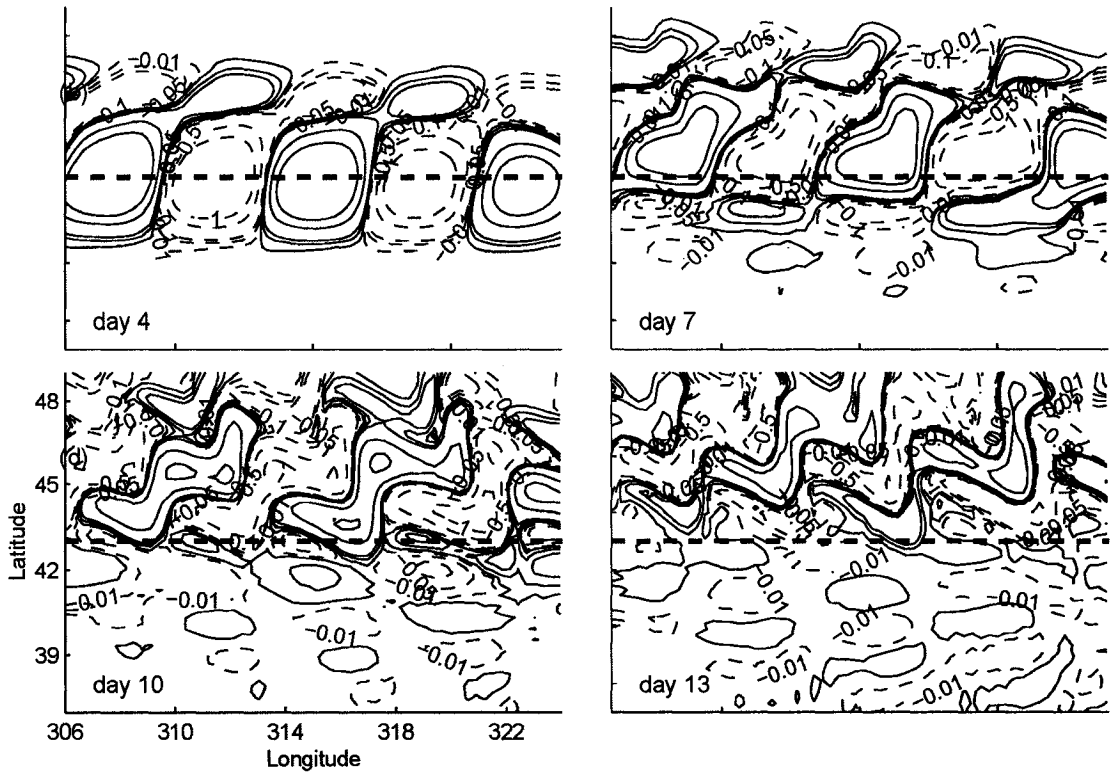

Figure 4.4: Temporal evolution of the inertial-band filtered zonal current at the sea surface in the prognostic run on a β-plane (unit: m s^{-1}). The dashed line represents the storm track.

where τ is the amplitude of the tangential wind stress with respect to the storm center (the radial wind stress is set to zero), and r is the radial distance from the center. Here, we put r_{min} = 30 km, r_{max} = 300 km, and τ_{max} = 3 N m^{-2} for a typical storm, the same as in *Zhai et al.* (2004a). The storm track is specified to be zonal from 55°W to 35°W at 43°N latitude and the translation speed of the storm is 8.5 $m\ s^{-1}$. Radiation open boundary conditions are used at the south and the north boundaries. Since the boundaries are far away from the area we are interested in, they are small in their effect.

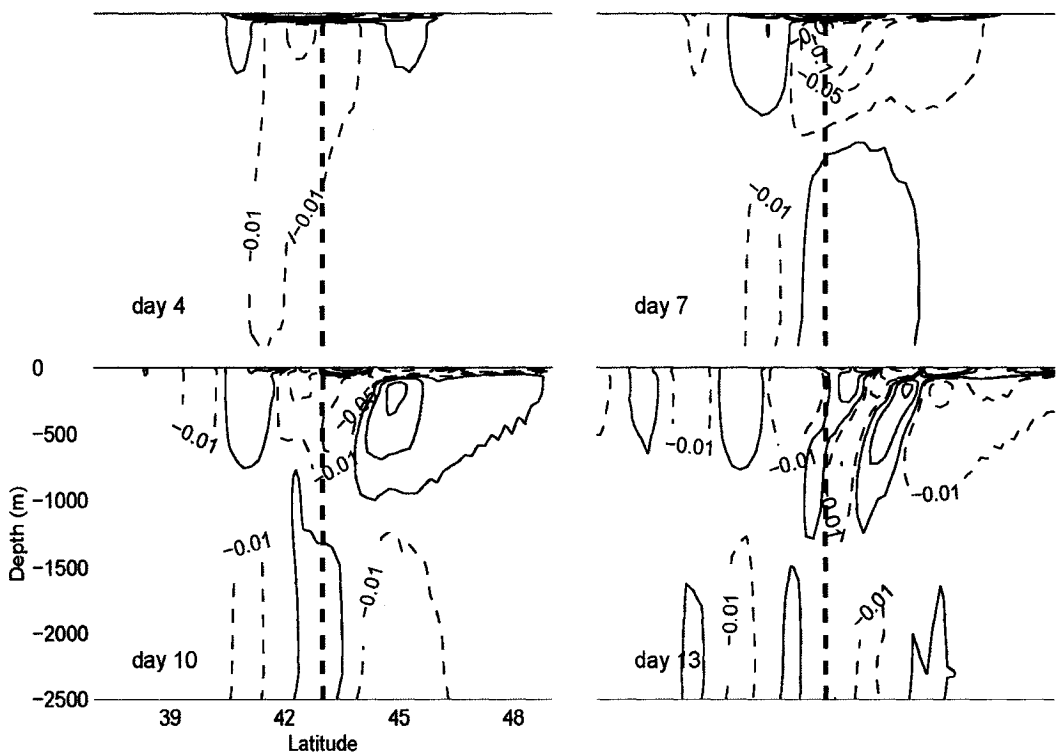

Figure 4.5: Vertical transect showing the temporal evolution of the inertial-band filtered zonal current in the prognostic run on a β-plane (unit: m s^{-1}) in the upper 2500 m. The dashed line shows where the storm center intersects the transect.

4.4 Results

4.4.1 On a β-plane

Two prognostic model runs are conducted on a β-plane, one with the storm forcing and the other without the storm forcing. The velocity differences between the two model runs are used to represent the oceanic response to the storm forcing. In order to extract the near-inertial response, a bandpass filter centered at the local (43°N) inertial frequency is used. The temporal and spatial evolution of the inertial-band filtered zonal currents at the sea surface is shown in Fig. 4.4. The near-inertial currents are initially biased to the right of the storm track (not shown) consistent with previous studies (e.g., *Price* (1981)). They are gradually advected poleward and the inertial oscillations are almost centered at the storm track at day 4. As the inertial oscillations are carried further poleward, they are squeezed meridionally as predicted by the linear theory, while the zonal wavenumber is well preserved. The β-dispersion effect is also evident after day 7, indicated by the near-inertial waves propagating equatorward, but it seems that most energy is carried poleward of the storm track. A vertical transect along the middle longitude is shown in Fig. 4.5. This figure is similar to Fig. 12 in *Gill* (1984), but note that the source of the equatorward-propagating waves is carried several hundred kilometers poleward of the storm track by the background flow. In addition, in contrast to the situation in *Gill* (1984) where the background flow is zero, the presence of the poleward background flow inhibits the equatorward dispersion of baroclinic modes higher than the first mode (see the end of Section 2). In fact, it seems only the first baroclinic mode can make its way equatorward, as indicated by the 180^o phase difference between the near-surface and near-bottom currents equatorward of the storm track in Figure 4.5.

Two additional diagnostic model runs (i.e., one with the storm forcing and one without) are conducted on the β-plane, with the density field specified from the initial condition, in which case the horizontal pressure gradients are independent of the model-calculated temperature so that the baroclinic dispersion of the inertial-gravity waves is excluded. This effect is evident in Fig. 4.6. There is no baroclinic dispersion and the near-inertial energy

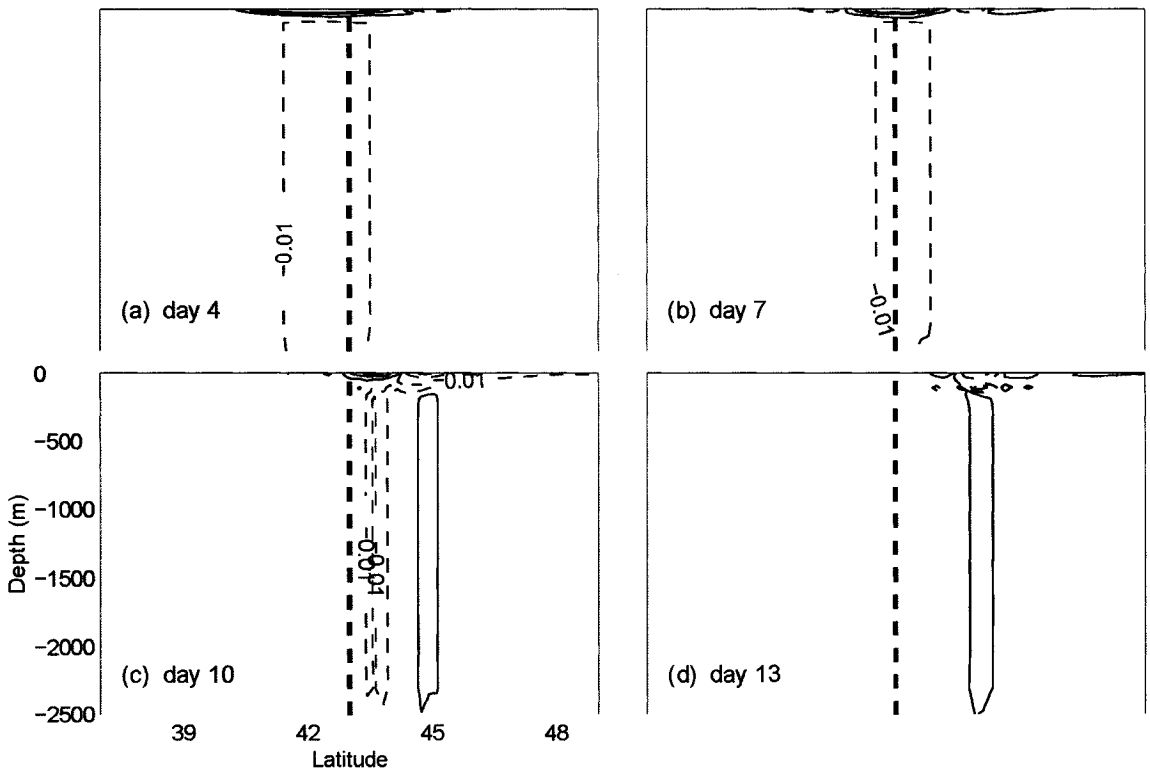

Figure 4.6: Vertical transect showing the temporal evolution of the inertial-band filtered zonal current in the diagnostic run on a β-plane (unit: m s^{-1}) in the upper 2500 m. The dashed line shows where the storm center intersects the transect.

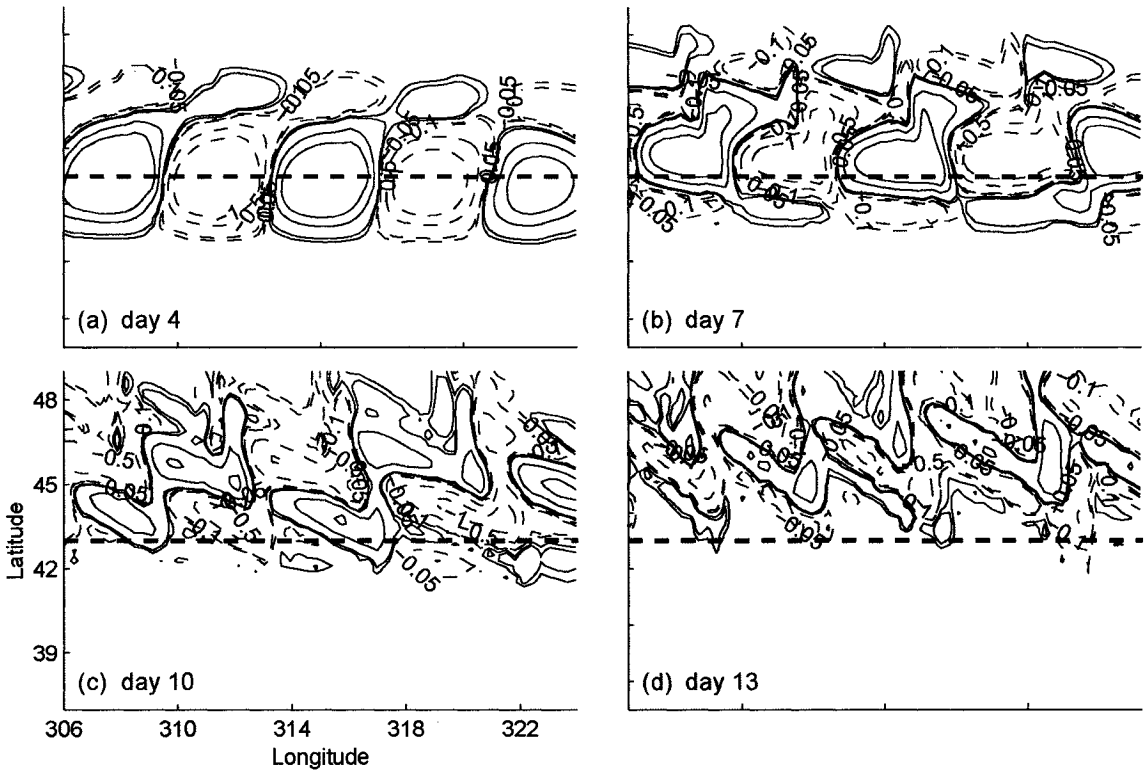

Figure 4.7: Temporal evolution of the inertial-band filtered zonal current at the sea surface in the diagnostic run on a β-plane (unit: m s^{-1}). The dashed line represents the storm track.

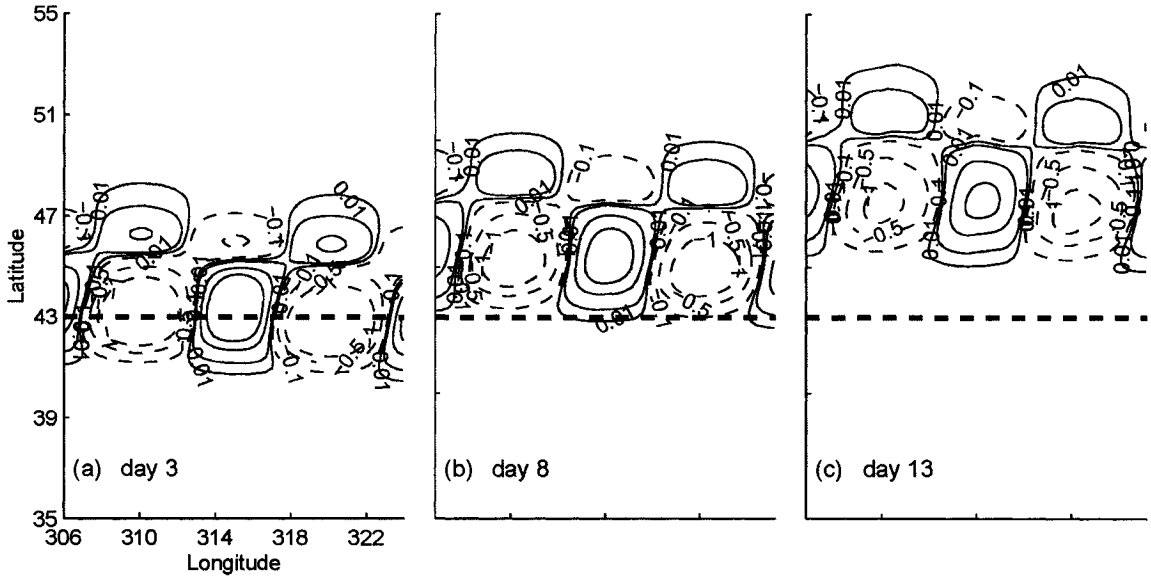

Figure 4.8: Temporal evolution of the zonal current at the sea surface in the diagnostic run on a f-plane (unit: m s^{-1}). The dashed line represents the storm track.

is confined in the mixed layer except for the (deep) inertial pumping which is also carried poleward of the storm track. The inertial oscillations act like passive tracers in the diagnostic case and the near-inertial energy occurs only poleward of the storm track at day 13, and is eventually dissipated there. For $t \approx 10$ days and $V \approx 50\, m\, s^{-1}$, the advection distance is roughly about 430 km, which is consistent with what is shown in Fig. 4.7. The meridional width of the inertial oscillations is about 300 km at day 13 after being advected poleward for about 500 km, close to the analytical prediction in Fig. 4.2. The advection distance of the inertial oscillations in the prognostic run is a little shorter than that in the diagnostic run, due to the second term in equation (4.14), which is negative and representing the wave propagation. The most revealing fact is that the diagnostic run captures the essential features of the prognostic run, i.e., the poleward advection of the near-inertial energy and the meridional squeezing of the near-inertial oscillations (compare Fig. 4.4 with Fig. 4.7).

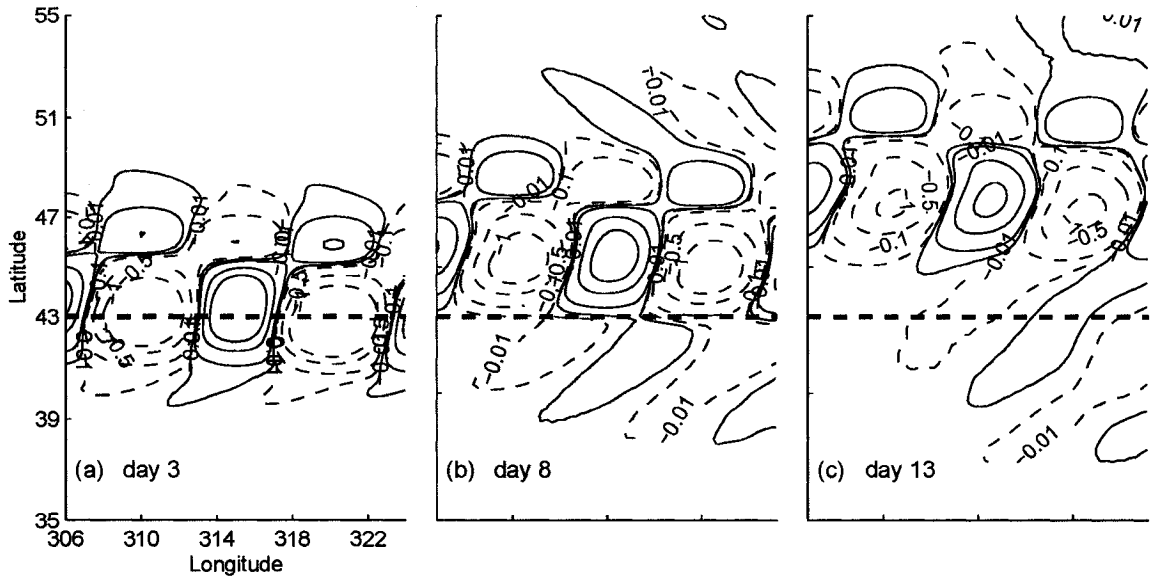

Figure 4.9: Temporal evolution of the zonal current at the sea surface in the prognostic run on a f-plane (unit: m s^{-1}). The dashed line represents the storm track.

4.4.2 On an f-plane

In the diagnostic run on the f-plane, the inertial oscillations act solely as passive tracers (Fig. 4.8). There is no squeezing of the meridional wavelength and the shape of the inertial oscillations are well preserved during the advection, which is consistent with the analytical solution. In the prognostic case on the f-plane, baroclinic dispersion takes effect and there is energy leakage both northward and southward through the propagation of the near-inertial waves (Fig. 4.9). This can be explained by the concepts of modal separation and modal interference as described in *Gill* (1984) and *Zervakis and Levine* (1995). The inertial oscillations, though carried northward by the background current, do not change much in their shape in contrast to what happens on the β-plane.

4.5 Summary and Discussion

Inertial oscillations can be carried poleward by a background flow beyond their turning latitude due to the Doppler shift effect. The inertial oscillations shrink meridionally with

latitude during this advection. As the scales become smaller, the near-inertial waves are more vulnerable to nonlinear interactions, which could eventually lead to small-scale dissipation and mixing. This advection-induced mixing occurs poleward of their source regions. Since a given energy level at higher latitudes causes much more mixing than at lower latitudes (*Gregg et al.* (2003); *Garrett* (2003)), a mechanism for transporting inertial energy to higher latitudes could lead to more efficient mixing than would otherwise be the case. We believe therefore that the mechanism described in this paper could be important for understanding mixing in the ocean. The phenomenon discussed in this paper could be applied to the North Atlantic Current (e.g. off eastern Canada), the Norwegian Coastal Current, and other poleward currents, even though those are more complicated environments and subject to additional physics.

Acknowledgments

We wish to thank Youyu Lu and Kevin Lamb for helpful discussions. This project is supported by funding from CFCAS.

Bibliography

Alford, M.H., 2003: Redistribution of energy available for ocean mixing by long-range propagation of internal waves. *Nature*, **423**, 159-162.

Anderson, D.L.T., and A.E. Gill, 1979: Beta dispersion of inertial waves, *J. Geophys. Res.*, **84**, 1836-1842.

Chang, S.W., and R.A. Anthes, 1978: Numerical simulations of the ocean's nonlinear baroclinic response to translating hurricanes, *J. Phys. Oceanogr.*, **8**, 468-480.

Chiswell, S.M., 2003: Deep equatorward propagation of inertial oscillations, *Geophys. Res. Lett.*, **30**, 1533-1536.

D'Asaro, E.A., 1995: Upper-ocean inertial currents forced by a strong storm. Part III:

Interaction of inertial currents and mesoscale eddies, *J. Phys. Oceanogr.*, **25**, 2953-2958.

Fu, L.L., 1981: Observations and models of inertial waves in the deep ocean, *Rev. Geophys. Space Phys.*, **19**, 141-170.

Garrett, C., 2001: What is the "Near-Inertial" band and why is it different from the rest of the internal wave spectrum, *J. Phys. Oceanogr.*, **31**, 962-971.

Garrett, C., 2003: Mixing with latitude, *Nature*, **422**, 477-478.

Geisler, J.E., and R.E. Dickinson, 1972: The role of variable Coriolis parameter in the propagation of inertia-gravity waves during the process of geostrophic adjustment, *J. Phys. Oceanogr.*, **2**, 263-272.

Gill, A.E., 1982: *Atmosphere-Ocean Dynamics*, Academic Press, 662 pp.

Gill, A.E., 1984: On the behavior of internal waves in the wake of storms, *J. Phys. Oceanogr.*, **14**, 1129-1151.

Greatbatch, R.J., 1983: On the response of the ocean to a moving storm: The nonlinear dynamics, *J. Phys. Oceanogr.*, **13**, 357-367.

Gregg, M.C., T.B. Sanford, and D.P. Winkel, 2003: Reduced mixing from the breaking of internal waves in equatorial waters, *Nature*, **422**, 513-515.

Kunze, E., 1985: Near-inertial propagation in geostrophic shear, *J. Phys. Oceanogr.*, **15**, 544-565.

Lee., C.M., and C.C. Eriksen, 1997: Near-inertial internal wave interactions with mesoscale fronts: Observations and models, *J. Geophys. Res.*, **102**, 3237-3253.

Olbers, D.J., 1981: The propagation of internal waves in a geostrophic current, *J. Phys. Oceanogr.*, **11**, 1224-1233.

Orvik, K.A., and M. Mork, 1995: A case study of Dopper-shifted inertial oscillations in the Norwegian Coastal Current, *Continental Shelf Res.*, **15**, 1369-1379.

Price, J.F., 1981: Upper ocean response to a hurricane, *J. Phys. Oceanogr.*, **11**, 153-175.

White, W.B., 1972: Dopper shift in the frequency of inertial waves observed in moored spectra, *Deep Sea Res.*, **19**, 595-600.

Zervakis, V., and M.D. Levine, 1995: Near-inertial energy propagation from the mixed

layer: Theoretical consideration, *J. Phys. Oceanogr.*, **25**, 2872-2889.

Zhai, X., R.J. Greatbatch, and J. Sheng, 2004: Advective spreading of storm-induced inertial oscillations in a model of the northwest Atlantic Ocean, *Geophys. Res. Lett.*, **31**, L14315, doi:10.1029/2004GL020084.

Chapter 5

Enhanced Vertical Propagation of Storm-Induced Near-Inertial Energy in an Eddying Ocean Channel Model[1]

The interaction between inertial oscillations generated by a storm and a mesoscale eddy field is studied using a Southern Ocean channel model. It is shown that the leakage of near-inertial energy out of the surface layer is strongly enhanced by the presence of the eddies, with the anticyclonic eddies acting as a conduit to the deep ocean. Given the ubiquity of the atmospheric storm tracks (a source of near-inertial energy for the ocean) and regions of strong ocean mesoscale variability, we argue that this effect could be important for understanding pathways by which near-inertial energy enters the ocean and is ultimately available for mixing.

[1]**Citation:** Zhai, X., R. J. Greatbatch and J. Zhao (2005), Enhanced vertical propagation of storm-induced near-inertial energy in an eddying ocean channel model, *Geophys. Res. Lett.*, *32*, L18602, doi:10.1029/2005GL023643.

5.1 Introduction

There is a remarkable coincidence of regions with strong mesoscale variability (storm tracks) in both the atmosphere and the ocean. This coincidence inevitably means that regions where there is a strong energy input to the ocean at near-inertial frequency (Figure 5.1a) are also regions of strong mesoscale variability in the ocean (Figure 5.1b). The question therefore arises as to how the presence of an eddy field in the ocean affects the vertical propagation of near-inertial energy from the surface layer to depth where, ultimately, it is available for mixing (*Munk and Wunsch* (1998)). In the absense of eddies or a mean flow, near-inertial energy generated at the surface spreads both vertically and horizontally (*Gill* (1984); *Zervakis and Levine* (1995)). The near-inertial wave propagation and energy transport are largely governed by the horizontal scale of the near-inertial motions, which, on an f plane, is primarily set by the scale and propagation speed of the applied wind field (*Kundu and Thomson* (1985)). Including the β-effect, it has been shown that near-inertial energy generated at a particular latitude is free to propagate equatorward, but is restricted in its poleward propagation by the planetary vorticity gradient (*Anderson and Gill* (1979); *D'Asaro* (1989); *Garrett* (2001); *Alford* (2003a)). Similar to the β effect, the horizontal gradient of the relative vorticity can also be important for near-inertial energy propagation and the decay of the near-inertial energy in the mixed layer (*van Meurs* (1998)). *Kunze* (1985) had earlier argued that near-inertial waves propagating in geostrophic shear are subject to the absolute, not the planetary, vorticity gradient, and can be trapped in regions of negative relative vorticity. The ubiquity of the atmospheric and oceanic storm tracks strongly suggests that the transfer of near-inertial energy out of the surface layer into the deep ocean should not be studied without considering the inhomogeneity of the absolute vorticity field associated with mesoscale eddies. *Young and ben Jelloul* (1997) have studied how near-inertial oscillations propagate through a three-dimensional geostrophic flow and noted that a field of eddies with horizontal scale much smaller than that of the inertial oscillations can greatly increase the vertical propagation rate of the near-inertial energy. *Klein and llewellyn Smith* (2001) studied the horizontal dispersion of near-inertial oscillations in a mesoscale eddy field and found the prevalence of the trapping regime, inside regions of

negative relative vorticity. *Lee and Niiler* (1998) have also pointed out the possibility that anticyclonic eddies can act as a chimney, draining near-inertial energy from the surface to the deep ocean.

In this letter, we consider the response of an eddy-rich channel model to a moving storm, and, in particular, how the presence of the eddies affects the vertical propagation of the near-inertial energy generated by the storm.

5.2 The Model

The model is a 5000 m depth reentrant channel of length 50° longitude. The numerical code is the same as used by *Eden et al.* (2004) and is a revised version of the MOM2 code. The northern and southern boundaries of the channel are at 30°S and 38°S, respectively. The horizontal resolution is $1/3^o$ in longitude (in both latitude and longitude) and there are 45 unevenly spaced z levels in the vertical. The initial conditions are a state of rest and a horizontally homogeneous but vertically stratified ocean. A cosine-shape eastward wind stress is applied at the surface to generate baroclinic instability. A quadratic drag law is used for bottom friction with a coefficient of 1.5×10^{-2}. Lateral biharmonic viscosity of $2 \times 10^{11}\ m^4/s$ and explicit vertical viscosity of $2 \times 10^{-4}\ m^2/s$ are also employed. The QUICKER advection scheme is used for the only tracer (potential temperature) with no explicit diffusion.

A year-long spin-up forced by the cosine-shape zonal wind was used to allow the turbulence to fully develop and reach a quasi-equilibrium state before the storm forcing is introduced. The wind stress for the storm is specified following *Chang and Anthes* (1978) as

$$\tau = \tau_{max} \times \begin{cases} r/r_{min} & 0 \le r \le r_{min} \\ (r_{max} - r)/(r_{max} - r_{min}) & r_{min} \le r \le r_{max} \\ 0 & r \ge r_{max} \end{cases} \tag{5.1}$$

where τ is the amplitude of the tangential wind stress with respect to the storm center, and r is the radial distance from the center (the radial wind stress is put to zero). Here, we put

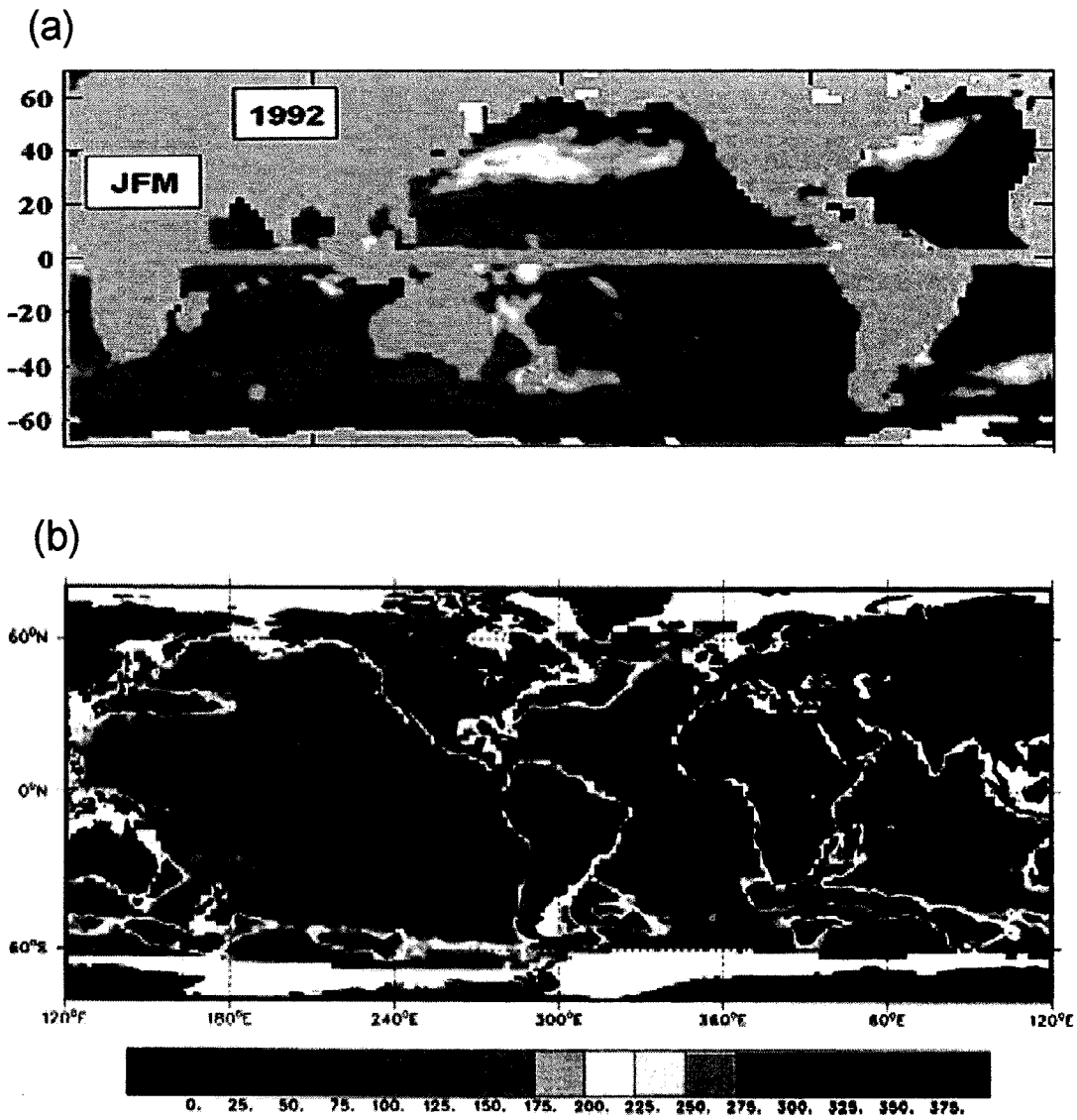

Figure 5.1: (a) Near-inertial energy input at the surface of the world ocean in the winter season (adopted from *Alford* (2003b)); (b) Eddy kinetic energy at the surface of the world ocean (adopted from *Stammer and Wunsch* (1999)). Note the use of different reference longitudes in the two figures.

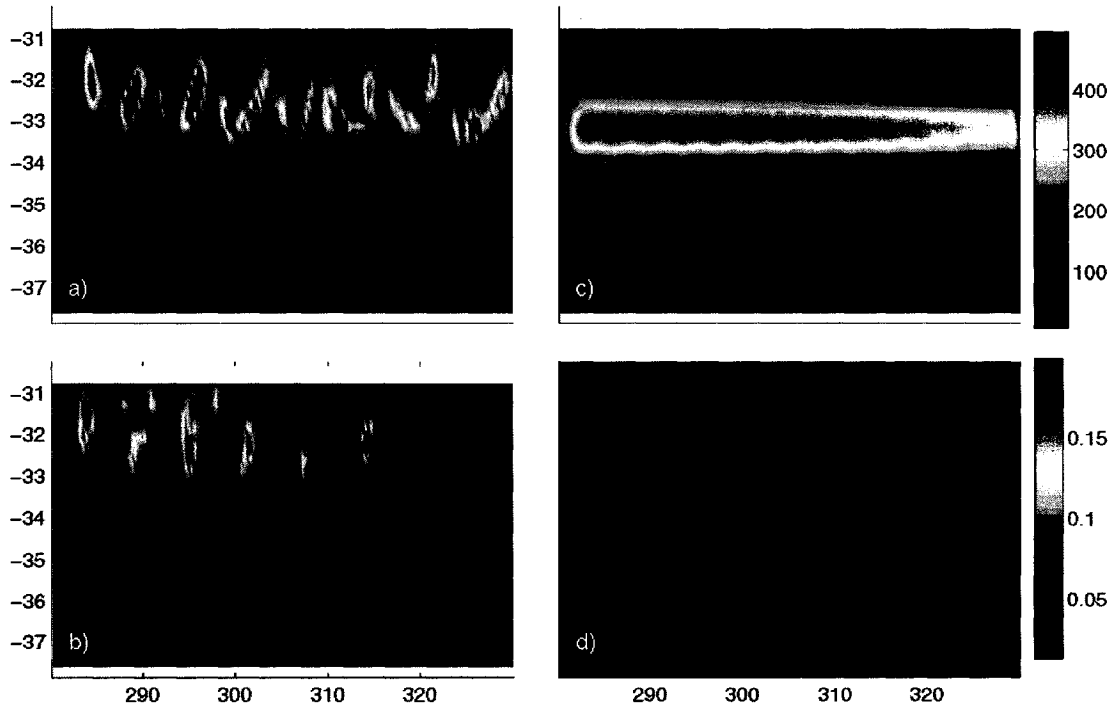

Figure 5.2: Near-inertial energy associated with the storm at 5 m depth [(a) and (c)] and 1641 m depth [(b) and (d)] and integrated over a 15 day period following the storm. (a) and (b) are for the case with eddies, (c) and (d) for the case without eddies. The units are m^2s^{-2}. Note that the scale used at 5 m depth [(a)and (c)] is different from that used at 1641 m depth [(b) and (d)].

r_{min} = 30 km, r_{max} = 300 km, and τ_{max} = 3 Nm^{-2}. The storm centre moves along 34°S from the west to the east at 10 ms^{-1} and decays so as not to reenter the channel at its western end. The storm forcing was added to the zonal wind stress at the end of the spin-up. A model run using the storm forcing applied to a resting ocean was also carried out and used to determine the difference between the response of an eddying and a resting ocean to the storm.

5.3 Model Results

At the end of the spin-up, the model domain is characterized by strong warm-core anticyclonic eddies aligned close to the north wall of the channel (see Figure 5.3b below) and weaker cold-core cyclonic eddies further south. The maximum velocity reaches 2 $m\ s^{-1}$ at the surface. In order to isolate the near-inertial response of the model, a 5th order Butterworth bandpass filter centred at the local (32^oS) inertial frequency was applied to the model-computed velocities. Figure 5.2 shows the kinetic energy calculated from the bandpass filtered velocity fields and integrated over a 15 day period following the passage of the storm. When the ocean ahead of the storm is at rest (Figure 5.2c), the near-inertial energy at the surface is found along and to the left (north) of the storm track, and integrates over the area of the channel to a value of $3.5 \times 10^5\ m^2 s^{-2}$. The leftward bias results from the surface current being turned by the Coriolis force in the same direction as the wind stress to the left of the track, but in the opposite direction to the right of the track (*Chang and Anthes* (1978)). When there are eddies, a much more complicated pattern results (Figure 5.2a). Several "hot spots" are formed, reflecting the pattern of the eddy field. Nevertheless, integrating over the area of the channel, the total near-inertial energy at the surface is now only $2.0 \times 10^5\ m^2 s^{-2}$, nearly half of that when there are no eddies. A different picture emerges at 1641 m depth (Figure 5.2b,d). In the absense of eddies, the energy level is so low that no contours appear on the plot (Figure 5.2d), whereas in the presence of eddies (Figure 5.2b), there are localized regions where the integrated, near-inertial energy is at least one order of magnitude larger. Integrated over the area of the channel, the total near-inertial energy in Figure 5.2c is more than 40 $m^2 s^{-2}$ compared to only about 8 $m^2 s^{-2}$ in Figure 5.2d. These results indicate a much more efficient transfer of near-inertial energy to depth when there are eddies compared to when there are not.

Figure 5.3 compares the difference in integrated, near-inertial energy between Figures 5.2b and 5.2d (Figure 5.3a) with the temperature field at the same depth (Figure 5.3b). It should be noted that Figure 5.3b is a snapshot, whereas Figure 5.3a shows the difference between quantities integrated over a 15 day period. Nevertheless, the two figures roughly correspond to the same time period, and clearly show that each hot-spot for near-inertial

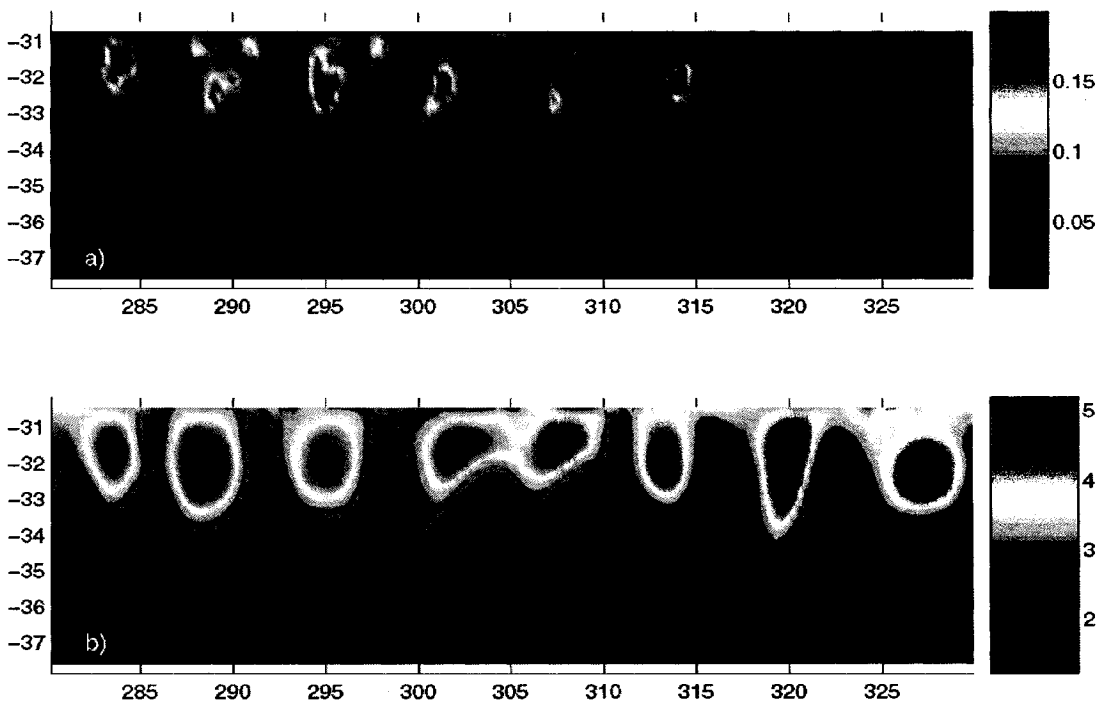

Figure 5.3: (a) The difference between Figures 5.2b and 5.2d in $m^2 s^{-2}$ and (b) a snapshot of the temperature (^oC) field at 1641 m depth.

energy at 1641 m depth (Figure 5.3a) corresponds to an individual anticyclonic (warm) eddy (Figure 5.3b). The correspondence is not exact because the anticyclonic eddies are not steady, but rather move around, and the near-inertial energy trapped in these anticyclones is carried by them and redistributed. Nevertheless, our results support the contention of *Lee and Niiler* (1998) that anticyclonic eddies can act as a conduit, draining near-inertial energy to depth (what they call the "chimney effect"). Figure 5.4 shows vertical transects of the near-inertial energy along 32°S for the two cases, with and without eddies. The chimney effect can be clearly seen in Figure 5.4a. Each high-energy conduit corresponds to an anticyclonic eddy (Figure 5.3b) and carries the near-inertial energy to more than 1500 m depth in the case with eddies (Figure 5.4a), compared to the much weaker and more diffuse downward spreading of near-inertial energy in the case without eddies (Figure 5.4b). *Young and ben Jelloul* (1997) describe an example in which the horizontal scale of the near-inertial oscillations is much larger than that of the eddy field and also find enhanced propagation of the near-inertial energy to depth in association with the eddies. By contrast, our model results show a strong correspondence between the horizontal scale of the storm-generated near-inertial oscillations, and that of the eddy field, and highlight the importance of the chimney effect.

The basic mechanism at work was introduced by *Kunze* (1985). He argued that in the presence of the relative vorticity ζ, the effective Coriolis parameter, f_{eff}, is replaced by

$$f_{eff} = f + \zeta/2 \tag{5.2}$$

where f is the planetary vorticity. To examine this effect, we have looked at time series of the bandpass filtered velocities within the hot spots at depth 1641 m. These reach up to 4 cm/s, somewhat greater than the 1 cm/s maximum found in the case with no eddies. A spectral analysis shows that the dominant frequency is shifted from about 19 hours (the local inertial period) when there are no eddies to near 23 hours when there are eddies. For a typical anticyclonic eddy in the channel, the relative vorticity ζ is roughly $2 \times 10^{-5}\ s^{-1}$. Based on equation (5.2), the effective inertial period in such an eddy is approximately 23 hours, consistent with the model results. The same frequency shift can also be seen in

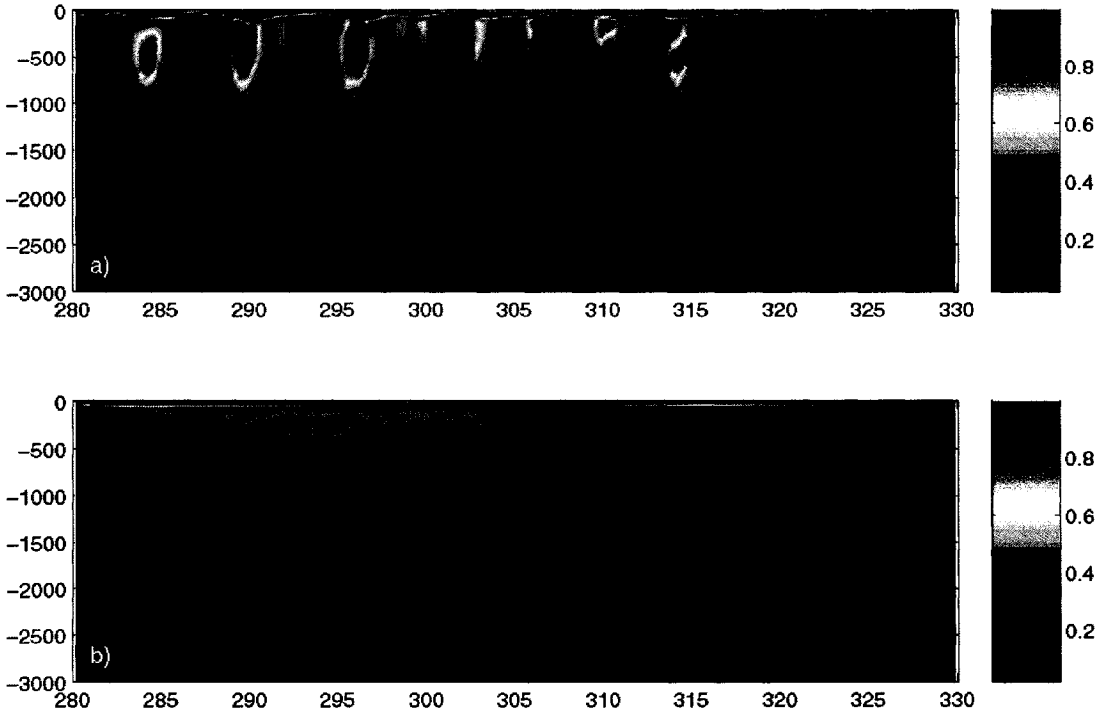

Figure 5.4: Vertical transect of the near-inertial energy in $m^2 s^{-2}$ along 32°S in the experiment (a) with eddies; (b) without eddies.

the surface level of the model where it is also consistent with equation (5.2). This result differs from *D'Asaro* (1995), who found a much smaller frequency shift associated with near-inertial oscillations generated in the Northeast Pacific by a strong storm. The reason for this difference is not clear.

5.4 Discussion and Summary

The thermohaline circulation of the ocean results primarily from deep water formation at sites in the Nordic and Labrador Seas, and around Antarctica, and upwelling throughout the rest of the global ocean. Mechanical energy input from the wind and tides is thought to be necessary to generate the diapycnal mixing required to support the upwelling branch of the thermohaline circulation (*Munk and Wunsch* (1998), *Wunsch* (2002)). Global maps of the wind-induced energy flux to inertial motions at the surface have been drawn by *Watanabe and Hibiya* (2002) and *Alford* (2003b), but there is a question as to how the near-inertial energy generated at the surface is transferred to the deep ocean where it is available to participate in deep ocean mixing.

Wind-induced near-inertial energy is thought to be redistributed by the propagation of inertial-gravity waves to lower latitudes, for example by the beta-dispersion effect (see *Alford* (2003a) and *Chiswell* (2003)), and by advective processes (e.g., *Zhai et al.* (2004a) and *Zhai et al.* (2005a)). However, there is a strong similarity between the distribution of the input of near-inertial energy at the surface (*Alford* (2003b)) and the distribution of eddy kinetic energy in the world ocean (*Stammer and Wunsch* (1999); see Figure 5.1), making it necessary to examine the effect of a mesoscale eddy field on the vertical propagation of the near-inertial energy.

Our model results suggest that the vertical propagation of near-inertial energy is strongly enhanced by the presence of eddies. *Young and ben Jelloul* (1997) had earlier arrived at a similar conclusion. However, in contract to *Young and ben Jelloul* (1997), our model results emphasise the important role played by anticyclonic eddies, which in our model, drain near-inertial energy quickly to the deep ocean through the "inertial chimney" effect

of *Lee and Niiler* (1998). Since a given energy level at higher latitudes causes much more mixing than at lower latitudes (*Gregg et al.* (2003), *Garrett* (2003)), the "inertial chimneys" could be an efficient way to generate mixing at depth, since they can drain wind-generated near-inertial energy to depth more locally, at middle to high latitudes, rather than transferring it first to lower latitudes as in the β-dispersion effect (*Garrett* (2001)). We argue that the "inertial chimney" effect could be particularly important in the Southern Ocean, where there is both an abundance of eddies, and strong near-inertial energy input at the surface due to passing storms. Such an effect could be important for understanding diapycnal mixing levels in the Southern Ocean, and ultimately, the pathways of the meridional overturning circulation.

Acknowledgments

This project has been supported by grants from NSERC and CFCAS through the Canadian CLIVAR Research Network. We are grateful to Carsten Eden for providing us with the basic numerical code used here. We also wish to thank two reviewers for critical comments that led to a significantly improved manuscript.

Bibliography

Alford, M.H., Redistribution of energy available for ocean mixing by long-range propagation of internal waves, *Nature*, *423*, 159-162, 2003a.

Alford, M.H., Improved global maps and 54-years history of wind-work on ocean inertial motions, *Geophys. Res. Lett.*, *30(8)*, 1424, doi:10.1029/2002GL016614, 2003b.

Anderson, D.L.T., and A.E. Gill, Beta dispersion of inertial waves, *J. Geophys. Res.*, *84*, 1836-1842, 1979.

Chang, S.W., and R.A. Anthes, Numerical simulations of the ocean's nonlinear baroclinic response to translating hurricanes, *J. Phys. Oceanogr.*, *8*, 468-480, 1978.

Chiswell, S.M., Deep equatorward propagation of inertial oscillations, *Geophys. Res.*

Lett., *30*, 1533-1536, 2003.

D'Asaro, E., The decay of wind-forced mixed layer inertial oscillations due to the β effect, *J. Geophys. Res.*, *94*, 2045-2056, 1989.

D'Asaro, E.A., Upper-ocean inertial currents forced by a strong storm. Part III: Interaction of inertial currents and mesoscale eddies, *J. Phys. Oceanogr.*, *25*, 2953-2958, 1995.

Eden, C., R.J. Greatbatch, and C.W. Böning, Adiabatically correcting an eddy-permitting model using large-scale hydrographic data: Application to the Gulf Stream and the North Atlantic Current, *J. Phys. Oceanogr.*, *34*, 701-719, 2004.

Garrett, C., What is the "Near-Inertial" band and why is it different from the rest of the internal wave spectrum, *J. Phys. Oceanogr.*, *31*, 962-971, 2001.

Garrett, C., Mixing with latitude, *Nature*, *422*, 477-478, 2003.

Gill, A.E., On the behavior of internal waves in the wake of storms, *J. Phys. Oceanogr.*, *14*, 1129-1151, 1984.

Gregg, M.C., T.B. Sanford, and D.P. Winkel, Reduced mixing from the breaking of internal waves in equatorial waters, *Nature*, *422*, 513-515, 2003.

Klein, P., and S.G. Llewellyn Smith, Horizontal dispersion of near-inertial oscillations in a turbulent mesoscale eddy field, *J. Mar. Res.*, *59*, 697-723, 2001.

Kundu, P.K., and R.E. Thomson, Inertial oscillations due to a moving front, *J. Phys. Oceanogr.*, *15*, 1076-1084, 1985.

Kunze, E., Near-inertial propagation in geostrophic shear, *J. Phys. Oceanogr.*, *15*, 544-565, 1985.

Lee, D.K., and P.P. Niiler, The inertial chimney: The near-inertial energy drainage from the ocean surface to the deep layer, *J. Geophys. Res.*, *103*, 7579-9791, 1998.

Munk, W., and C. Wunsch, Abyssal recipes II, Energetics of tidal and wind mixing, *Deep Sea Res., Part I, 45*, 1977-2010, 1998.

Stammer, D., and C. Wunsch, Temporal changes in eddy energy of the oceans, *Deep-Sea Res., II46*, 77-108, 1999.

van Meurs, P., Interactions between near-inertial mixed layer currents and the mesoscale: The importance of spatial variabilities in the vorticity field, *J. Phys. Oceanogr.*, *28*,

1363-1388, 1998.

Watanabe, M., and T. Hibiya, Global estimates of the wind-induced energy flux to inertial motions in the surface mixed layer, *Geophys. Res. Lett., 29(8)*, doi:10.1029/2001GL014422, 2002.

Wunsch, C., What is the thermohaline circulation? *Science, 298*, 1179-1181, 2002.

Young, W.R., and M. Ben Jelloul, Propagation of near-inertial oscillations through a geostrophic flow, *J. Mar. Res., 55*, 735-766, 1997.

Zervakis, V., and M.D. Levine, Near-inertial energy propagation from the mixed layer: Theoretical consideration, *J. Phys. Oceanogr., 25*, 2872-2889, 1995.

Zhai, X., R.J. Greatbatch, and J. Sheng, Advective spreading of storm-induced inertial oscillations in a model of the northwest Atlantic Ocean, *Geophys. Res. Lett., 31*, L14315, doi:10.1029/2004GL020084, 2004.

Zhai, X., R.J. Greatbatch, and J. Sheng, Doppler-shifted inertial oscillations on a β plane, *J. Phys. Oceanogr., 35*, 1480-1488, 2005.

Chapter 6

Spreading of Near-Inertial Energy in a $1/12^o$ Model of the North Atlantic Ocean[1]

Near-inertial energy in the ocean is thought to be redistributed by β-dispersion, whereby near-inertial waves generated at the surface by wind forcing propagate downward and equatorward. In this letter, we examine the spreading of near-inertial energy in a realistic $1/12^o$ model of the North Atlantic driven by synoptically varying wind forcing. We find that (i) near-inertial energy is strongly influenced by the mesoscale eddy field and appears to be locally drained to the deep ocean, largely by the chimney effect associated with anticyclonic eddies, and (ii) the interior of the subtropical gyre shows very low levels of near-inertial energy, contrary to expectations based on the β-dispersion effect.

[1]**Citation:** Zhai, X., R. J. Greatbatch, and C. Eden (2007), Spreading of near-inertial energy in a 1/12 model of the North Atlantic Ocean, *Geophys. Res. Lett.*, *34*, L10609, doi:10.1029/2007GL029895. Copyright 2007 American Geophysical Union. Reproduced by permission of American Geophysical Union.

6.1 Introduction

Near-inertial waves are believed to be an important source of energy for generating diapycnal mixing in the ocean, contributing to the maintenance of the meridional overturning circulation (*Munk and Wunsch* (1998)). The traditional view is that near-inertial energy is redistributed in the ocean largely by the β-dispersion effect, whereby near-inertial waves are free to propagate equatorward, but are restricted in their poleward propagation by the planetary vorticity gradient (e.g., *Anderson and Gill* (1979); *Garrett* (2001)). Observational evidence has been found to support this idea (e.g., *Chiswell* (2003); *Alford* (2003a)). However, the ocean is not homogeneous, and similar to the idea of β-dispersion, the horizontal gradient of the relative vorticity can influence the propagation of near-inertial waves (*Kunze* (1985); *Young and ben Jelloul* (1997); *van Meurs* (1998); *Lee and Niiler* (1998); *Klein and llewellyn Smith* (2001); *Zhai et al.* (2005b)). It has also been pointed out (*Zhai et al.* (2005b)) that there is a remarkable coincidence between regions with strong mesoscale variability (storm tracks) in both the atmosphere and the ocean. It follows that regions where there is a strong energy input to the ocean at near-inertial frequency (the atmospheric storm tracks) and also regions of strong mesoscale variability in the ocean, making studies of the interaction between near-inertial waves and mesoscale eddies necessary. Using an idealized ocean channel model, *Zhai et al.* (2005b) showed the important role played by anticyclonic eddies for draining near-inertial energy from the surface to the deep ocean through the "inertial chimney" effect (e.g. *Kunze* (1985), *Lee and Niiler* (1998)). The basic mechanism at work was discussed by *Kunze* (1985) (see also *Mooers* (1975)), who showed that in the presence of the relative vorticity ζ, the effective Coriolis parameter, f_{eff}, is

$$f_{eff} = f + \zeta/2 \tag{6.1}$$

where f is the planetary vorticity. It then follows that if the relative vorticity gradient is strong enough, near-inertial energy generated inside anticyclonic eddies can be trapped and reflected downward locally to the deep ocean.

Most previous studies on the interaction between near-inertial oscillations and mesoscale

eddies have been conducted in idealized model set-ups, and it is not clear how significant the chimney effect is in reality in comparison with β-dispersion. In this letter, we make a first attempt to address this issue using a realistic eddy-resolving ($1/12^o$) model of the North Atlantic Ocean driven by synoptically varying wind forcing.

6.2 The Model

The model used in this study is based on a rewritten version of MOM2, and is idential to the one used in *Eden et al.* (2007b). The horizontal resolution is about 10 km at the equator decreasing to about 5 km in high latitudes, corresponding to roughly $1/12^o$ in longitude. The model domain extends between open boundaries at 20^oS and 70^oN formulated following *Stevens* (1990), with a restoring zone in the eastern Mediterranean Sea. There are 45 vertical geopotential levels with increasing thickness with depth, ranging from 10 m at the surface to 250 m near the maximal depth of 5500 m. The model was spun-up for 10 years with monthly climatological forcing. After that, it was forced using daily wind stress taken from 24-hour forecasts of the operational weather forecast model from ECMWF started from operational analyses at 12 Universal Coordinated Time (UTC) on each day from year 2001 to 2004 (see *Eden and Jung* (2006)). The horizontal resolution of the ECMWF model is about 40×40 km and here we use forcing from 2001 starting on January 1.

The model variables are saved every 0.1 day, so aliasing of the near-inertial frequency band in the model output is not a problem. We examine the model results in winter when the near-inertial energy input is at its maximum, and leave the question of seasonality to a future study. To compute near-inertial energy, the horizontal velocity is filtered (using a Butterworth filter) to retain periods of less than 1.3 days. By near-inertial energy in the model we mean the kinetic energy computed from the high pass filtered velocity. The cutoff period of 1.3 days is sufficient for the regions that we are interested in, and further refinement of the band-pass filter does not lead to any major changes of the near-inertial properties in the model.

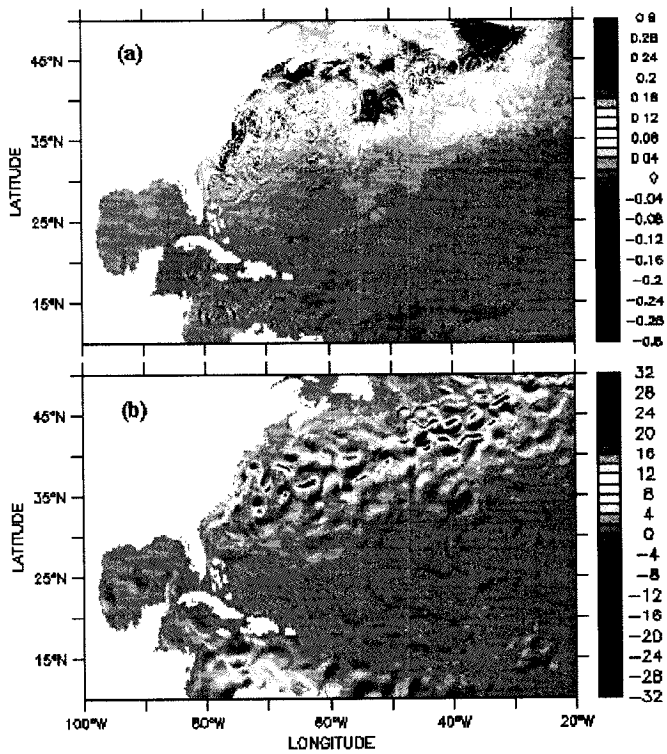

Figure 6.1: (a) Energy input to near-inertial motions. (b) Total wind work. Both are integrated for 10 days. Unit, $\times 8640$ N m^{-1}.

6.3 Model Results

Figure 6.1a shows the input of near-inertial energy at the sea surface calculated using $\tau \cdot \mathbf{u_I}$, where τ is the wind stress vector and $\mathbf{u_I}$ the high pass filtered surface velocity, and integrated for 10 days starting on March 8. For simplicity, we focus on the subtropical gyre and its neighbourhood. The overall pattern and magnitude is broadly consistent with the estimate given by *Alford* (2003b) who used a slab model and did not account for mesoscale eddies. In particular, south of the atmospheric storm track, over the subtropical gyre, much lower levels of energy input are found than beneath the atmospheric storm track itself. Clearly, however, integrations using wind forcing with higher temporal resolution and averaged over many years will be required to provide a reliable comparison with *Alford* (2003b). Our purpose here is simply to show that the energy input to the inertial frequency band in the model is at a reasonable level. For comparison, Figure 6.1b shows the total wind work ($\tau \cdot \mathbf{u}$, where $\mathbf{u}$ is the total surface velocity) over the same region, integrated over the same 10 days. Here, the mesoscale eddy field clearly dominates; in particular, the wind transfers energy into (and out of) the ocean mostly through the mesoscale eddy field (*Zhai and Greatbatch* (2007)), and the peak value is more than one order of magnitude larger than that of the near-inertial energy input.

The distribution of the near-inertial energy itself is illustrated in Figure 6.2. At the surface (Fig. 6.2a), the near-inertial energy shows a smooth maximum over the Grand Banks of Newfoundland, where the relative vorticity is small compared with the Coriolis frequency. By contrast, much smaller spatial scales, reflecting the mesoscale eddy field, are found in other parts of the figure, in contrast to expectations based on traditional theory in which the spatial scale is set by the scale of the applied wind field (e.g. *Greatbatch* (1984); *Kundu and Thomson* (1985)). The same effect can be seen by comparing Figures 6.2a and 6.2c in the idealised study of *Zhai et al.* (2005b), and has been noted in observed data by *Kunze and Sanford* (1984) for a frontal situation, demonstrating the influence of the mesoscale in regulating the near-inertial energy field. Deeper down at 516 m depth, large near-inertial energy levels are also confined in the western boundary current region and again exhibit small spatial scales associated with the eddy field. Vertical transects

(Figures 6.2c,d) reveal a similar picture, with relatively high levels of near-inertial energy in "chimneys" confined to the neighbourhood of the Gulf Stream. The association between high levels of near-inertial energy and negative relative vorticity is shown in Figure 6.3. The Gulf of Mexico (Figures 6.3a,c) offers a very clear example of the "chimney effect" with nearly all the significant inertial energy confined within two warm core rings (see also Figure 6.4). The situation is more complicated in the neighbourhood of the Gulf Stream, where advection (*Zhai et al.* (2004a)) and doppler shift effects (e.g. *Zhai et al.* (2005a)) are likely to be important, but there is still a clear association between high levels of near-inertial energy and regions of negative relative vorticity.

Finally, we see no evidence in the model of the equatorward spreading of near-inertial energy from its generation over the Gulf Stream region, in association with the passage of atmospheric storms, to the interior of the subtropical gyre further south. Both the horizontal plan views and the vertical transects (Figure 6.2) indicate very low levels of near-inertial energy south of 35°N and below the surface layer of 100m depth, much lower, for example, than found by *Nagasawa et al.* (2000) in their study without eddies using a $1/6^o$ model of the North Pacific. Rather the picture that emerges is of near-inertial energy input at the surface in the western boundary current region that propagates locally down to the deep ocean, with no significant leaking equatorward through β-dispersion. Therefore, the majority of the subtropical gyre, apart from the top 100 m, can be described as a "desert" for the near-inertial energy. It should be noted that the model run starts from January 1 with synoptic wind forcing, so near-inertial waves should have adequate time to ventilate the subtropical gyre by the time in March of our plots if β-dispersion is at work (*Anderson and Gill* (1979); *Nagasawa et al.* (2000)).

6.4 Discussion and Summary

Near-inertial energy is traditionally thought to be redistributed in the ocean largely by β-dispersion, whereby the near-inertial energy propagates both equatorward and downward

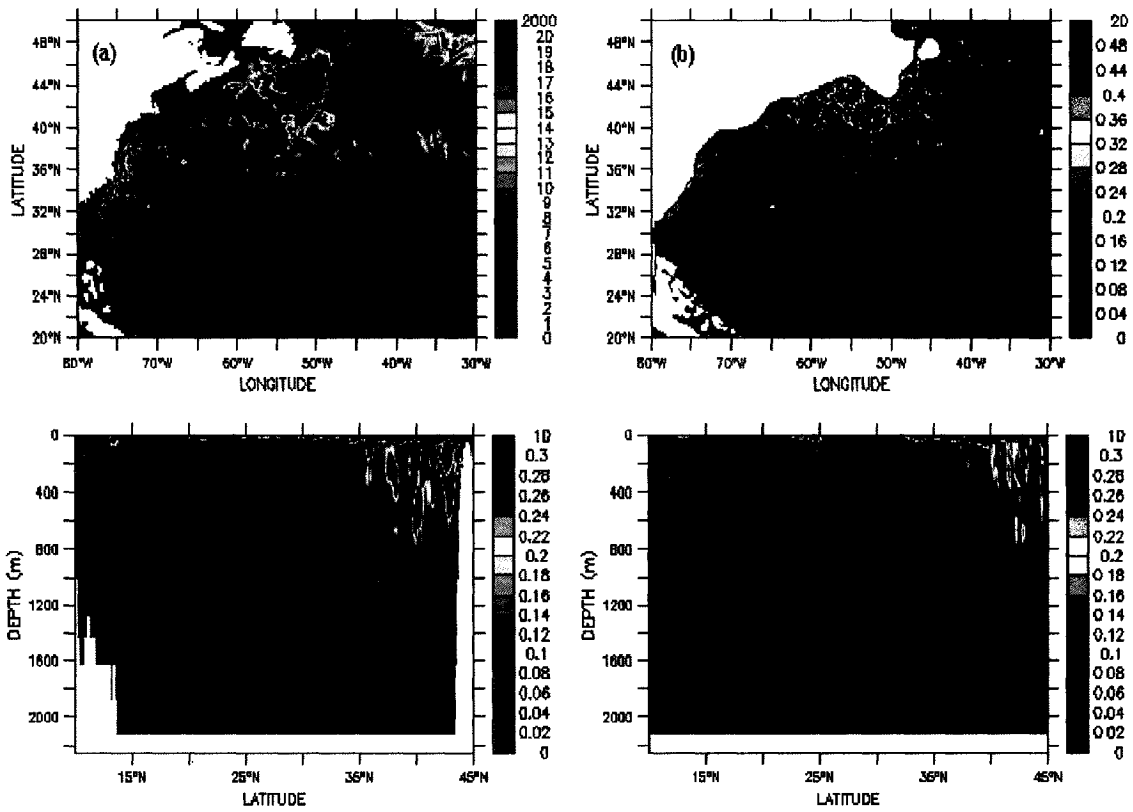

Figure 6.2: Near-inertial energy at (a) 5 m depth, (b) 516 m depth, (c) 59°W and (d) 45°W. (a), (b) and (c) are on March 8th, and (d) is on March 13th. All are averaged over a day. Unit, 10^{-3} m^2 s^{-2}.

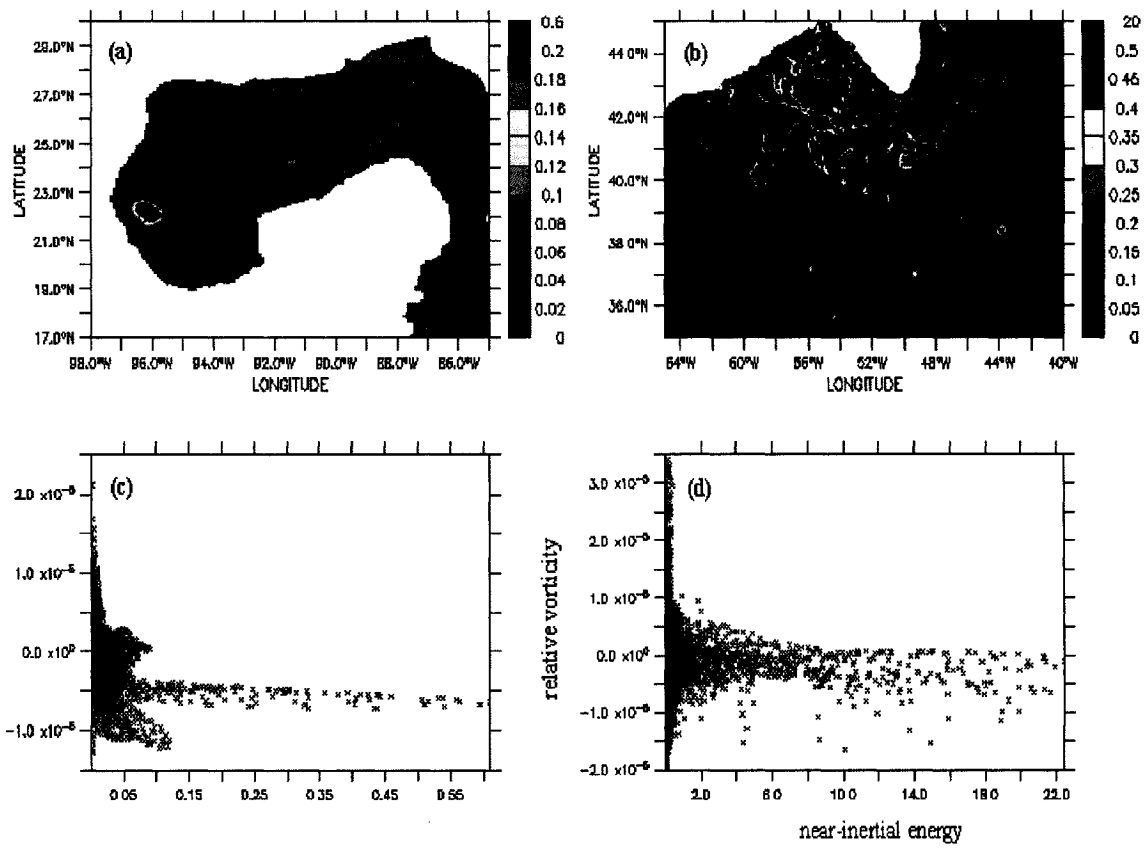

Figure 6.3: The relative vorticity (contours) and near-inertial energy (colour shading) (a) in the Gulf of Mexico and (b) in the western boundary current region. (c) and (d) are corresponding scatter plots. Unit for the near-inertial energy, 10^{-3} m^2 s^{-2}; unit for the relative vorticity, s^{-1}.

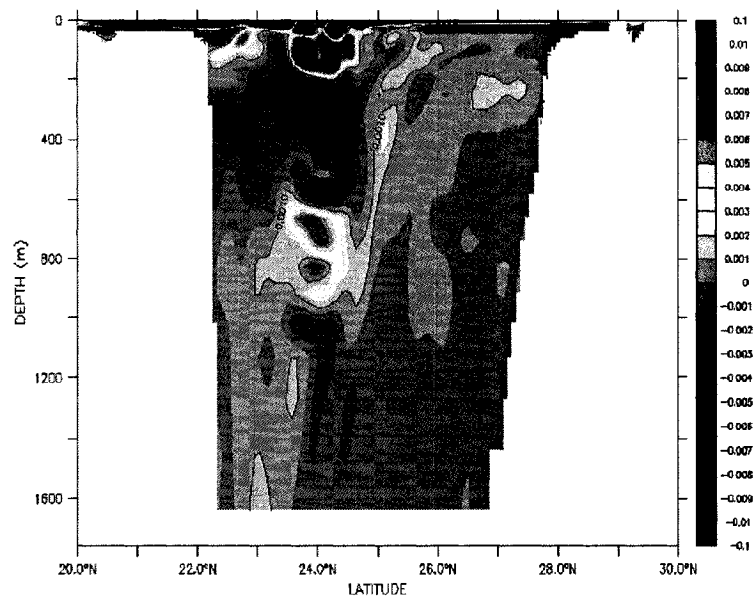

Figure 6.4: Instantaneous eastward velocity component of the near-inertial filtered velocity along 92°W in the Gulf of Mexico on March 16th. Unit, m s^{-1}. The trapping of near-inertial energy inside a warm core ring is evident.

(e.g. *Garrett* (2001)). If this is the case, then near-inertial energy generated in the western boundary current region could fuel the deep subtropical ocean, where there is only a limited energy source at the surface. However, the ocean is turbulent and inhomogeneous in its nature, and the propagation of near-inertial waves can be strongly influenced by the mesoscale flow field. For example, enhanced near-inertial energy levels have been observed on the negative vorticity sides of fronts (e.g., *Kunze and Sanford* (1984); *Mied et al.* (1986)) and in warm eddies (e.g., *Kunze and Sanford* (1986)). Given the remarkable coincidence of the atmospheric storm tracks (the source regions for near-inertial energy in the ocean) and the oceanic storm track, mesoscale eddies need to be taken into account when studying the distribution of near-inertial energy in the ocean. Using an idealized model, *Zhai et al.* (2005b) showed the important role played by anticyclonic eddies for draining near-inertial energy from the surface to the deep ocean through the "inertial chimney" effect (e.g. *Kunze* (1985), *Lee and Niiler* (1998)). However, there have been no previous studies with high-resolution realistic simulations. In this letter, we examine the spreading of near-inertial energy in an eddy-resolving ($1/12^o$) model of the North Atlantic Ocean driven by synoptic wind forcing. The picture that emerges from this study is as follows:

1) The horizontal scale of variations in near-inertial energy in the model, both at the surface and subsurface, is strongly influenced by the mesoscale eddy field and, as a result, is much smaller than that of the applied wind forcing.

2) Most of the near-inertial energy input at the surface is drained locally to the deep ocean by the mesoscale eddy field, and in particular, by the chimney effect associated with anticyclonic eddies.

3) The interior of the subtropical gyre is a "desert" for near-inertial energy, contrary to expectations from β-dispersion theory (*Garrett* (2001), *Nagasawa et al.* (2000)).

Enhanced near-inertial energy in warm eddies has been observed to generate turbulence and mixing through shear instability at the critical depth where the vertical group velocity goes to zero (e.g., *Lueck and Osborn* (1986); *Kunze et al.* (1995)). Therefore, strong diapycnal mixing associated with near-inertial wave breaking is expected to occur in the Gulf Stream system and other regions of the world ocean with high levels of eddy kinetic energy

(e.g. the Southern Ocean). Furthermore, since a given energy level at higher latitude causes much more mixing than at lower latitudes (*Gregg et al.* (2003); *Garrett* (2003)), mesoscale eddies could be efficient in generating mixing at depth, since they can drain the near-inertial energy to depth locally, rather than transferring it to lower latitudes as in β-dispersion.

More detailed calculations are necessary to provide accurate estimates of the near-inertial energy input to the ocean in the presence of a mesoscale eddy field, updating *Alford* (2003b), and also to study the fate of near-inertial energy within eddies and the associated mixing, building on the observation work of *Lueck and Osborn* (1986) and *Kunze et al.* (1995). Longer integrations, including the seasonal cycle, and using wind stress forcing with higher temporal and spatial resolution are clearly required, as well as further relatively short model integrations using even higher model resolution than we have used here. Nevertheless, our results clearly suggest that energy input from the wind to the near-inertial frequency band may well be dissipated, and lead to mixing, locally within mesoscale eddies in the ocean rather than being spread equatorward by β-dispersion. If this result holds up to closer scrutiny, then the diapycnal diffusivity that is specified in the ocean component of climate models will need to be adjusted accordingly, with relatively large values in regions of relatively large eddy kinetic energy in the ocean, complementing recent work by *Hibiya et al.* (2006) on the spatial distribution of the diapycnal diffusivity resulting from tidal forcing.

Acknowledgments

This project was initiated with support from the Canadian CLIVAR Research Network, funded jointly by NSERC and CFCAS. and completed with support from RJG's NSERC Discovery Grant. XZ and RJG are grateful to IFM-GEOMAR for their hospitality during a visit in October 2006. We are also grateful to Dr. Thomas Jung for providing us with the wind forcing used to drive the model, and to two reviewers for their helpful comments on our manuscript.

Bibliography

Alford, M.H., Redistribution of energy available for ocean mixing by long-range propagation of internal waves, *Nature*, *423*, 159-162, 2003a.

Alford, M.H., Improved global maps and 54-years history of wind-work on ocean inertial motions, *Geophys. Res. Lett.*, *30(8)*, 1424, doi:10.1029/2002GL016614, 2003b.

Anderson, D.L.T., and A.E. Gill, Beta dispersion of inertial waves, *J. Geophys. Res.*, *84*, 1836-1842, 1979.

Chiswell, S.M., Deep equatorward propagation of inertial oscillations, *Geophys. Res. Lett.*, *30*, 1533-1536, 2003.

Eden, C., and T. Jung, Wind-driven eddies and plankton blooms in the North Atlantic Ocean. ECMWF, Reading, UK, Technical Memorandum 490, 2006.

Eden, C., R.J. Greatbatch, and J. Willebrand, A diagnosis of thickness fluxes in an eddy-resolving model, *J. Phys. Oceanogr.*, *37*, 727-742, 2007.

Garrett, C., What is the "Near-Inertial" band and why is it different from the rest of the internal wave spectrum, *J. Phys. Oceanogr.*, *31*, 962-971, 2001.

Garrett, C., Mixing with latitude, *Nature*, *422*, 477-478, 2003.

Greatbatch, R.J., On the response of the ocean to a moving storm: Parameters and scales, *J. Phys. Oceanogr.*, *14*, 59-77, 1984.

Gregg, M.C., T.B. Sanford, and D.P. Winkel, Reduced mixing from the breaking of internal waves in equatorial waters, *Nature*, *422*, 513-515, 2003.

Hibiya, T., M. Nagasawa, and Y. Niwa, Global mapping of diapycnal diffusivity in the deep ocean based on the results of expendable current profiler (XCP) surveys, *Geophys. Res. Lett.*, *33*, L03611, doi:10.1029/2005GL025218, 2006.

Klein, P., and S.G. Llewellyn Smith, Horizontal dispersion of near-inertial oscillations in a turbulent mesoscale eddy field, *J. Mar. Res.*, *59*, 697-723, 2001.

Kundu, P.K., and R.E. Thomson, Inertial oscillations due to a moving front, *J. Phys. Oceanogr.*, *15*, 1076-1084, 1985.

Kunze, E., Near-inertial propagation in geostrophic shear, *J. Phys. Oceanogr.*, *15*, 544-565, 1985.

Kunze, E., and T.B. Sanford, Observations of near-inertial waves in a front, *J. Phys. Oceanogr.*, *14*, 566-581, 1984.

Kunze, E., and T.B. Sanford, Near-inertial wave interaction with mean flow and bottom topography near Caryn Seamount, *J. Phys. Oceanogr.*, *16*, 109-120, 1986.

Kunze, E., R.W. Schmitt, and J.M. Toole, The energy balance in a warm-core ring's near-inertial critical layer, *J. Phys. Oceanogr.*, *25*, 942-957, 1995.

Lee, D.K., and P.P. Niiler, The inertial chimney: The near-inertial energy drainage from the ocean surface to the deep layer, *J. Geophys. Res.*, *103*, 7579-7591, 1998.

Lueck, R., and T. Osborn, The dissipation of kinetic energy in a warm-core ring, *J. Geophys. Res.*, *91*, 803-818,1986.

Mied, R.P., C.Y. Shen, C.L. Trump, and G.J. Lindemann, Internal-inertial waves in a Sargasso Sea front, *J. Phys. Oceanogr.*, *16*, 1751-1762, 1986.

Mooers, C.N.K., Several effects of a baroclinic current on the cross-stream propagation of inertial-internal waves, *Geophys. Fluid Dyn.*, *6*, 245-275.

Munk, W., and C. Wunsch, Abyssal recipes II, Energetics of tidal and wind mixing, *Deep Sea Res., Part I, 45*, 1977-2010, 1998.

Nagasawa, M., Y. Niwa, and T. Hibiya, Spatial and temporal distribution of the wind-induced internal wave energy available for deep water mixing in the North Pacific, *J. Geophys. Res.*, *105*, 13,933-13,943, 2000.

Stevens, D.P., On open boundary conditions for three dimensional primitive equation ocean circulation models, *Geophys. Astrophys. Fluid Dyn.*, *51*, 103-133, 1990.

van Meurs, P., Interactions between near-inertial mixed layer currents and the mesoscale: The importance of spatial variabilities in the vorticity field, *J. Phys. Oceanogr.*, *28*, 1363-1388, 1998.

Wunsch, C., The work done by the wind on the oceanic general circulation, *J. Phys. Oceanogr.*, *28*, 2332-2340, 1998.

Young, W.R., and M. Ben Jelloul, Propagation of near-inertial oscillations through a geostrophic flow, *J. Mar. Res.*, *55*, 735-766, 1997.

Zhai, X., R.J. Greatbatch, and J. Sheng, Advective spreading of storm-induced inertial

oscillations in a model of the northwest Atlantic Ocean, *Geophys. Res. Lett.*, *31*, L14315, doi:10.1029/2004GL020084, 2004.

Zhai, X., R.J. Greatbatch, and J. Zhao, Enhanced vertical propagation of storm-induced near-inertial energy in an eddying ocean channel model, *Geophys. Res. Lett.*, *32*, L18602, doi:10.1029/2005GL023643, 2005a.

Zhai, X., R.J. Greatbatch, and J. Sheng, Doppler-shifted inertial oscillations on a β plane, *J. Phys. Oceanogr.*, *35*, 1480-1488, 2005b.

Zhai, X., and R.J. Greatbatch, Wind work in a model of the northwest Atlantic Ocean, *Geophys. Res. Lett.*, *34*, L04606, doi:10.1029/2006GL028907, 2007.

Chapter 7

The Possible Role in the Ocean Heat Budget of Eddy-Induced Mixing due to Air-Sea Interaction[1]

The traditional point of view is that in the ocean, the meridional transport of heat is achieved by the wind-driven and meridional overturning circulations. Here we point out the fundamental role played by ocean mixing processes. We argue that mixing (i.e. water mass conversion) associated with eddies, especially in the surface mixed layer, can play an important role in closing the ocean heat budget. Our results argue that the lateral mixing applied at the surface of ocean/climate models should be playing an important role in the heat balance of these models, indicating the need for physically-based parameterizations to represent this mixing.

[1]**Citation:** Greatbatch, R. J., X. Zhai, C. Eden, and D. Olbers The possible role in the ocean heat budget of eddy-induced mixing due to air-sea interaction, *Geophys. Res. Lett.*, *34*, L07604, doi:10.1029/2007GL029533, 2007.

7.1 Introduction

The earth exhibits a net radiative gain of heat from the sun in the tropics and middle latitudes, but a net loss in higher latitudes. The earth's fluid envelope is therefore required to redistribute heat from low to high latitudes in order to maintain balance (*Gill* (1982)). The ocean is believed to play an important role in this process and the traditional picture is that ocean heat transport is achieved by the circulation (e.g. *Bryan* (1991)). In the North Atlantic, it is thought the meridional overturning circulation dominates (*Hall and Bryden* (1982), *Roemmich and Wunsch* (1985)), with warm water flowing northward in the upper part of the water column and colder water returning southward at depth, giving a net northward transport of heat when integrating over the depth of the water column (*Bryan* (1962)). Recently *Boccaletti et al.* (2005) have pointed out that the shallow wind-driven overturning cells also contribute to this process. Here we present an alternative point of view and emphasise the fundamental role played by mixing processes in the ocean heat budget. The necessary mixing can arise either from interaction with the atmosphere in the surface mixed layer or from interior mixing. Estimates of the diapycnal diffusivity in the interior of the ocean (*Ledwell et al.* (1993)) are of the order 10^{-5} m^2 s^{-1}, and we argue that this level of mixing is insufficient to close the heat budget (see Sections 2 and 3). Although more enhanced mixing has been found over rough topography, e.g. *Ledwell et al.* (2000), this mixing takes place at too great a depth to affect the heat budget for the top 1 km or so of the ocean where the thermocline is located - see Figure 7.1. Mixing inferred from water mass transformation theory (e.g. *Speer* (1997)) also supports the small values found in the ocean interior. Eddies, on the other hand, are known to play an important role in shaping the large-scale ocean circulation, especially in the Southern Ocean (*Danabasoglu et al.* (1994), *Rintoul et al.* (2001)), but it has not been clear what role the eddies play in the overall heat balance. Early work suggested that eddies do not have a fundamental role to play (*Drijfhout* (1994), *Bryan* (1996)). In this letter, we combine a new theory (*Eden et al.* (2007a)) with observed data to argue, by contrast, that the redistribution of heat by eddies plays a fundamental role. Our approach is an extension of that taken by *Radko and Marshall* (2004) (see also *Marshall et al.* (2002), *Hughes* (2002)), except that rather than

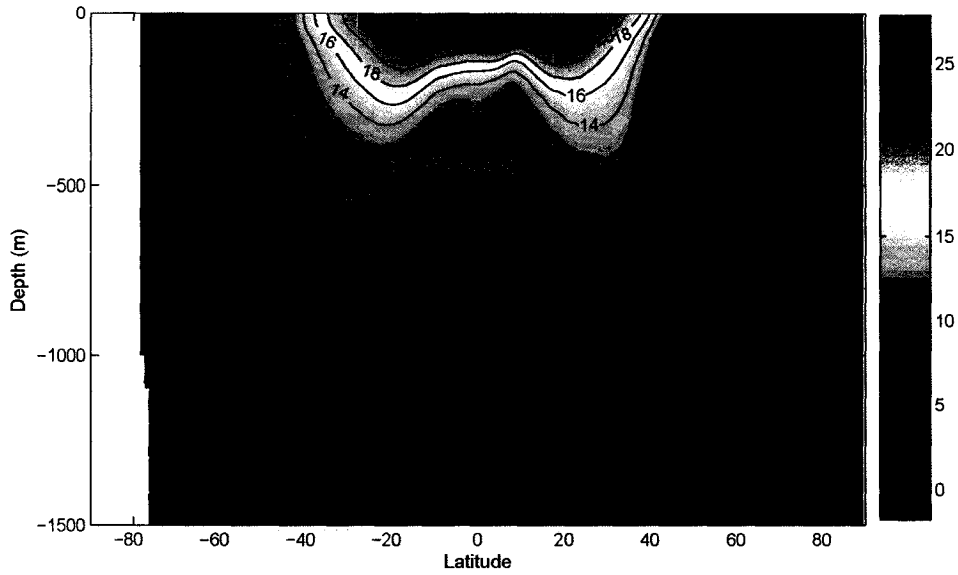

Figure 7.1: Zonally-averaged potential temperature (°C) from the World Ocean Atlas 1998 (*Levitus et al.* (1998)).

analyse an idealised model set-up (as in *Radko and Marshall* (2004)), we apply the theory to ocean data. Importantly, we emphasise the role played by the surface mixed layer and, in particular, we stress a new aspect, namely the importance of mixing that arises from the damping of the sea surface temperature (SST) variance by the surface heat flux (see *Zhai and Greatbatch* (2006b)). Our ultimate aim is to show the importance of heat transfer associated with mesoscale eddies in the 3-D heat budget of the ocean. However, to do this we must begin with the heat budget for the ocean after zonal averaging (Section 2), for which standing eddies are important, and then make use of the zonally-averaged case to extend the theory to three-dimensions in Section 3, where the importance of mesoscale eddies is revealed.

7.2 Zonal Averaging

The potential temperature in the ocean reveals a bowl-shaped warm water pool, with isentropes outcropping at the surface on both sides of the equator (see Figure 7.1). The question

arises as to how the heat input at the surface at low latitudes escapes from the "bowl" and redistributes itself poleward in order to maintain balance. Following zonal averaging at fixed height and time averaging to ensure a statistically steady state, the equation for the ocean heat budget, following *Eden et al.* (2007a), can be written as:

$$\nabla \cdot (L_w \mathbf{u}^* \bar{T}) = \bar{Q} + \nabla \cdot (L_w K_e \nabla \bar{T}) \tag{7.1}$$

where the overbar denotes the averaging operator (zonal and time averaging), T is the potential temperature, $\mathbf{u}^*$ is the "residual mean" velocity (sum of the Eulerian mean and eddy-induced transport velocity; see *Gent et al.* (1995)), L_w is the zonal width of the ocean as a function of latitude and depth, and Q is the total, instantaneous thermal forcing associated, in the surface mixed layer, with the surface heat flux and 3-D turbulence (e.g. leading to entrainment/detrainment etc..) and, in the ocean interior, with microstructure mixing (*Gregg et al.* (2003)). K_e is the thermal diffusivity associated with the departures from the average. *Eden et al.* (2007a) give the following expression for K_e in statistical steady conditions:

$$K_e |\nabla \bar{T}|^2 = -\overline{Q'T'} + \text{higher order terms} \tag{7.2}$$

where the prime denotes the departure from the zonal/time average. Noting that, in statistically steady state, the equation for the eddy variance, $\overline{\phi} = \frac{\overline{T'^2}}{2}$ is

$$\nabla \cdot (L_w \overline{\mathbf{u}\phi}) = L_w[-\overline{\mathbf{u}'T'} \cdot \nabla \bar{T} + \overline{Q'T'}] \tag{7.3}$$

we see that the second term on the right hand side of (7.2) is the same as the $\overline{Q'T'}$ term in (7.3). The higher order terms in (7.2) arise from rotational fluxes used to absorb the advective flux of variance on the left hand side of (7.3) - see *Eden et al.* (2007a) for details - leaving a balance between production, $-\overline{\mathbf{u}'T'} \cdot \nabla \bar{T}$ and dissipation $\overline{Q'T'}$ to determine K_e. Furthermore, the $\overline{Q'T'}$ term is negative when variance is being dissipated, in which case K_e emerges as a positive coefficient. (Equations (7.7) and (7.11) provide a simple illustration of K_e when Q is a Newtonian relaxation term.) We now integrate (7.1) over the area (called the "control volume") between the sea surface and a mean isentrope, say $\bar{T} = T_o$.

The residual mean advection term integrates to zero and plays no role in the subsequent balance (using the fact that the normal component of $\mathbf{u}^*$ is zero at the sea surface and $\nabla \cdot (L_w \mathbf{u}^*) = 0$). Physically, this is because the potential temperature of the water that is advected into the control volume (the "bowl" of warm water) is the same as the potential temperature of the water that is advected out. The resulting balance (see *Walin* (1982)) is therefore

$$\int_s L_w (K_s + K_e) \frac{\partial \bar{T}}{\partial n} ds = \frac{\mathcal{H}}{\rho c_p} \tag{7.4}$$

where the integral is taken along the isentrope $\bar{T} = T_o$, n is the coordinate perpendicular to the isentrope, and ρ, c_p are the density of sea water and the specific heat at constant pressure, respectively. In (7.4) we have split the thermal forcing Q into two parts: K_s is the diffusivity associated with the 3-D mixing, in particular microstructure mixing in the ocean interior, and $\mathcal{H}$ is the net input of heat at the surface. (7.4) says that the heat input at the surface, $\mathcal{H}$, is balanced by mixing processes, either the 3-D mixing associated with K_s acting on the mean gradient, or mixing (i.e. water mass conversion) associated with the eddies, i.e. the departures from the averaging operator, and represented by K_e. A striking feature of equation (7.4) is that there is no appearance of the mean circulation associated with the wind-driven or meridional overturning circulations, as in the traditional view of ocean heat transport (*Bryan* (1991)). Furthermore, the essential role played by mixing processes for balancing the heat budget is made very clear.

Let us now consider the heat budget for the control volume that is bounded by the sea surface and the 14 °C isentrope. The 14 °C isentrope spans roughly the range of latitudes between about 40°N and 40°S (see Figure 7.1). We use the ocean heat transport estimates shown in Figure 3 of *Wunsch* (2005) (see also *Ganachaud and Wunsch* (2000)) to estimate the total surface heat input to our control volume to be about 1 PW (1 PW is 10^{15} W). It should be noted that the error bars are such that the actual net heat input could be as much as 2 PW or as little as 0 PW (as implied by *Grist and Josey* (2003)). Taking $\mathcal{H} = 1$ PW, $K_s = 10^{-5}$ m^2 s^{-1}, as found from microstructure measurements (*Ledwell et al.* (1993)), and $\partial \bar{T}/\partial n = 2$ °C/100 m from Figure 7.1, the integrated contribution from the small-scale mixing is almost one order of magnitude too small to balance the surface heat input.

Furthermore, since the 14 °C isentrope is confined to the upper few hundred meters of the water column, we cannot invoke enhanced mixing over rough topography (e.g., *Ledwell et al.* (2000)) to close the budget. It is also easy to show that 3-D mixing in the surface mixed layer associated with the K_s term is insufficient to balance the budget, since the horizontal length scales associated with 3-D mixing are too small to provide the necessary diffusivity. It follows that if one accepts that the net heat input is 1 PW, then to close the heat budget one needs to invoke the K_e term; that is, mixing associated with the departures from the zonal/time average. Diagnoses using the 16 °C or 18 °C isentropes add support to this conclusion because as the water mass contained in our control volume warms, one can be increasingly confident that the lower bound on the estimate for the net heat input, $\mathcal{H}$, is significantly above 0 PW.

K_e is the diffusivity arising from the departures from the zonal/time average and we can use the theory of *Eden et al.* (2007a) to estimate its value. In our case, these departures are associated with mesoscale eddies, standing eddies arising from the departure of the time-mean flow from the zonal average, and also the seasonal cycle. The latter is a complication we expect to be associated with a negative diffusive effect. This is because when the variations in the thermal forcing, Q', are seasonal only, the temperature and forcing changes, T', Q' respectively, are positively correlated, as can be seen from Figure 1 in *Gill and Turner* (1976), leading to a negative diffusivity using (7.2). (Note that the effect of seasonal forcing is to enhance the equator to pole temperature contrast, rather than reduce it.) Clearly, however, if K_e is negative, then the heat budget given by (7.4) cannot be balanced. It follows that either the mesoscale eddies or the standing eddies dominate. A second complication is the role of along-isopycnal mixing. Since potential temperature is the dominant influence on density over most of the ocean (at least the subtropical regions we are interested in), we neglect this effect in what follows. On the other hand, the eddy-induced diffusivity, whether this comes from the mesoscale or the standing eddies, will be important in the surface mixed layer where the ocean has contact with the atmosphere (e.g. *Tandon and Garrett* (1996)). We therefore assume that K_e is dominated by the contribution

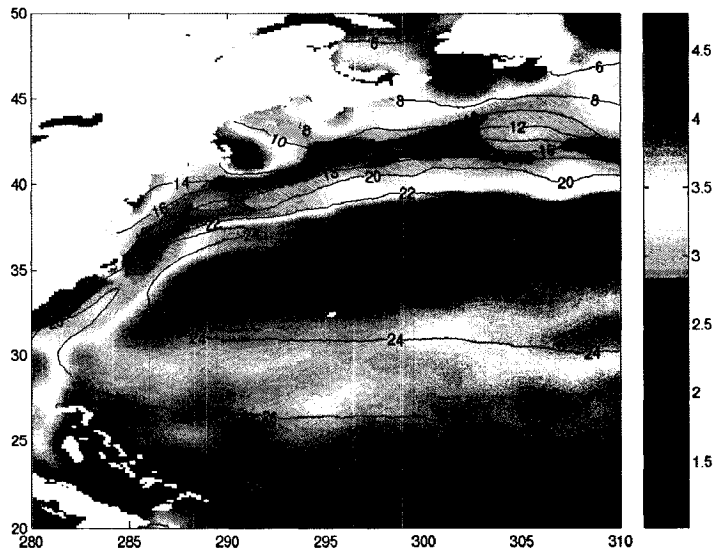

Figure 7.2: Surface eddy diffusivity in units of $m^2\ s^{-1}$ estimated from equation (7.11) using *Haney* (1971) and color coded using a log scale to base 10, together with the mean SST (^oC) contours.

from the surface mixed layer and write equation (7.4) as

$$2\bar{h}K_e L_w \frac{\partial \bar{T}}{\partial y} \approx \frac{\mathcal{H}}{\rho c_p} \tag{7.5}$$

where we have neglected the contribution from 3-D mixing (the K_s term) and $\bar{h}$ represents a mean mixed layer depth. To estimate $\bar{h}$, we use the climatology of the mixed layer depth taken from the U.S. Naval Research Laboratory (*Kara et al.* (2003)), which is on the order of 100 m at 40^o latitude in both hemispheres. The diffusivity, K_e, diagnosed from equation (7.4) using $\mathcal{H} = 1$ PW is then close to $10^4\ m^2\ s^{-1}$.

The eddy diffusivity in the surface mixed layer can also be estimated directly from theory. We neglect the higher order terms (which can be shown to be small) in equation (7.2) to obtain

$$K_e|\bar{T}_y|^2 \approx -\overline{Q'T'} \tag{7.6}$$

where $\bar{T}_y$ is the meridional gradient of the zonally-averaged sea surface temperature (SST),

and T' is the departure of the SST from the zonal/time average. To illustrate the importance of the damping of SST variance by the atmosphere, we replace Q' by a simple restoring boundary condition, in which SST is relaxed back to climatology on a time scale $(1/\gamma)$ of 50 days (*Haney* (1971)), so that

$$K_e|\bar{T}_y|^2 \approx \gamma\overline{T'^2}. \tag{7.7}$$

In order to estimate $\overline{T'^2}$, we use climatological SST data from the World Ocean Atlas and compute the variance based on the departures from the zonal average. Taking $|\bar{T}_y|$ from Figure 7.1, then gives values of K_e that are significantly larger than 10^4 m^2 s^{-1}, indicating that sufficient mixing is indeed available in the surface mixed layer to close the ocean heat budget in the zonally-averaged case. It should be noted that this estimate for the diffusivity is based on the standing eddies only (analogous to the gyre component in *Bryan* (1962)) and does not include the effect of mesoscale eddies. In the 3-D case discussed next, only transient eddies are available to provide the necessary mixing.

7.3 The 3-D Case

Following *Eden et al.* (2007a), the equation for the ocean heat budget in the 3-D case in statistically steady state is:

$$\nabla \cdot (\mathbf{u}^*\bar{T}) = \bar{Q} + \nabla \cdot (K_e \nabla \bar{T}) \tag{7.8}$$

where here the overbar represents a time mean carried out in height coordinates, ∇ is now a 3-D operator, $\mathbf{u}^*$ the 3-D "residual mean" velocity (different from $\mathbf{u}^*$ in equation (7.1)) and K_e is the diffusivity in the 3-D case given in statistical steady conditions by

$$K_e|\nabla\bar{T}|^2 = -\overline{Q'T'} + \text{higher order terms.} \tag{7.9}$$

As before, the diffusivity, K_e, in general will be positive (in association with the irreversible removal of variance). Taking the control volume to be the volume of water between the sea surface and a mean isentropic surface, say $T = T_0$, it follows, exactly as before, that the

residual advection term drops out from the heat balance, again revealing the central role played by mixing processes, and leaving the balance

$$\int_A (K_s + K_e)\frac{\partial \bar{T}}{\partial n} dA = \frac{\mathcal{H}}{\rho c_p} \tag{7.10}$$

where the integral is now taken over the isentropic surface $T = T_o$, and $\mathcal{H}$ is the total surface heat input to the control volume. We now use the surface heat flux climatology of *Grist and Josey* (2003) to adjust our estimate for the net surface heat input in the zonally-averaged case in order to account for the fact that the 14 ^{o}C isentrope does not outcrop exactly along the latitude lines 40^{o}N and 40^{o}S. This adjustment turns out to be negligibly small compared to 1 PW, and we therefore take 1 PW as our estimate for the net surface heat input to our control volume in the 3-D case, as for the zonally-averaged case (while recognising the uncertainty in this estimate noted above). It follows, as before, that we expect mixing associated with K_e to play an important role in balancing the ocean heat budget. Since in the 3-D case we are using time averaging, the influence of standing eddies is excluded, and mesoscale eddies are the only mechanism available to provide the mixing necessary to overwhelm the negative diffusive effect from the seasonal cycle. We now concentrate, as before, on the mixing arising due to interaction between mesoscale eddies and the surface heat flux. To provide some indication of the likely magnitude of K_e in this case, we replace Q' in (7.9) by a simple restoring boundary condition, as before, and neglect the higher order terms to obtain

$$K_e |\nabla \bar{T}|^2 \approx \gamma \overline{T'^2}. \tag{7.11}$$

where $\overline{T'^2}$ is the SST variance which, here, is derived from satellite data. The SST data have a resolution of 14 km and are taken from the NOAA Satellite and Information Service website (for details, see http://www.class.noaa.gov/nsaa/products). The selected dataset spans the period from August 2001 to September 2005, and is available once a week. The SST anomaly (T') is computed after the seasonal cycle has been removed and is the departure from the mean over the whole study period. Figure 7.2 shows the estimated diffusivity

for the Gulf Stream region computed from the variance using (7.11) and a time scale of 50 days for $1/\gamma$. In the region of the Gulf Stream front, the estimated values are of order 1000 $m^2\ s^{-1}$ due to the strong mean gradient in SST there. Much larger values (of order 10^4 $m^2\ s^{-1}$) are found immediately south of the Gulf Stream where the mean gradient is relatively weak. We note that the net northward flux of heat computed by multiplying the local value of the diffusivity by the local value of the gradient of mean SST is comparable to the flux implied by (7.5), suggesting that as in the zonally-averaged case, there is sufficient mixing available in the surface mixed layer due to air-sea interaction processes alone to balance the 3-D ocean heat budget. Clearly future work should focus on estimating the diffusivity K_e globally and on developing parameterizations for K_e for use in climate models. A first attempt at estimating the diffusivity from satellite data has been given by *Zhai and Greatbatch* (2006a) and agrees quite well in both amplitude and spatial structure with the estimate in Figure 7.2. *Zhai and Greatbatch* (2006b) have estimated the eddy-induced surface diffusivity from a model and also find a similar pattern and amplitude. In particular, the large values, approaching 10^4 $m^2\ s^{-1}$ immediately south of the Gulf Stream, are feature of diagnoses from both observations (*Zhai and Greatbatch* (2006a)) and models (*Zhai and Greatbatch* (2006b)) and appear to be robust.

7.4 Conclusions

Equations (7.4) and (7.10) show that mixing (either 3-D mixing acting on the mean gradient or eddy-induced mixing) is the essential ingredient for closing the ocean heat budget. Our results have emphasised the diabatic aspect of the mesoscale eddies (*Tandon and Garrett* (1996)). In particular, we argue that eddy-induced mixing in the surface mixed layer due to air-sea interaction processes can play an important role in closing the ocean heat budget (illustrated schematically in Figure 7.3). It follows that the lateral mixing applied near the surface in non-eddy resolving ocean/climate models may be required to play an important role in closing the ocean heat budget in these models, and that careful attention should be given to how the lateral mixing in these models is specified. The current practise is

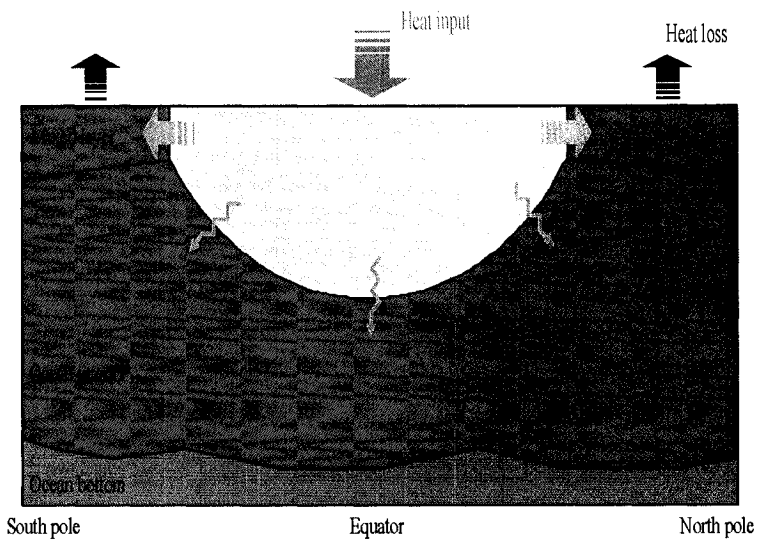

Figure 7.3: Schematic illustrating the oceanic heat budget.

often to simply replace the isopycnal mixing in the ocean interior by horizontal mixing at the surface, with no guarantee that the magnitude and spatial structure of the mixing is appropriate. There is clearly a need to develop physically-based parameterizations for eddy-induced mixing, especially in the surface mixed layer. The important role played by the damping of SST variance by the surface heat flux has been emphasised in this paper, an effect that has been illustrated using a model by *Zhai and Greatbatch* (2006b).

Acknowledgments

This work has been funded by NSERC and CFCAS in support of the Canadian CLIVAR Research Network. XZ thanks Ms Jie Ou for help with the plotting. Comments from several anonymous reviewers and Dr. Meric Srokosz led to improvements in the manuscript.

Bibliography

Boccaletti G., R. Ferrari, A. Adcroft, D. Ferreira, and J. Marshall (2005), The vertical structure of ocean heat transport, *Geophys. Res. Lett.*, *32*, L10603, doi:10.1029/2005GL022474.

Bryan, K. (1962), Measurements of meridional heat transport by ocean currents, *J. Geophys. Res.*, *67*, 3403-3414.

Bryan, K. (1991), Poleward heat transport in the ocean. A review of a hierarchy of models of increasing resolution, *Tellus*, *43*, 104-115.

Bryan, K. (1996), The role of mesoscale eddies in the poleward transport of heat by the oceans: a review, *Physca D*, *98*, 249-257.

Danabasoglu, G., J.C. McWilliams, and P. Gent (1994), The role of mesoscale tracer transport in the global ocean circulation, *Science*, *264*, 1123-1126.

Drijfhout, S. (1994), Heat transport by mesoscale eddies in an ocean circulation model, *J. Phys. Oceanogr.*, *24*, 353-369.

Eden, C., R.J. Greatbatch, and D. Olbers (2007), Interpreting eddy fluxes, *J. Phys. Oceanogr.*, *37*, 1282-1296.

Ganachaud, A., and C. Wunsch (2000), Improved estimates of global ocean circulation, heat transport and mixing from hydrological data, *Nature*, *408*, 453-457.

Gent, P., J. Willebrand, T.J. McDougall, and J.C. McWilliams (1995), Parameterizing eddy-induced tracer transports in ocean circulation models, *J. Phys. Oceanogr.*, *25*, 463-474.

Gill. A.E. (1982), *Atmosphere-Ocean Dynamics*, Academic Press, 662pp.

Gill, A.E., and J.S. Turner (1976), A comparison of seasonal thermocline models with observations, *Deep-Sea Res.*, *23*, 391-401.

Gregg, M.C., T.B. Sanford, and D.P. Winkel (2003), Reduced mixing from the breaking of internal waves in equatorial waters, *Nature*, *422*, 513-515.

Grist, J.P., and S.A. Josey (2003), Inverse analysis adjustment of the SOC air-sea flux climatology using ocean heat transport constraints, *J. Climate*, *16*, 3274-3295.

Hall, M.M., and H.L. Bryden (1982), Direct estimates and mechanisms of ocean heat transport, *Deep-Sea Res.*, *29*, 339-359.

Haney, R.L. (1971), Surface thermal boundary condition for ocean circulation models, *J. Phys. Oceanogr.*, *1*, 241-248.

Hughes, C.W. (2002), An extra dimension to mixing, *Nature*, *416*, 136-139.

Kara, A.B., P.A. Rochford, and H.E. Hurlburt (2003), Mixed layer depth variability over the global ocean, *J. Geophys. Res.*, *108*, doi:10.1029/2000JC000736.

Ledwell, J.R., A.J. Watson, and C.S. Law (1993), Evidence for slow mixing across the pycnocline from an open ocean tracer release experiment, *Nature*, *364*, 701-703.

Ledwell, J.R. et al. (2000), Evidence for enhanced mixing over rough topography in the abyssal ocean, *Nature*, *403*, 179-182.

Levitus, S. et al. (1998), *World Ocean Database 1998*, *Vol. 1*, U.S. Government Printing Office, Washington, DC.

Marshall, J.C., H. Jones, R. Karsten, and R. Wardle (2002), Can eddies set ocean stratification? *J. Phys. Oceanogr.*, *32*, 26-38.

Radko, T., and J.C. Marshall (2004), Eddy-induced diapycnal fluxes and their role in the maintenance of the thermocline, *J. Phys. Oceanogr.*, *34*, 372-383.

Rintoul, S., C. Hughes, and D. Olbers, (2001), *Ocean Circulation and Climate: Observing and Modeling the Global Ocean* (eds Siedler, G., Church, C., and Gould, J.), 271-302, Academic Press.

Roemmich, D., and C. Wunsch (1985), Two transatlantic sections: meridional circulation and heat flux in the subtropical North Atlantic Ocean, *Deep-Sea Res.*, *32*, 619-664.

Speer, K.G. (1997), A note on average cross-isopycnal mixing in the North Atlantic ocean, *Deep-Sea Res.*, *44*, 1981-1990.

Tandon, A., and C. Garrett (1996), On a recent parameterization of mesoscale eddies, *J. Phys. Oceanogr.*, *26*, 406-411.

Walin, G. (1982), On the relation between sea-surface heat flow and thermal circulation in the ocean, *Tellus*, *34*, 187-195.

Wunsch, C. (2002), What is the thermohaline circulation? *Science*, *298*, 1179-1181.

Wunsch, C. (2005), The total meridional heat flux and its oceanic and atmosphic patitions, *J. Climate*, *18*, 4374-4380.

Zhai, X., and R.J. Greatbatch (2006a), Inferring the eddy diffusivity for heat in the surface mixed layer using satellite data, *Geophys. Res. Lett.*, *33*, L24607, doi:10.1029/2006GL027875.

Zhai, X., and R.J. Greatbatch (2006b), The surface eddy diffusivity for heat in a model of the northwest Atlantic Ocean, *Geophys. Res. Lett.*, *33*, L24611, doi:10.1029/2006GL028712.

Chapter 8

Inferring the Eddy-Induced Diffusivity for Heat in the Surface Mixed Layer Using Satellite Data[1]

The eddy-induced diffusivity for heat at the surface of the western North Atlantic Ocean is estimated using satellite altimetry and sea surface temperature data. A rotational eddy flux is removed from the total eddy flux following the ideas of Marshall and Shutts (1981). The resulting eddy-induced diffusivity shows considerable spatial variability with a value near 10^4 m^2 s^{-1} just to the south of the Gulf Stream and values in the range 1-2 $\times$ 10^3 m^2 s^{-1} within the Gulf Stream itself.

[1]**Citation:** Zhai, X., and R. J. Greatbatch, Inferring eddy-induced diffusivity for heat in the surface mixed layer using satellite data, *Geophys. Res. Lett.*, *33*, L24607, doi:10.1029/2006GL027875, 2006.

8.1 Introduction

Eddies play an important role in determining the large-scale ocean circulation and in tracer transport, and models used for climate studies and prediction must rely on their parameterization for some time into the future. Most climate models currently use the parameterization of *Gent and McWilliams* (1990) (hereafter GM) to mimic the flattening of isopycnals and the associated release of available potential energy due to baroclinic instability. The GM parameterization can be interpreted in terms of thickness diffusion on isopycnal surfaces, and several attempts have been made to diagnose the "thickness diffusivity" using output from eddy-resolving models, e.g., *Rix and Willebrand* (1996), *Bryan et al.* (1999), *Peterson and Greatbatch* (2001) and *Eden et al.* (2007b). The GM parameterization is an adiabatic parameterization; that is, the effect of the eddies is assumed to be completely adiabatic, and the resulting eddy flux is entirely advective in character. However, while adiabaticity is a good approximation in the ocean interior, where the observed level of diapycnal mixing is low, the adiabatic assumption breaks down in the surface mixed layer, where the ocean has contact with the atmosphere (*Tandon and Garrett* (1996), *Treguier et al.* (1997)). In fact, although baroclinic instability is itself an intrinsically adiabatic process, eddies generated by baroclinic (or any other) instability processes are strongly modified in the surface mixed layer by interaction with the atmosphere, leading to irreversible diapycnal mixing (i.e. water mass conversion) associated with eddies. It has also been proposed that diapycnal eddy fluxes play a significant role in the maintenance of the thermocline and in balancing the ocean heat budget (e.g., *Marshall et al.* (2002), *Karsten et al.* (2002), *Hughes* (2002), *Radko and Marshall* (2004), *Greatbatch et al.* (2007)).

Recently *Eden et al.* (2007a) have provided a comprehensive theory in which the eddy heat (or tracer) flux is decomposed in a consistent fashion into advective (i.e., adiabatic), diffusive (i.e., diabatic) and rotational parts, extending the theory of *Marshall and Shutts* (1981) to the completely general situation. In *Eden et al.* (2007a), the diabatic effect of eddies is associated with the irreversible removal of variance at small scale (or the local growth of variance in non-statistically steady situations). Here, we combine satellite-derived geostrophic velocity anomalies with sea surface temperature (SST) data to estimate

the eddy-induced diffusivity for heat in the surface mixed layer of the western North Atlantic, based on the theory of *Eden et al.* (2007a). It should be noted that the mixing we are talking about here is strictly diabatic and differs from the thickness mixing/diffusivities associated with the adiabatic eddy tracer transport, and also from the mixing length approach for estimating diffusivities taken by *Holloway* (1986), *Keffer and Holloway* (1988) and *Stammer* (1998). In particular, following *Eden et al.* (2007a), we emphasise the dissipation of the eddy variance of SST through interaction with the tmosphere.

8.2 Data Description

The SST data has a resolution of 14 km and is taken from the NOAA Satellite and Information Service website. It is a composite gridded-image derived from 8-km resolution SST observations. SST is defined as the sea surface temperature tuned to in situ data at 1 meter depth (for details, see http://www.class.noaa.gov/nsaa/products). The geostrophic velocity anomaly (GVA) is derived from maps of sea surface height anomalies optimally interpolated to a $1/3^o$ Mercator grid and downloaded from the CLS Space Oceanography Division website (*LeTraon et al.* (1998)). The study area is the western Atlantic Ocean, extending from 20°N to 50°N and from 280°W to 310°W. The reason for choosing this region is that the ocean here is subject to strong eddy activity. To overcome the mismatch between GVA and SST data grids, we linearly interpolate the GVA data to the SST data grids. The interpolated GVA fields preserve very well the features in the original GVA data. The selected datasets span the period from August 2001 to September 2005, with a temporal resolution of a week (two times a week in the later years). Both the GVA ($\mathbf{u}'$) and the SST (T') anomalies are computed after the seasonal cycle has been removed[2] and are departures from the mean over the whole study period. The surface temperature flux associated with the Ekman flow anomalies is about two orders of magnitude smaller than the eddy temperature flux associated with the GVA, and is neglected in this study. It should be noted that in the following computations, both the mean temperature gradient and the

[2]The seasonal cycle is obtained by fitting a sine curve with annual period to the data.

final diffusivities are spatially smoothed over a scale of 100 kms.

8.3 Results

By considering the full hierarchy of tracer moments, *Eden et al.* (2007a) express the eddy-induced diffusivity for heat, K_e, in quasi-steady state as

$$K_e|\nabla\bar{T}|^2 = -\overline{Q'T'} + \mathcal{D}(\overline{\phi_2 Q}) - \frac{1}{2}\mathcal{D}^2(\overline{\phi_3 Q}) + \frac{1}{3!}\mathcal{D}^3(\overline{\phi_4 Q}) + \cdots \tag{8.1}$$

where the operator $\mathcal{D}() = \nabla \cdot \left(\nabla\bar{T}|\nabla\bar{T}|^{-2}()\right)$, Q is the diabatic forcing and $\overline{\phi_n}$ are the moments of variance ($\overline{\phi_n} = \frac{\overline{T'^n}}{n}$) and T is here the SST. In the surface mixed layer, Q is controlled by the surface heat flux and entrainment. We begin by neglecting the higher order terms and use the balance

$$K_e|\nabla\bar{T}|^2 \approx -\overline{Q'T'}. \tag{8.2}$$

It is instructive to replace Q by a simple restoring boundary condition, as in *Haney* (1971), where SST is relaxed towards climatology on a time scale $(1/\gamma)$, so that

$$Q = -\gamma(T - T^*) \tag{8.3}$$

where T is the instantaneous SST and T^* is a specified restoring temperature. Substituting into (8.2), we obtain

$$K_e|\nabla\bar{T}|^2 \approx \gamma\overline{T'^2}. \tag{8.4}$$

It follows that in this simple case, the surface eddy diffusivity can be estimated from the variance of the SST ($\overline{T'^2}$) shown in Figure 8.1a. For simplicity, we begin by putting the time scale $1/\gamma$ equal to 100 days (the spatial distribution of this time scale is discussed later). The resulting diffusivity, K_e, is shown in Figure 8.1b. Large values of order 10^4 $m^2\ s^{-1}$ are found to the south of the Gulf Stream, where the mean temperature gradient is relatively weak, whereas smaller values are found in the Gulf Stream itself, where the

mean gradient is relatively strong, even though the variance (Figure 8.1a) is relatively large there.

Next we estimate the diffusivity using the eddy flux, $\overline{\mathbf{u}'T'}$. Following *Eden et al.* (2007a), the eddy flux can be decomposed as

$$\overline{\mathbf{u}'T'} = \nabla \times \theta + \mathbf{B} \times \nabla\bar{T} - K_e \nabla\bar{T} \tag{8.5}$$

where all the vectors and vector operators are three dimensional (3-D). $\nabla \times \theta$ serves as a rotational flux which drops out when the (3-D) divergence of the eddy flux is taken, and $\mathbf{B}$ is the vector streamfunction for the eddy-induced transport velocity. From (8.5) the eddy-induced diffusivity K_e is given by

$$K_e = -|\nabla\bar{T}|^{-2}(\overline{\mathbf{u}'T'} - \nabla \times \theta) \cdot \nabla\bar{T}. \tag{8.6}$$

We note that for a particular choice of rotational flux, θ, (8.6) and (8.1) are equivalent (see equation (43) in *Eden et al.* (2007a)). However, we begin by ignoring the rotational flux (i.e. put $\theta = 0$) and also assume that the vertical gradient of the mean temperature field is zero (i.e. that the surface layer is well mixed). Figure 8.2 shows the horizontal component of the raw eddy flux ($\overline{\mathbf{u}'T'}$) plotted together with the mean temperature. ("Raw" here means that no rotational flux has been removed.) The raw eddy flux shows considerable spatial variability, with large amplitude associated with the Gulf Stream, especially after it separates at Cape Hatteras, and a significant component along the mean temperature contours. The eddy-induced diffusivity, K_{raw}, is diagnosed using (8.6) from the raw eddy fluxes by putting $\theta = 0$, i.e.,

$$K_{raw} = -\frac{\overline{\mathbf{u}'T'} \cdot \nabla\bar{T}}{|\nabla\bar{T}|^2} \tag{8.7}$$

and is shown in Figure 8.3a. The raw eddy diffusivity is largely positive in the study area, indicating that the raw eddy flux is mostly down the mean temperature gradient, although some regions with negative diffusivity are found. The large-scale structure of K_{raw} reveals a pattern that is basically similar to K_e as derived using *Haney* (1971) (see Figure 8.1b),

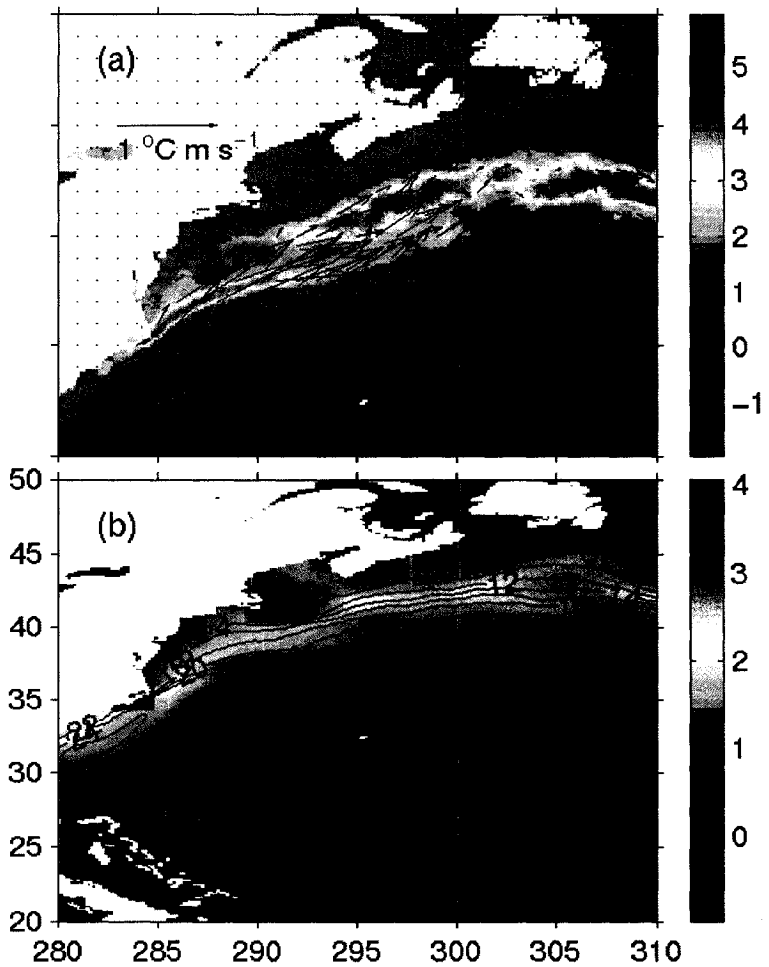

Figure 8.1: (a) Rotational eddy flux plotted together with the variance ($^oC^2$). (b) Surface eddy diffusivity K_e estimated using *Haney* (1971) and plotted on a log scale with base 10; unit: $m^2\ s^{-1}$. Black contours are the annual-mean SST (^{o}C).

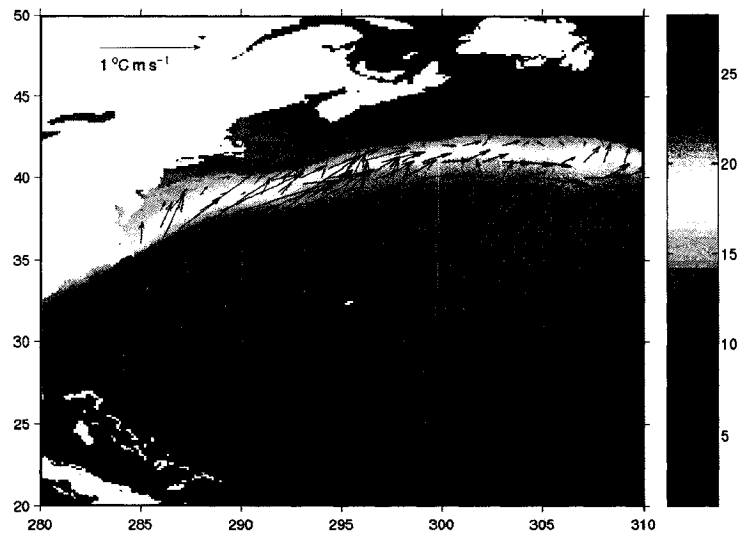

Figure 8.2: Surface eddy flux plotted together with the annual-mean SST; Unit: °C.

with maximum values on the order of 10^4 m^2 s^{-1} immediately to the south of the Gulf Stream and values typically between 1000 m^2 s^{-1} and 2000 m^2 s^{-1} in the region of the Gulf Stream front itself. It should be noted that the component of the eddy flux normal to the mean contours (not shown) is largest along the Gulf Stream front and is relatively small in magnitude in the subtropical ocean. The eddy diffusivity, on the other hand, is relatively large in the subtropical ocean because of the weak mean temperature gradient there.

Rotational fluxes can be large in amplitude, and it is important to realize their presence when interpreting eddy fluxes either in models (*Bryan et al.* (1999), *Jayne and Marotzke* (2002)) or observations (*Illari and Marshall* (1983)). Here, we note that in the decomposition of *Marshall and Shutts* (1981), the rotational flux circulates along the variance contours. We therefore follow *Eden et al.* (2007b) and estimate the horizontal component of the rotational flux using

$$(\overline{\mathbf{u}'T'})_R = -\frac{\overline{\mathbf{u}'T'} \cdot \nabla\bar{\phi}}{|\nabla\bar{\phi}|^2} \nabla\bar{\phi} \tag{8.8}$$

where $\nabla = (-\frac{\partial}{\partial y}, \frac{\partial}{\partial x})^T$ denotes anti-clockwise rotation of the gradient vector by 90°, as

in *Eden et al.* (2007b). We also tried using the more general approach for estimating rotational fluxes of *Medvedev and Greatbatch* (2004) and *Eden et al.* (2007a). However, the results are not very satisfactory, probably because the vertical flux of variance (which unfortunately is not available to us) is required to make (8.6) and (8.1) equivalent (see *Eden et al.* (2007a)). It is should also be noted that the two-dimensional divergence of $(\overline{\mathbf{u}'T'})_R$ is not, in general, zero. However, it is easy to add a vertical component to make the 3-D divergence zero, as required by the theory. The horizontal component of the rotational flux is plotted together with the variance in Figure 1a. (The spatial distribution of the variance in the study area is of its own special interest. The maximum variance is found in the Gulf Stream separation region at Cape Hatteras and there is a spatial shift of the region of high variance associated with the presence of the New England Seamounts near 39°N, 295°W.) We now estimate the eddy-induced diffusivity after removing the rotational flux using

$$K_e = -\frac{(\overline{\mathbf{u}'T'} - (\overline{\mathbf{u}'T'})_R) \cdot \nabla \bar{T}}{|\nabla \bar{T}|^2} \tag{8.9}$$

where $(\overline{\mathbf{u}'T'})_R$ is defined using equation (8.8). The resulting eddy diffusivity (Figure 8.3b) is similar in structure but generally reduced in amplitude compared to the raw diffusivity (Figure 8.3a), though there are still "hot spots" where the eddy diffusivity is close to 10^4 m^2 s^{-1}. Regions with negative diffusivity are also generally reduced compared to Figure 8.3a. Overall, the amplitude and large-scale structure of the eddy diffusivity diagnosed in this study compares reasonably well (but with differences in detail) with the diffusivity derived from surface drifter data by *Zurbas and Oh* (2004). The values we have diagnosed are also generally larger than previous estimates (e.g. *Stammer* (1998) - see also *Holloway* (1986) for the North Pacific and *Marshall et al.* (2006) for the Southern Ocean), the reason being the fundamental role played in our approach by the damping of SST variance by the surface heat flux (illustrated explicitly by equation (8.4)). However, in common with *Marshall et al.* (2006) our diagnosed diffusivities are smaller in the core of the Gulf Stream jet and enhanced on the equatorial flank (see *Marshall et al.* (2006) for a discussion of this issue).

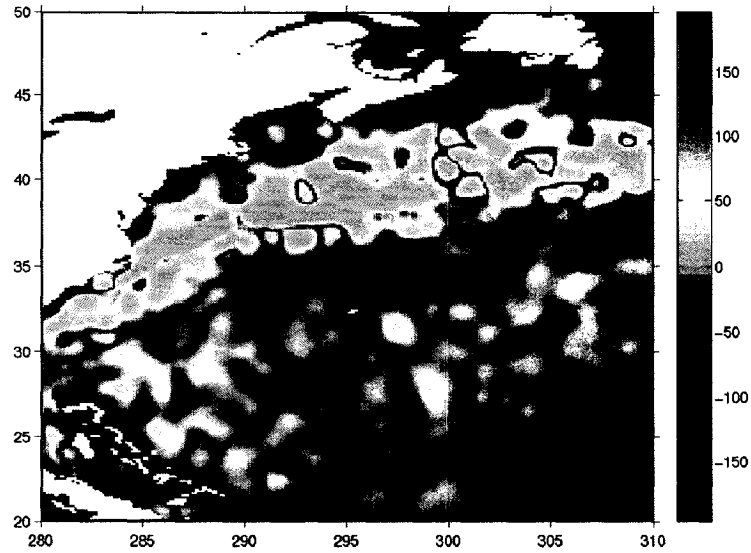

Figure 8.3: Estimated dissipation time scale $1/\gamma$. Unit: days

Finally, we can estimate the dissipation time scale by equating (8.4) and (8.7) to obtain

$$\gamma = -\frac{\overline{\mathbf{u}'T'} \cdot \nabla \bar{T}}{\overline{T'^2}}. \tag{8.10}$$

The (absolute) value of the time scale $1/\gamma$ is shown in Figure 8.4. The computed time scale shows considerable spatial variability, with shorter time scale along the Gulf Stream (about 20-30 days) and longer time scales (100 days and longer) in less eddy rich regions. This difference in time scales is broadly consistent with expectations from the theory of *Bretherton* (1982) (see also *Rahmstorf and Willebrand* (1995)) since surface thermal damping in the region of the Gulf Stream front is expected to be more rapid than in the relatively quiet gyre interior where SST is much more spatially homogeneous. It should be noted, however, that consistency with the above theory is not guaranteed because our estimate includes a contribution to the dissipation from entrainment whereas the *Bretherton* (1982) approach is based on the contribution from surface heat flux alone. The relatively short dissipation time scale along the Gulf Stream also explains why the estimated eddy diffusivity shown in Figure 8.1b is lower in amplitude than shown in Figure 8.3, since to produce Figure 8.1b

we used a spatially uniform time scale of 100 days.

8.4 Summary and Discussion

Observations in the atmosphere are easier to make and hence more abundent than those in the ocean, facilitating the diagnosis of eddy fluxes in the atmosphere (e.g., *Lau and Wallace* (1979), *Illari and Marshall* (1983)). Sea surface height and temperature seen from satellites provide a way to analyze the eddy properties near the surface of the ocean. *Greatbatch et al.* (2007) have argued that the eddy-induced diffusivity in the surface mixed layer plays a fundamental role in balancing the ocean heat budget and it is clearly important to provide estimates of this diffusivity from data, and to correctly parameterize the eddy-induced diffusivity in ocean/climate models. Here we have conducted a regional diagnosis of the eddy-induced diffusivity for heat by directly combining satellite-derived geostrophic velocity and sea surface temperature anomalies from the western North Atlantic Ocean. The eddy diffusivity derived from the raw fluxes (no rotational flux removed) exceeds 10^4 m^2 s^{-1} to the south of the Gulf Stream, where the mean temperature gradient is weak, and typically takes values in the range $1000 - 2000$ m^2 s^{-1} within the Gulf Stream itself. We estimated the rotational eddy flux based on the approach of *Marshall and Shutts* (1981). The resulting eddy diffusivity is reduced in amplitude but has the same basic spatial pattern as the diffusivity derived from the raw fluxes. It still has values close to 10^4 m^2 s^{-1} south of the Gulf Stream. A similar spatial structure and amplitude is also found when the eddy-induced diffusivity is derived using a simple restoring boundary condition (*Haney* (1971)) applied to SST. We can also estimate the dissipation time scale for SST anomalies in the study area by inversion using the eddy flux and the variance. The estimated time scale compares (perhaps surprisingly) favourably with the theory of *Bretherton* (1982), indicating a time of 20-30 days in the Gulf Stream itself and longer time scales (100 days and longer) in less eddy-rich regions. We note that values of the eddy diffusivity diagnosed here are generally larger than found in previous studies (e.g. *Holloway* (1986), *Stammer* (1998),

Marshall et al. (2006)) but are consistent with (i) *Zurbas and Oh* (2004), (ii) considerations based on the ocean heat budget (*Greatbatch et al.* (2007)), and (iii) estimates from a model (*Zhai and Greatbatch* (2006b)). We argue that ocean climate models should include a surface eddy diffusivity applied to temperature with a magnitude and spatial structure similar to that diagnosed here, while noting that a different eddy diffusivity is required in the salinity equation to reflect the different dissipation mechanism for surface salinity anomalies.

Acknowledgments

This work has been funded by NSERC and CFCAS in support of the Canadian CLIVAR Research Network. We thank Dr. John Marshall and an anonymous reviewer for useful comments. XZ thanks Ms Jie Ou for help with the data.

Bibliography

Bretherton, F.P. (1982), Ocean climate modeling, *Progress in Oceanogr.*, *11*, 93-129.

Bryan, K., J.K. Dukowicz, and R.D. Smith (1999), On the mixing coefficient in the parameterization of bolus velocity, *J. Phys. Oceanogr.*, *29*, 2442-2456.

Eden, C., R.J. Greatbatch, and D. Olbers (2007a), Interpreting eddy fluxes, *J. Phys. Oceanogr.*, *37*, 1282-1296.

Eden, C., R.J. Greatbatch, and J. Willebrand (2007b), A diagnosis of thickness fluxes in an eddy-resolving model, *J. Phys. Oceanogr.*, *37*, 727-742.

Gent, P.R., and J.C. McWilliams (1990), Isopycnal mixing in ocean circulation models, *J. Phys. Oceanogr.*, *20*, 150-155.

Greatbatch, R.J., X. Zhai, C. Eden, and D. Olbers (2007), The possible role in the ocean heat budget of eddy-induced mixing due to air-sea interaction, *Geophys. Res. Lett.*, *34*, L07604, doi:10.1029/2007GL029533.

Haney, R.L. (1971), Surface thermal boundary condition for ocean circulation models, *J.*

Phys. Oceanogr., *1*, 241-248.

Holloway, G. (1986), Estimation of oceanic eddy transports from satellite altimetry, *Nature*, *323*, 243-244.

Hughes, C.W. (2002), An extra dimension to mixing, *Nature*, *416*, 137-139.

Illari, L., and J.C. Marshall (1983), On the interpretation of eddy fluxes in a blocking episode, *J. Atmos. Sci.*, *40*, 2232-2242.

Jayne, S.R., and J. Marotzke (2002), The oceanic eddy heat transport, *J. Phys. Oceanogr.*, *32*, 3328-3345.

Karsten, R., H. Jones, and J.C. Marshall (2002), The role of eddy transfer in setting the stratification and transport of a Circumpolar Current, *J. Phys. Oceanogr.*, *32*, 39-54.

Keffer, T., and G. Holloway (1988), Estimating Southern Ocean eddy flux of heat and salt from satellite altimetry, *Nature*, *332*, 624-626.

Lau, N.C., and J.M. Wallace (1979), On the distribution of horizontal transports by transient eddies in the Northern Hemisphere wintering circulation, *J. Atmos. Sci.*, *36*, 1844-1861.

LeTraon, P.-Y., F. Nadal, and N. Ducet (1998), An improved mapping method of multi-satellite altimeter data, *J. Atmos. Oceanic Technol.*, *15*, 522-534.

Marshall, J.C., and G.J. Shutts, A note on rotational and divergent eddy fluxes, *J. Phys. Oceanogr.*, *11*, 1677-1680.

Marshall, J.C., H. Jones, R. Karsten, and R. Wardle (2002), Can eddies set ocean stratification? *J. Phys. Oceanogr.*, *32*, 26-38.

Marshall, J.C., E. Shuckburgh, H. Jones, and H. Hill (2006), Estimates and implications of surface eddy diffusivity in the Southern Ocean derived from tracer transport, *J. Phys. Oceanogr.*, *36*, 1806-1821.

Medvedev, A.S., and R.J. Greatbatch (2004), On advection and diffusion in the mesosphere and lower thermosphere: The role of rotational fluxes, *J. Geophys. Res.*, *109*, D07104, doi:10.1029/2003JD003931.

Peterson, K.A., and R.J. Greatbatch (2001), Vorticity fluxes in shallow water ocean models, *Atmos.-Ocean.*, *39*(1), 1-14.

Radko, T., and J.C. Marshall (2004), Eddy-induced diapycnal fluxes and their role in the maintenance of the thermocline, *J. Phys. Oceanogr.*, *34*, 372-383.

Rahmstorf, S., and J. Willebrand (1995), The role of temperature feedback in stabilizing the thermohaline circulation, *J. Phys. Oceanogr.*, *25*, 787-805.

Rix. N., and J. Willebrand (1996), Parameterization of mesoscale eddies as inferred from a high-resolution circulation model, *J. Phys. Oceanogr.*, *26*, 2281-2285.

Stammer, D. (1998), On eddy characteristics, eddy transports, and mean flow properties, *J. Phys. Oceanogr.*, *28*, 727-739.

Tandon, A., and C. Garrett (1996), On a recent parameterization of mesoscale eddies, *J. Phys. Oceanogr.*, *26*, 406-411.

Treguier, A.M., I.M. Held, and V.D. Larichev (1997), On the parameterization of quasi-geostrophic eddies in primitive equation models, *J. Phys. Oceanogr.*, *27*, 567-580.

Zhai, X., and R.J. Greatbatch (2006), The surface eddy diffusivity for heat in a model of the northwest Atlantic Ocean, *Geophys. Res. Lett.*, *33*, L24611, doi:10.1029/2006GL028712.

Zurbas, V., and I.M. Oh (2004) Drifer-derived maps of lateral diffusivity in the Pacific and Atlantic Oceans in relation to surface circulation patterns, *J. Geophys. Res.*, *109*, doi:10.1029/2003JC002241.

Chapter 9

The Surface Eddy Diffusivity for Heat in a Model of the Northwest Atlantic Ocean[1]

Eddies influence the surface heat budget both by modifying the surface heat flux and by the lateral transfer of heat within the surface mixed layer. It is shown that the presence of eddies modifies the surface heat flux in a model of the northwest Atlantic Ocean by more than 100 W m^{-2} over the Gulf Stream system. The diffusive effect of eddies is then illustrated by comparing two model runs, in the second of which the surface heat flux acts only on large spatial scales and interaction with the mesoscale eddies is suppressed. This second run exhibits finer-scale structure and tighter thermal fronts than in the fully interactive run. Finally, we estimate the surface eddy diffusivity associated with surface thermal damping from the fully interactive run. The estimated diffusivity takes large values (more than 10^3 m^2 s^{-1}) south of the Gulf Stream and smaller values elsewhere.

[1]**Citation:** Zhai, X., and R. J. Greatbatch, Surface eddy diffusivity for heat in a model of the northwest Atlantic Ocean, *Geophys. Res. Lett.*, *33*, L24611, doi:10.1029/2006GL028712, 2006.

9.1 Introduction

Most state-of-the-art ocean/climate models use the parameterization of *Gent and McWilliams* (1990) (hereafter GM) to parameterize the role of eddies in the large-scale ocean circulation and ocean tracer transport. The GM parameterization assumes the tracer fluxes associated with eddies are completely adiabatic. However, eddies can be strongly modified in the surface mixed layer by interaction with the atmosphere, leading to irreversible mixing and water mass conversion (e.g *Tandon and Garrett* (1996), *Treguier et al.* (1997), *Zhai and Greatbatch* (2006a)), with the implication that eddy fluxes also have a diffusive effect that needs to be taken into account in ocean/climate models. Furthermore, *Greatbatch et al.* (2007) have argued that the diffusive effect of eddies, especially in the surface mixed layer, plays an important role in the global ocean heat balance. However, studies of the diffusive effect of eddies are still quite limited, though some efforts have been spent on drifter data (e.g., *Zurbas and Oh* (2004)) and satellite products (e.g. *Holloway* (1986), *Stammer* (1998), *Marshall et al.* (2006), *Zhai and Greatbatch* (2006a), *Ferrari and McWilliams* (2007)). Furthermore, it is only recently (*Eden et al.* (2007a)) that a firm theoretical basis for decomposing eddy tracer fluxes into advective, diffusive and rotational parts has been proposed. *Eden et al.* (2007a) generalise the seminal work of *Marshall and Shutts* (1981) to show how, in the completely general situation of inhomogeneous turbulence, it is possible to choose the rotational component of the flux to ensure that the diffusive part is associated, in statistically steady state, with the irreversible removal of eddy variance, and hence can be expected to be down the mean tracer gradient. (Note that the rotational flux has no divergence and so does not appear explicitly in the mean tracer budget, but it does appear in the eddy variance equation. In the theory of *Eden et al.* (2007a), the rotational flux absorbs the advection of variance term that appears in the eddy variance equation). In this letter, we illustrate the diffusive effect of eddies by comparing two sets of model runs, in one of which the dissipation of eddy variance is suppressed by experimental design. We also use our model set-up to illustrate the large impact eddies can have on the surface heat loss to the atmosphere over the Gulf Stream system.

9.2 Ocean Model and Method

9.2.1 Model Description

The model is the same as the northwest Atlantic Ocean model described in *Greatbatch and Zhai* (2006). The model domain spans the area between 30°W and 76°W and 35°N and 66°N with a horizonal resolution at each latitude of $1/5^o$ in longitude. There are 31 unevenly spaced z levels. The model is initialized with January mean temperature and salinity fields and forced by 12-hourly NCEP wind stress starting at the beginning of January 1990. The net heat flux through the sea surface ($\mathcal{H}$) is the sum of the climatological surface heat flux ($\mathcal{H}_{clim}$), taken from *da Silva et al.* (1994), and a restoring term ($\mathcal{H}_{res}$) as in *Sheng et al.* (2001), where $\mathcal{H}_{res} = \beta(SST_{clim} - SST_{model})$. SST_{clim} is the interpolated monthly mean climatological sea surface temperature (SST), SST_{model} the modeled SST, and β is the coupling coefficient with value 31 W m^{-2} K^{-1}. The sea surface salinity in the model is restored to the monthly mean climatology on a time scale of 15 days, but different from *Greatbatch and Zhai* (2006), only on large spatial scales (larger than 300 km), in order to reduce the damping of the eddies due to the surface boundary condition (note that precipitation does not fall preferentially on the saltier eddies, nor does evaporation occur more frequently over the fresher eddies). Along the model's open boundaries, temperature and salinity are restored to climatology and the transport is specified as described by *Sheng et al.* (2001).

9.2.2 The Semi-Diagnostic Method (SDM)

All the model runs here use the SDM introduced in *Zhai et al.* (2004b). The SDM is a special case of the semi-prognostic method (*Greatbatch et al.* (2004)) in which, on large spatial scales, the density variable in the model's hydrostatic equation is an input density field (in our case computed from the climatological data of *Geshelin et al.* (1999)), whereas on the mesoscale, the corresponding density variable is the model density. In this way, the large scale flow in the model is strongly constrained, while the mesoscale is completely free, ensuring a rich eddy field. It is also possible to carry out a diagnostic model run

in which the specified density field in the model's hydrostatic equation is the same as the large scale density field seen by the semi-diagnostic model run. The difference between the semi-diagnostic model run and the corresponding diagnostic model run is then entirely attributable to the eddies present in the semi-diagnostic run but missing from the diagnostic model run. Readers are referred to *Zhai et al.* (2004b) for details. Use of the SDM eliminates the common problems of Gulf Stream overshooting and the disappearance of the northwest corner in models (*Willebrand et al.* (2001)). Here we carry out a companion diagnostic model run to show the role of eddies in driving the surface heat flux.

9.2.3 Experiment Design

Following *Eden et al.* (2007a), the equation for the time-averaged (annual mean) potential temperature, $\bar{T}$, is

$$\bar{T}_t + \nabla \cdot (\mathbf{u}^* \bar{T}) = \nabla \cdot (K_e \nabla \bar{T}) + \bar{Q}, \tag{9.1}$$

where an overbar denotes a time average, $\mathbf{u}^*$ is the "residual" velocity (the sum of the Eulerian mean and the eddy-induced transport velocity; see *Gent et al.* (1995)), Q is the total instantaneous thermal forcing, and K_e is the diabatic diffusivity associated with the eddies given, in statistically steady state, by

$$K_e |\nabla \bar{T}|^2 = -\overline{Q'T'} + \mathcal{D}(\overline{\phi_2 Q}) - \frac{1}{2}\mathcal{D}^2(\overline{\phi_3 Q}) + \frac{1}{3!}\mathcal{D}^3(\overline{\phi_4 Q}) + \cdots \tag{9.2}$$

In (9.2), the operator $\mathcal{D}() = \nabla \cdot \left(\nabla \bar{T} |\nabla \bar{T}|^{-2}()\right)$, ϕ_n is the higher order variance ($\phi_n = \frac{T'^n}{n}$), and a prime denotes departure from the time average. It should be noted that the advective effect of the eddies is contained entirely in $\mathbf{u}^*$, and that the diffusive effect of the eddies is contained in K_e, the diffusivity of heat associated with the eddies and which is the focus of our paper. The irreversible removal of eddy variance is associated with the $\overline{Q'T'}$ term in (9.2), while the higher order terms arise from the inhomogeneity of the eddy field and here are neglected. In this study, we consider only the contribution to the heating, Q, that is associated with the surface heat flux, $\mathcal{H}$ acting on the surface mixed layer (the relationship between Q and $\mathcal{H}$ is discussed further later). Neglecting the higher order terms, (9.1) then

reduces to

$$K_e|\nabla\bar{T}|^2 \approx -\overline{Q'T'} \tag{9.3}$$

where the term on the right hand side of the equation is now the dissipation of variance associated with the surface heat flux. Based on the theory, two semi-diagnostic model runs are conducted with the difference only in the way of dealing with the surface heat flux. The control run (TOTAL) is forced by the total net surface heat flux as described in the previous subsection. The SMOOTH run is forced by the same formulation for surface heat flux except that it acts only on large spatial scales, i.e.

$$\mathcal{H}_{SMOOTH} = \mathcal{H}_{clim} + \beta(SST_{clim} - \overline{SST_{model}}), \tag{9.4}$$

where the filter, denoted by an overbar, passes horizontal scales larger than a specified cut-off scale (here 300 km). By this design, the dissipation of mesoscale eddy variance by surface damping (associated with $-\overline{Q'T'}$ in (9.2)) is strongly suppressed in SMOOTH. A complication arises because of the seasonal cycle in the surface heat flux seen by the model. Using (9.2), the seasonal cycle generates a negative diffusivity because surface temperature and surface heat flux associated with seasonal forcing alone exhibit a positive correlation (see Figure 9.1 in *Gill and Turner* (1976)). In order to avoid contamination from the seasonal cycle in our estimate of the surface eddy diffusivity of heat, we therefore conduct another two model runs (TOTAL_m and SMOOTH_m) forced by the annual-mean forcing only.

9.3 Results

To begin, we first examine the net role of eddies in determining the annual mean surface heat flux in the model run with seasonally varying forcing (Figure 9.1). Since the climatological surface heat flux is identical in the semi-diagnostic and diagnostic models, the difference comes from the restoring term which relies on the difference between the modeled and climatological SST. The diagnostic model gains a lot of heat through the restoring

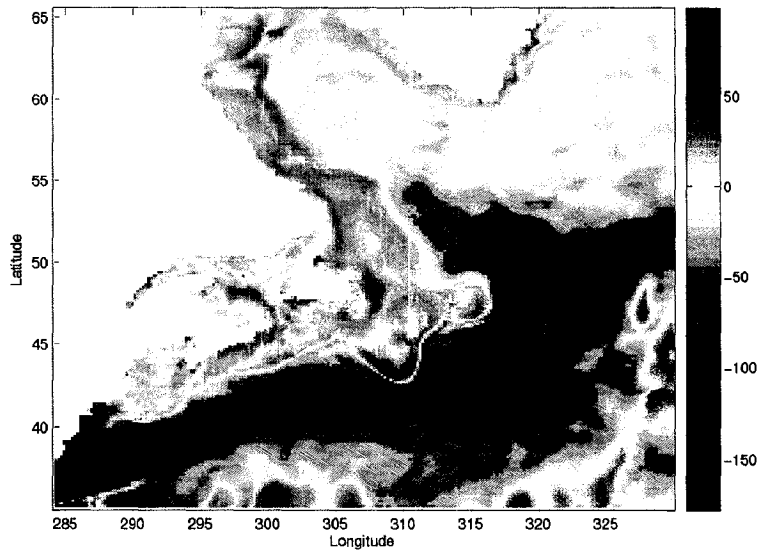

Figure 9.1: The difference, semi-diagnostic minus diagnostic, in the annual mean surface heat flux for Year 3; unit: W m^{-2}.

term over the Gulf Stream and in the northwest corner east of Newfoundland because its SST is colder than the climatology. The situation is greatly improved in the semi-diagnostic model. The main role of eddies in the semi-diagnostic model is to increase heat loss along the Gulf Stream and in the northwest corner (over 100 W m^{-2} on average). There is also a significant impact on the surface heat flux over the eastern Canadian shelf, including the Labrador Shelf. The impact of eddies arises partly from the changes to the mean flow discussed by *Zhai et al.* (2004b), but also from the diffusive effect we discuss next.

To illustrate the diffusive effect, we compare the model runs TOTAL and SMOOTH, also with seasonal forcing. Recall that the mesoscale thermal damping, which according to (9.2) determines the surface eddy diffusivity of heat, is suppressed by design in SMOOTH compared to TOTAL. Therefore, we expect to see tighter SST gradients in SMOOTH compared to TOTAL. The 3rd-year annual mean SSTs in the two model runs are shown in Figure 9.2. The large-scale patterns of SSTs are very much the same in the two models and compare well with the climatology (not shown). However, we do observe more fine-scale structure and tighter SST gradients in SMOOTH, e.g., the cold tongue associated with the

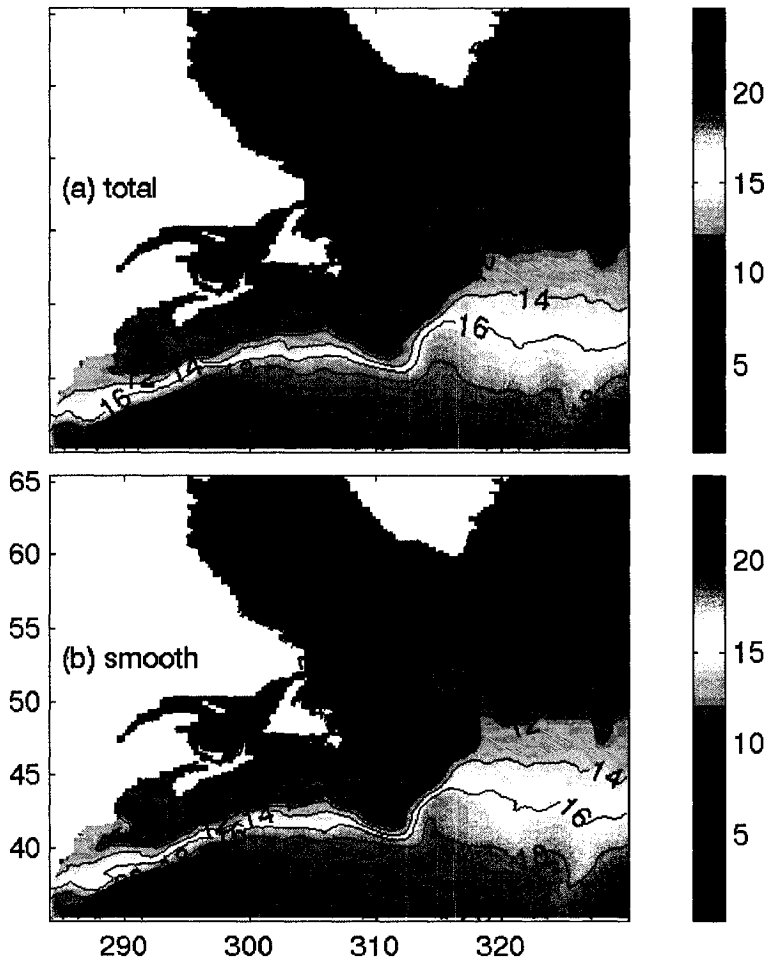

Figure 9.2: The 3rd-year annual mean SST in (a) TOTAL and (b) SMOOTH.

Labrador Current flowing along the shelf break around the Grand Banks of Newfoundland, and the thermal fronts south of Nova Scotia and southeast of Newfoundland associated with the Gulf Stream and the North Atlantic Current. The difference between Figures 9.2a and 9.2b is shown in Figure 9.3a and is consistent with the idea that an increased lateral diffusion of heat is operating in TOTAL compared to SMOOTH. It is particularly striking how in TOTAL, the SST is consistently colder (warmer) on the offshore, i.e. warm, (inshore, i.e. cold) side of the Gulf Stream, North Atlantic Current and Labrador Current, indicating that heat is being more efficiently exchanged across the thermal fronts associated with these currents in TOTAL than in SMOOTH. We recall that the only difference between TOTAL and SMOOTH is that in TOTAL, the surface heat flux acts on all spatial scales, and is an effective damping of the eddies, whereas in SMOOTH the surface heat flux acts only on large spatial scales, and is much less effective at damping the eddies. It follows that the more efficient heat exchange in TOTAL is a consequence of the thermal dissipation of the eddies that is present in TOTAL, but suppressed (by design) in SMOOTH. The model runs with the annual-mean forcing yield similar results (see Figure 9.3b) and we now turn to these runs to estimate the diffusivity using equation (9.3).

Since TOTAL_m has annual mean forcing, the fluctuations in surface heat flux, $\mathcal{H}'$, are associated entirely with the surface restoring term. It follows that $\overline{\mathcal{H}'T'} = -\beta\overline{T'^2}$, and indicates the damping of SST variance in the model by the surface heat flux. It is also clear that $\overline{\mathcal{H}'T'}$ is everywhere negative (as is indeed the case in the model - not shown) and is proportional to the SST variance, $\overline{T'^2}$. As can be seen from Figure 9.4a, $\overline{\mathcal{H}'T'}$ takes large values along the Gulf Stream and North Atlantic Current and in the northwest corner. There is also the indication of significant eddy activity further north, in the Labrador Sea. Figure 9.4b shows K_e estimated using equation (9.3) assuming that the surface heat flux acts on a uniform mixed layer depth of 50 m. K_e is positive everywhere, with values of more than 10^3 m^2 s^{-1} south of the Gulf Stream and North Atlantic Current, and in the range 10^2-10^3 m^2 s^{-1} within those current systems themselves. The pattern and magnitude of the estimated surface eddy diffusivity agree well with that inferred from satellite data by *Zhai and Greatbatch* (2006a). The rough similarity between the distributions of K_e and eddy

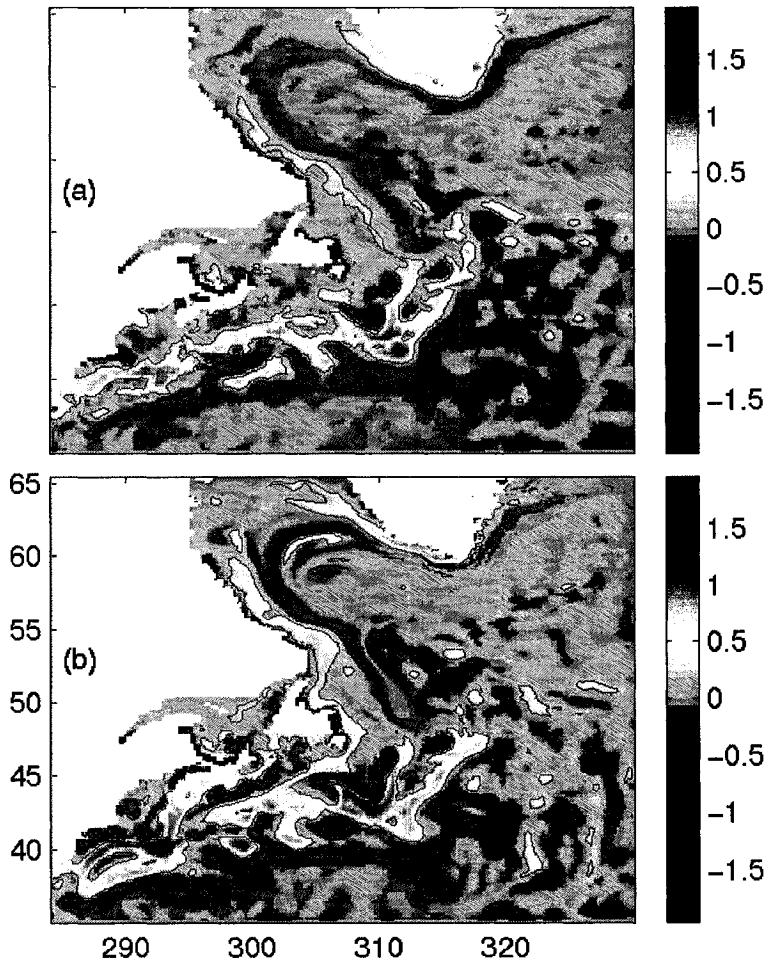

Figure 9.3: The difference (°C) in the 3rd-year annual mean SST (a) TOTAL minus SMOOTH, i.e., Figure 9.2a minus 9.2b; (b) TOTAL_m minus SMOOTH_m. Red and blue contours represent values of 0.25°C and -0.25°C, respectively.

kinetic energy (EKE) also provides some justification for using EKE as an index to parameterize the eddy diffusivity (*Stammer* (1998)), an issue to be explored further elsewhere. An attempt to take account of the contribution to the total heating Q from entrainment and mixing (i.e. taking account of the fact the mixed layer depth is, in reality, variable) shows a very noisy field, indicating that very much longer model runs (beyond our current capability) are required to obtain stable statistics on this contribution. Nevertheless, the general agreement between the diffusivity shown in Figure 4a, and the diffusivity derived from satellite data by *Zhai and Greatbatch* (2006a) (which includes the entrainment effect) suggests that our estimate using a fixed mixed layer depth is representative. Finally we note that since the diffusivity given by equations (9.2) and (9.3) clearly depends on the dissipation time scale, and since this dissipation time scale will be different for different tracers (e.g. salinity versus temperature), it is a prediction of the theory that the eddy-induced diffusivity will depend on the dissipation characteristics of individual tracers, and is therefore likely to be tracer dependent (see also the discussion in *Plumb and Mahlman* (1987)).

Finally, the contribution of the diffusive effect of the eddies to the eddy-induced surface heat flux shown in Figure 9.1 can be estimated by subtracting the surface heat flux in SMOOTH from that in TOTAL. Since the contribution comes entirely from the restoring term, the spatial pattern is the negative of that shown in Figure 9.3a, and is not shown here. We note, however, the amplitude reaches as much as 80 W m^{-2} locally near the Gulf Stream. It follows that while the diffusive effect does not dominate the difference shown in Figure 9.1, it can, locally, make a significant contribution and cannot be ignored.

9.4 Summary and Discussion

Most state-of-the-art ocean/climate models use the parameterization of *Gent and McWilliams* (1990) (hereafter GM) to mimic the role of eddies in determining the large-scale circulation and its tracer transport. The GM parameterization assumes the effect of eddies to be completely adiabatic since the mechanism generating the eddies (baroclinic instability) is an intrinsically adiabatic process. However, eddies generated by the instability process

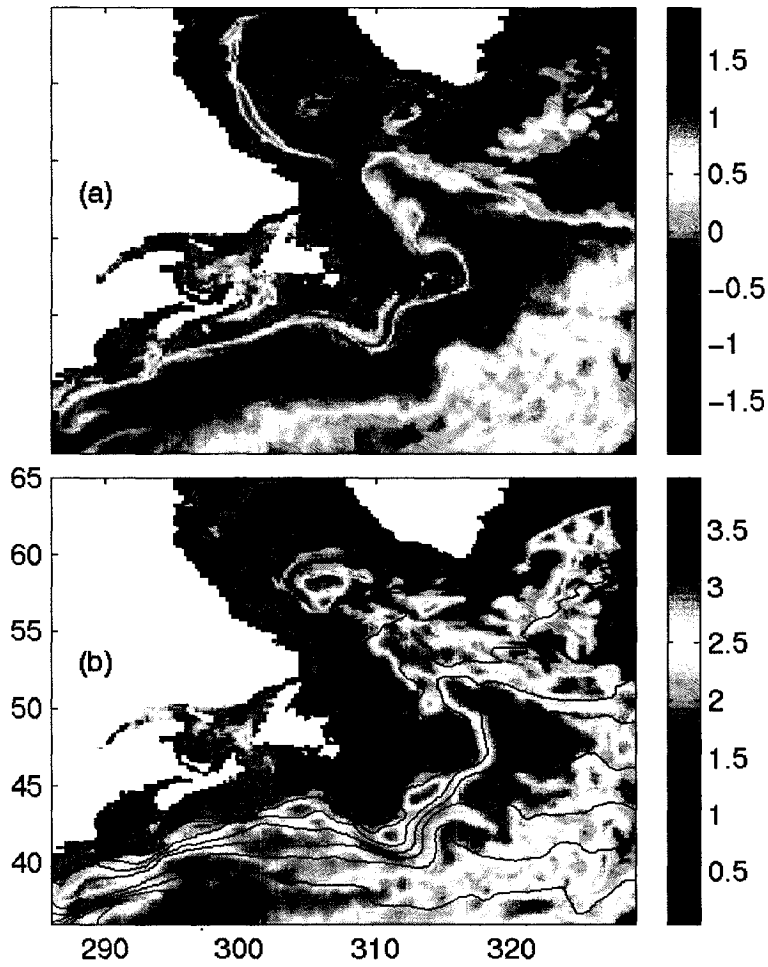

Figure 9.4: (a) $\overline{\mathcal{H}'T'}$ in TOTAL$_m$; unit: W m^{-2} ^{o}C. (b) The estimated surface eddy diffusivity for heat, K_e, plotted together with the annual-mean SST in TOTAL$_m$ (black contours) for a fixed mixed layer depth of 50 m; unit: m^2 s^{-1}. Both are plotted on a log scale with base 10.

can be strongly modified in the surface mixed layer by interaction with the atmosphere, or weakly modified in the ocean interior by microstructure mixing, leading to irreversible mixing and an associated eddy-induced diffusivity. Here we focus on the surface mixed layer, where the ocean has contact with the atmosphere, and the eddy-induced diffusivity is strongly enhanced by air-sea interaction processes (*Tandon and Garrett* (1996),*Treguier et al.* (1997)).

To illustrate the diffusive effect of eddies, we described two model runs, one (TOTAL) in which the surface heat flux is applied at all spatial scales, one (SMOOTH) in which the surface heat flux acts only on large spatial scales. By this design, damping of the eddy SST variance by the surface heat flux, and which basically sets the surface eddy diffusivity (see (9.2) and (9.3)), is present in TOTAL but suppressed in SMOOTH. As such, we observe finer-scale structures and tighter thermal fronts in SMOOTH, due to the suppression of the diffusive eddy effect. To avoid the complication associated with the seasonal cycle, the surface eddy diffusivity for heat, K_e, is estimated from a model run with annual mean forcing only. The estimated K_e is positive everywhere in the study area with values of more than 10^3 m^2 s^{-1} south of the Gulf Stream and North Atlantic Current, and in the range 10^2-10^3 m^2 s^{-1} within those current systems themselves. The coincidence of regions of high EKE and large K_e also provides some justification for using EKE as a proxy to parameterize K_e (e.g. *Stammer* (1998)). To diagnose K_e we did not take account of variations in mixed layer depth. An attempt to do so suggests that a very long model run would be required to obtain a stable estimate, and is beyond the scope of the present study. However, since our estimate has similar magnitude and spatial pattern to the diffusivity inferred from satellite data (*Zhai and Greatbatch* (2006a)), we believe our estimate to be realistic (a topic for future research). We recommend that coarse-resolution climate models, which do not resolve meso-scale eddies, need to incorporate the surface eddy diffusion effect, since this is almost certainly important to obtain the correct water mass formation rate (*Marshall* (1997)) and for balancing the heat budget (*Greatbatch et al.* (2007)). Finally we note that it is a prediction of the theory that the eddy-induced diffusivity for different tracers (e.g. salinity, carbon or CFC) depends on the dissipation characteristics for those

tracers and is unlikely to be the same as that for heat (see also *Plumb and Mahlman* (1987)), another topic to be explored in future work

Acknowledgments

This work has been funded by NSERC and CFCAS in support of The Canadian CLIVAR Research Network and RJG's Discovery Grant. We wish to thank Dr. Jinyu Sheng for his help with the model code. We also thank Dr. Stephen Griffies and one anonymous reviewer for critical comments that led to a significant improvement in the manuscript.

Bibliography

da Silva, A.M., C.C. Young, and S. Levitus (1994), *Atlas of Surface Marine Data 1994*, vol. 3, *Anomalies of Heat and Momentum Fluxes, NOAA Atlas NESDIS 8*, 413 pp., NOAA, Silver Spring, Md.

Eden, C., R.J. Greatbatch, and D. Olbers (2007), Interpreting eddy fluxes, *J. Phys. Oceanogr.*, *37*, 1282-1296.

Ferrari, R., and J.C. McWilliams (2007), Parameterization of eddy fluxes near oceanic boundaries, *Ocean Modelling*, submitted, 2007.

Gent, P.R., and J.C. McWilliams (1990), Isopycnal mixing in ocean circulation models, *J. Phys. Oceanogr.*, *20*, 150-155.

Gent, P., J. Willebrand, T.J. McDougall, and J.C. McWilliams (1995), Parameterizing eddy-induced tracer transports in ocean circulation models, *J. Phys. Oceanogr.*, *25*, 463-474.

Geshelin, Y., J. Sheng, and R.J. Greatbatch (1999), Monthly mean climatologies of temperature and salinity in the western North Atlantic, Canadian Data Report of Hydrography and Ocean Sciences, 153pp.

Gill, A.E., and J.S. Turner (1976), A comparison of seasonal thermocline models with observations, *Deep-Sea Res.*, *23*, 391-401.

Greatbatch, R.J., and X. Zhai (2006), Influence of assimilated eddies on the large-scale circulation in a model of the northwest Atlantic Ocean, *Geophys. Res. Lett.*, *33*, L02614, doi:10.1029/2005GL025139.

Greatbatch, R.J., et al. (2004), The semi-prognostic method, *Cont. Shelf Res.*, *24/18*, 2149-2165.

Greatbatch, R.J., X. Zhai, C. Eden, and D. Olbers (2007), The possible role in the ocean heat budget of eddy-induced mixing due to air-sea interaction, *Geophys. Res. Lett.*, *34*, L07604, doi:10.1029/2007GL029533.

Haney, R.L. (1971), Surface thermal boundary condition for ocean circulation models, *J. Phys. Oceanogr.*, *1*, 241-248.

Holloway, G. (1986), Estimation of oceanic eddy transports from satellite altimetry, *Nature*, *323*, 243-244.

Marshall, D.P. (1997), Subduction of water masses in an eddying ocean, *J. Marine Res.*, *55*, 201-222.

Marshall, J.C., and G.J. Shutts, A note on rotational and divergent eddy fluxes, *J. Phys. Oceanogr.*, *11*, 1677-1680.

Marshall, J.C., E. Shuckburgh, H. Jones, and H. Hill (2006), Estimates and implications of surface eddy diffusivity in the Southern Ocean derived from tracer transport, *J. Phys. Oceanogr.*, *36*, 1806-1821.

Plumb, R.A., and J.D. Mahlman (1987), The zonally averaged transport characteristics of the GFDL general circulation/transport model, *J. Atmos. Sci.*, *44*, 298-327.

Sheng, J., R.J. Greatbatch, and D.G. Wright (2001), Improving the utility of ocean circulation models through adjustment of the momentum balance, *J. Geophys. Res.*, *106*, 16,711-16,728.

Stammer, D. (1998), On eddy characteristics, eddy transports, and mean flow properties, *J. Phys. Oceanogr.*, *28*, 727-739.

Tandon, A., and C. Garrett (1996), On a recent parameterization of mesoscale eddies, *J. Phys. Oceanogr.*, *26*, 406-411.

Treguier, A.M., I.M. Held, and V.D. Larichev (1997), On the parameterization of quasi-geostrophic eddies in primitive equation models, *J. Phys. Oceanogr.*, *27*, 567-580.

Willebrand, J., et al. (2001), Circulation characteristics in three eddy-permitting models of the North Atlantic, *Prog. Oceanogr.*, *48*, 123-161.

Zhai, X., and R.J. Greatbatch (2006), Inferring the eddy diffusivity for heat in the surface mixed layer from satellite data, *Geophys. Res. Lett.*, *33*, L24607, doi:10.1029/2006GL027875.

Zhai, X., R.J. Greatbatch, and J. Sheng (2004), Diagnosing the role of eddies in driving the circulation of the northwest Atlantic Ocean, *Geophys. Res. Lett.*, *31*, L23304, doi:10.1029/2004GL021146.

urbas, V., and I.M. Oh (2004) Drifer-derived maps of lateral diffusivity in the Pacific and Atlantic Oceans in relation to surface circulation patterns, *J. Geophys. Res.*, *109*, doi:10.1029/2003JC002241.

Chapter 10

Diagnosing the Role of Eddies in Driving the Circulation of the Northwest Atlantic Ocean[1]

In this letter we present a variation of the recently proposed "semi-prognostic method" for use with ocean models. The new version has the advantage that model drift is effectively prevented, while at the same time the meso-scale eddy field is free to evolve. We use the method to probe the importance of the eddy-driven circulation in the northwest Atlantic Ocean. For the particular model we use here, it is shown that the eddies strongly reinforce the eastward Gulf Stream jet and the northern recirculation in the slope region, with over 50% of the total transport of this recirculation being directly eddy-driven. The eddies also play a role in setting the temperature and salinity properties of the "northwest corner" southeast of Newfoundland.

[1]**Citation:** Zhai, X., R. J. Greatbatch and J. Sheng, Diagnosing the role of eddies in driving the circulation of the Northwest Atlantic Ocean, *Geophys. Res. Lett.*, *31*, L23304, doi:10.1029/2004GL021146, 2004.

10.1 Introduction

Ocean models contain systematic errors because of both physical and numerical inaccuracies, e.g. in the parameterization of unresolved physical processes and numerical truncation error. Therefore ocean models almost inevitably show a tendency to drift away from climatology in multi-year simulations. For example, the Gulf Stream tends to separate too far to the north, and the recirculation in the slope region between the Gulf Stream and the eastern Canadian Shelf tends to disappear after several years of simulation (see, for example, *Willebrand et al.* (2001)). In addition, the model temperature can be in error by as much as 10^oC in the "northwest corner" region southeast of Newfoundland (*Lazier* (1994); see *Greatbatch et al.* (2004)). One way to correct for model drift is to follow *Sarmiento and Bryan* (1982) and add Newtonian relaxation terms to the tracer equations so as to "nudge" the model temperature and salinity towards climatology. This is equivalent to adding internal buoyancy sources and sinks to the model tracer equations, and is not consistent with the observation that the diapycnal mixing is weak in the ocean interior (e.g., *Gregg* (1989); *Ledwell et al.* (1998)). As an alternative, *Sheng et al.* (2001) proposed the "semi-prognostic" method, which has the advantage of adjusting the model momentum equations and leaving the tracer equations unchanged. *Eden et al.* (2004) modified the original semi-prognostic method and reduced some of the drawbacks of the original method (see *Greatbatch et al.* (2004) for an overview). However, the semi-prognostic method does not prevent model drift completely; instead, it just slows it down (as can be seen from Fig. 14 in *Sheng et al.* (2001)).

In this note, we explore a new technique based on the semi-prognostic method in which model drift is effectively prevented, while at the same time meso-scale eddies are allowed to evolve as freely as possible. We use the new method as a diagnostic tool to show the importance of eddies for driving the circulation in the northwest Atlantic Ocean. There is also a counterpart to this new method, which we point out but do not explore here.

10.2 Ocean Model and Methods

The model is the northwest Atlantic Ocean model developed by *Sheng et al.* (2001). The model domain spans the area between 30°W and 76°W and 35°N and 66°N with a horizontal resolution of about $1/3^o$ in longitude. There are 31 unevenly spaced z levels. The model is initialized with January mean temperature and salinity fields and forced by monthly mean COADS (Comprehensive Ocean-Atmosphere Data Set) surface heat flux and 12-hourly NCEP (National Center for Environmental Prediction) wind stress starting at the beginning of January 1990. The model sea surface salinity is restored to the monthly mean climatology on a time scale of 15 days. Along the model's open boundaries, temperature and salinity are restored to climatology and the transport is specified as described in *Sheng et al.* (2001).

10.2.1 The Semi-Prognostic Method

The semi-prognostic method was introduced originally by *Sheng et al.* (2001) for the purpose of adjusting a model to correct for systematic error. The adjustment is accomplished by replacing the density variable ρ in the model's hydrostatic equation by a linear combination of the model-computed density ρ_m and an input density ρ_c (in our case, climatological density):

$$\rho = \alpha\rho_m + (1-\alpha)\rho_c \equiv \rho_m + (1-\alpha)(\rho_c - \rho_m) \tag{10.1}$$

where $\rho_m = \rho(T, S, p_{ref})$ is the density calculated from the model potential temperature T and salinity S, p_{ref} is the reference pressure at the center of each z level, and α is the linear combination coefficient with a value between 0 and 1 (Sheng et al. chose 0.5). Using (10.1), the model's hydrostatic equation can be written as:

$$\frac{\partial p}{\partial z} = -g\rho_m - g(1-\alpha)(\rho_c - \rho_m), \tag{10.2}$$

where the second term on the right hand side of (10.2) appears as a correction term and g is the acceleration due to gravity. As noted by *Sheng et al.* (2001), the above procedure is

equivalent to adding a forcing term to the horizontal momentum equations. (It is important to note that the semi-prognostic method is adiabatic, leaving the temperature and salinity equations unconstrained). The presence of $\rho_m g$ in the correction term on the right hand side of (10.2) leads to damping of the meso-scale eddy field in the model. *Eden et al.* (2004) smoothed the second term to avoid this damping. However, the smoothing does not prevent the slow drift of the mean circulation.

10.2.2 The New (Semi-Diagnostic) Method

We start from a diagnostic model, where the density variable in the hydrostatic equation is specified from climatology ρ_c, i.e.,

$$\frac{\partial p}{\partial z} = -g\rho_c \tag{10.3}$$

We now rewrite (3) as

$$\frac{\partial p}{\partial z} = -g\rho_m - g(\rho_c - \rho_m) \tag{10.4}$$

(the same as (10.2) with $\alpha = 0$). The new method, which we call the "semi-diagnostic" method, uses equation (10.4) in the model, but with the correction term $g(\rho_c - \rho_m)$ spatially filtered so that

$$\frac{\partial p}{\partial z} = -g\rho_m - \overline{(\rho_c - \rho_m)}g. \tag{10.5}$$

Since $\overline{-g\rho_m - \overline{(\rho_c - \rho_m)}g} = -\overline{\rho_c}g$, it follows that the large-scale flow field of the model is strongly constrained by the large-scale climatology, $\overline{\rho_c}$. Meanwhile, the eddy field, which depends on the first term $-g\rho_m$, is free to develop. Furthermore, there is no coefficient α involved in equation (10.5), as in the semi-prognostic method, avoiding the difficulty of choosing its value. In the semi-prognostic method, the mean flow field of the model is not as strongly constrained as in the new method. This is because in Sheng et al.'s case, $\overline{-g\rho_m - 0.5(\rho_c - \rho_m)g} = -\overline{(0.5\rho_c + 0.5\rho_m)}g$, which means that only 50% of the mean flow field of the model is constrained by the climatology, and this is true for both the original semi-prognostic (*Sheng et al.* (2001)) and the smoothed semi-prognostic (*Eden et al.*

(2004)) methods. It is for this reason that the semi-prognostic method cannot completely prevent model drift.

We have applied the semi-diagnostic method to the northwest Atlantic Ocean model using spatial filtering on a scale of roughly 300 km (sufficient to release the eddy field) for the overbar in (10.5). The input density, ρ_c, is taken from the high resolution climatology of *Geshelin et al.* (1999). Use of the semi-diagnostic method maintains the northern recirculation, between the Gulf Stream and the eastern Canadian shelf (Fig. 10.1a), whereas in the semi-prognostic case ($\alpha = 0.5$, Fig. 10.1b) the recirculation gradually disappears. (It is important to note that the semi-prognostic model nevertheless shows much less drift than a prognostic model with the same model parameters (*Sheng et al.* (2001))). Furthermore, the semi-diagnostic case has been run for 10 years with no evidence of model drift. The transport carried by the recirculation is about 15-20 Sverdrups (Sv) in the semi-diagnostic model, and is comparable to estimates from observations (e.g., *Hogg et al.* (1986)). The semi-diagnostic method also generates a sharper front at the Gulf Stream than the semi-prognostic case (Figs. 10.1a,b).

It is not hard to imagine the counterpart to the semi-diagnostic method. This time we start with the hydrostatic equation seen by a prognostic model, i.e.,

$$\frac{\partial p}{\partial z} = -g\rho_m \equiv -g\rho_c - (\rho_m - \rho_c)g \tag{10.6}$$

rather than (3). By spatially filtering the second term, we get

$$\frac{\partial p}{\partial z} = -g\rho_c - \overline{(\rho_m - \rho_c)}g. \tag{10.7}$$

Since $\overline{-g\rho_c - \overline{(\rho_m - \rho_c)}g} = -\overline{\rho_m}g$, the large-scale flow field of the model is free to evolve in this case. Here we do not envisage the input density ρ_c as being the climatological density field, but rather high-frequency density fluctuations derived from altimetric data (e.g., *Cooper and Haines* (1996)) or from a higher resolution model (as in a nested modelling system; *Zhai et al.* (2004c)). We leave exploration of the counterpart method to a later paper.

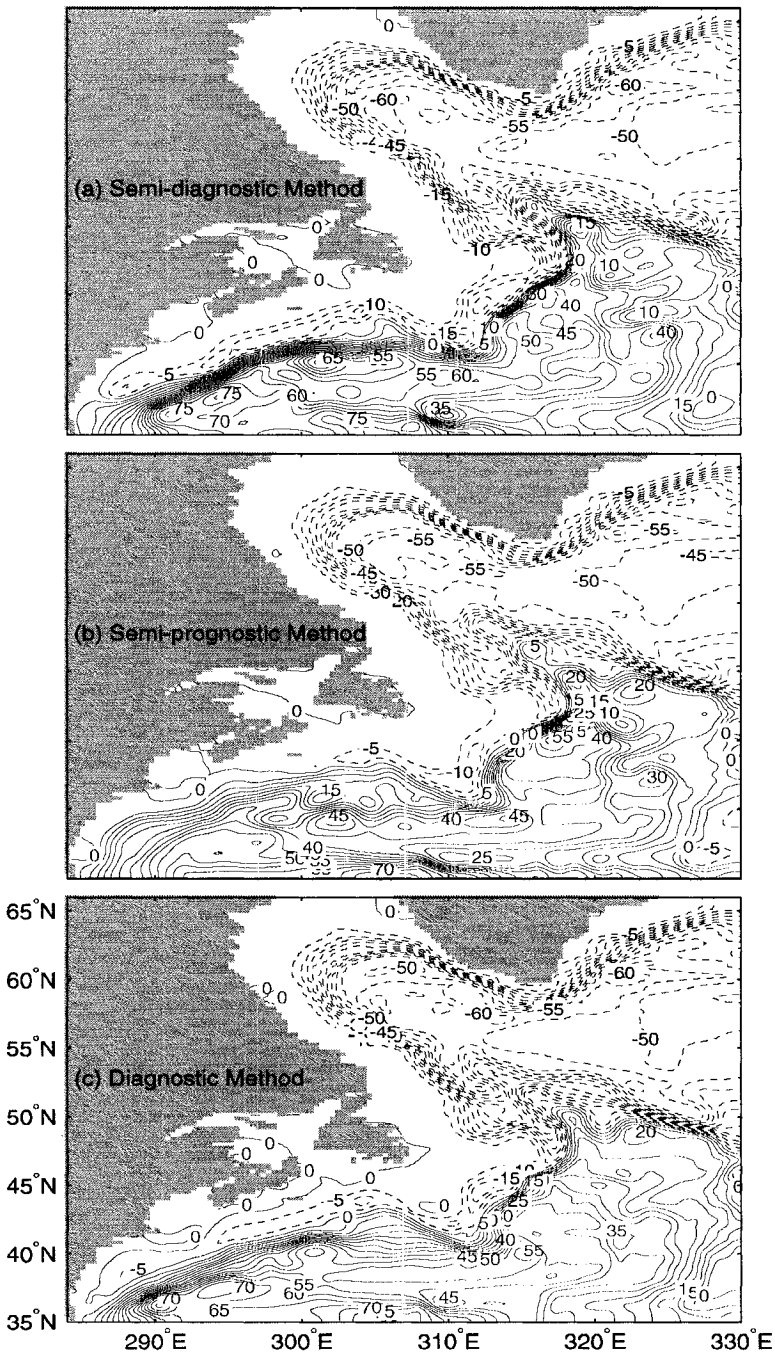

Figure 10.1: Model-calculated annual mean horizontal transport streamfunctions in year 3 using the (a) semi-diagnostic, (b) semi-prognostic and (c) diagnostic methods. The red contours represent anticyclonic transport and blue contours cyclonic transport. The contour interval is 5 Sv.

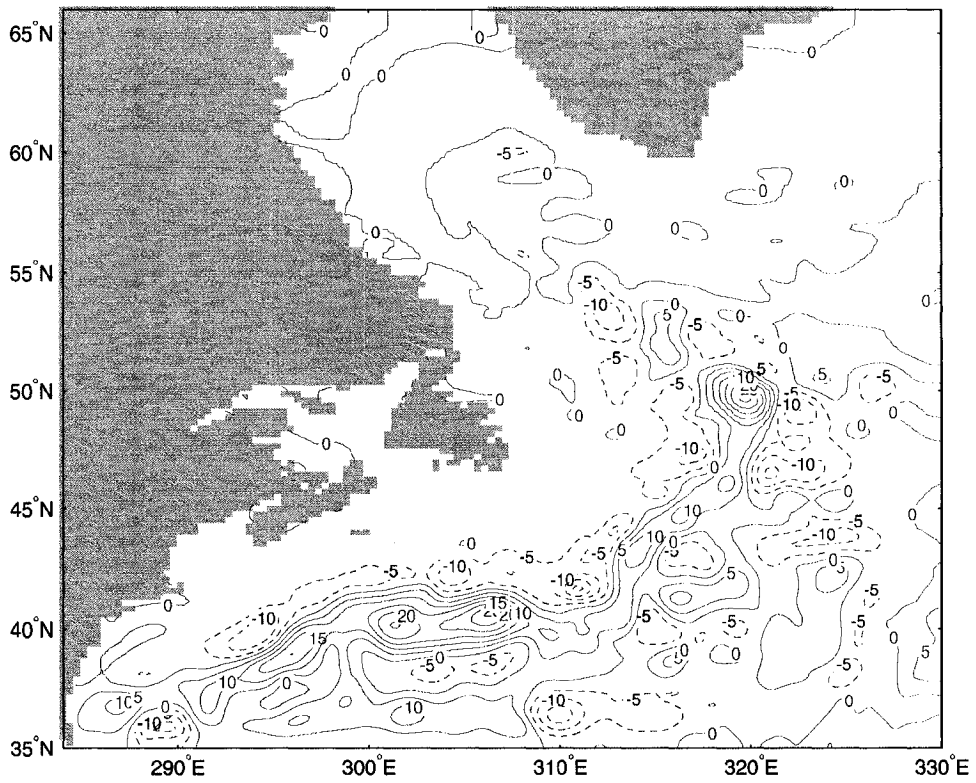

Figure 10.2: The eddy-driven annual mean transport (in Sv) computed by the model.

10.3 The Eddy-Driven Circulation in the Northwest Atlantic Ocean

It has long been known that eddies are an essential element in understanding the general circulation both in the atmosphere (e.g., *Philips* (1956)) and the ocean (e.g., *Gill et al.* (1974); *Holland and Lin* (1975)). For example, the northern recirculation gyre of the Gulf Stream is thought to be mostly driven by eddies (e.g., *Holland and Rhines* (1980); *Hogg* (1983)). However, since the flow is highly geostrophic, momentum balances are not a useful way for determining the importance of the eddies; the Reynolds stresses are usually one or two orders of magnitude smaller than the Coriolis and pressure gradient terms (*Holland and Lin* (1975)). As we now show, the semi-diagnostic method provides a simple way to determine the importance of eddies for driving the mean circulation.

At discussed in Section 2, use of the semi-diagnostic method can maintain the large-scale circulation, while at the same time leaving the mesoscale eddies free to develop. If the first term in (10.5) is filtered spatially in the same way as the second term, we get

$$\frac{\partial p}{\partial z} = -\overline{\rho_m} g - \overline{(\rho_c - \rho_m)} g = -\overline{\rho_c} g. \tag{10.8}$$

To understand the role of the eddies, an additional diagnostic model run is conducted using (10.8) in place of the model hydrostatic equation. In this calculation, there are no eddies (because the model is diagnostic) and temperature and salinity are treated as passive tracers. It follows that the difference between the annual mean fields in the semi-diagnostic and diagnostic cases is due entirely to the presence of mesoscale eddies in the semi-diagnostic case and their absense in the diagnostic case. In comparison with Fig. 10.1a, the annual mean transport streamfunction in the diagnostic case (Fig. 10.1c) shows a weaker front marking the Gulf Stream, and a weaker northern recirculation; only about 5-10 Sv annual transport (Fig. 10.1b) compared to 15-20 Sv in the semi-diagnostic case. The difference between Fig. 10.1a and Fig. 10.1c represents the eddy-driven circulation (Fig. 10.2). The eddies strengthen the Gulf Stream jet and the North Atlantic Current in the northwest corner (by 10-15 Sv) and strongly reinforce the northern recirculation gyre of the Gulf Stream by over 50%, and, correspondingly the outflow along the slope of the subpolar gyre (by 5-10 Sv) (Fig. 10.2). The eddies alter the mean flow by fluxing momentum up the gradient in the Gulf Stream and adjacent northwest corner region (*Holland and Lin* (1975), *Wardle and Marshall* (2000)). Our results also support the theoretical study by *Greatbatch* (1987).

The annual mean temperature field at 45 m depth in the semi-diagnostic and diagnostic model runs is shown in Fig. 10.3. It is important to note that the temperature field is not directly constrained in the model and has the same evolution equation as in an uncorrected model. In both cases, the model temperature field compares well with climatology. However, in the semi-diagnostic case, the northwest corner region is more strongly developed and penetrates more strongly into the Labrador Sea. The difference between these two model versions can be explained entirely by the presence of the eddies in the semi-diagnostic model, but not in the diagnostic model. It follows that the eddies play a role in

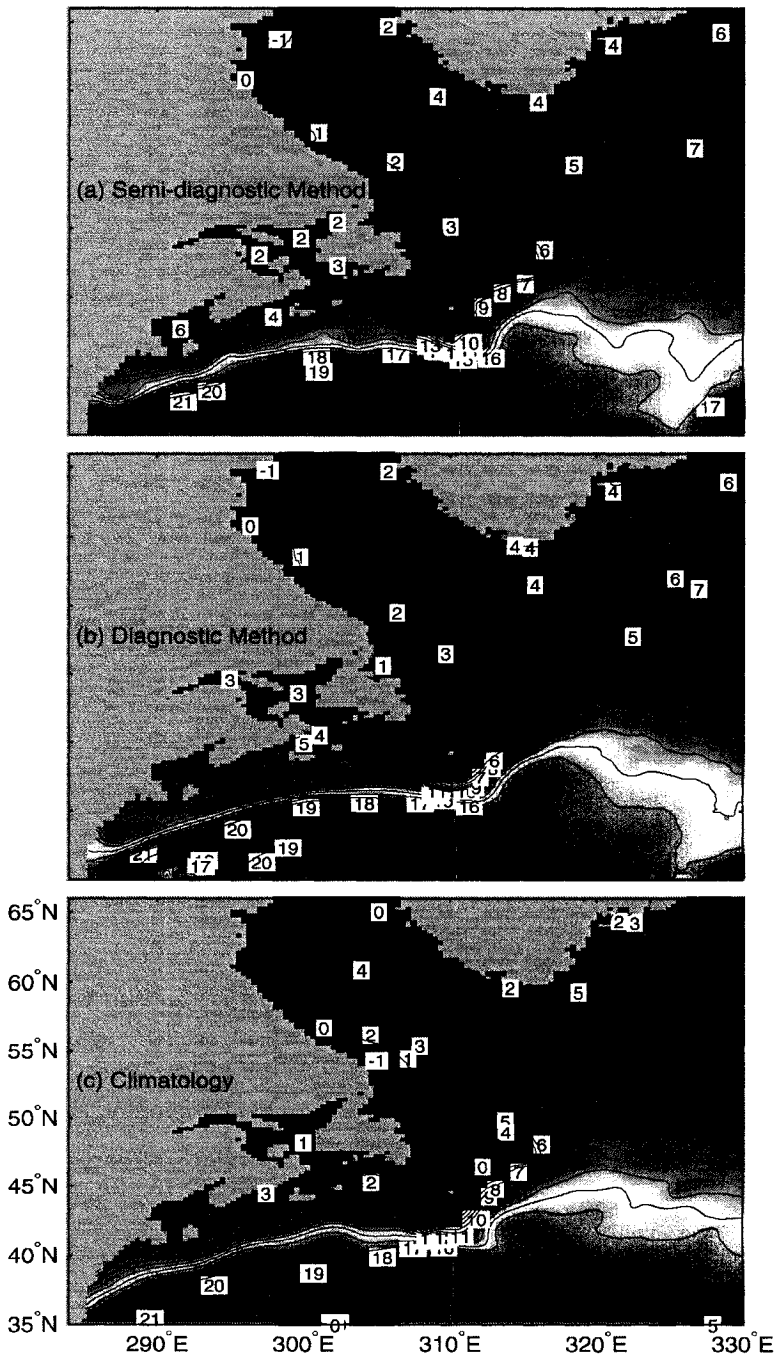

Figure 10.3: Model-calculated annual mean temperature at 45 m depth in year 3 using the (a) semi-diagnostic and (b) diagnostic methods. (c) Climatological temperature at the same depth. The contour interval is 2°C.

shaping the hydrographic structure of the northwest corner region in the semi-diagnostic case.

10.4 Summary and Discussion

Many studies (e.g. transient tracers or the carbon cycle) require ocean models to be run for many decades. Model drift can be a serious problem in such situations calling into questioning the fidelity of the model results (see *Zhao et al.* (2004)). Nudging in the tracer equations is not desirable, since unrealistic diapycnal mixing is introduced into the model. The semi-diagnostic method introduced here adjusts the model momentum equations, as in the semi-prognostic method, leaving the model tracer equations unchanged. Different from the semi-prognostic method, which can only slow model drift, the semi-diagnostic method strongly inhibits model drift. Meanwhile, meso-scale eddies are allowed to develop freely, enabling the method to be used as a diagnostic tool to probe the importance of eddies for driving the circulation. In a model of the northwest Atlantic Ocean, we found that the eddies strongly reinforce the Gulf Stream jet and the North Atlantic Current. Over half of the transport of the northern recirculation gyre of the Gulf Stream is driven by eddies. The eddies also play a role in shaping the hydrographic structure of the northwest corner region. We note, however, that while these results are broadly consistent with the role we expect eddies to play in this region, the particular diagnosis we have carried out depends on both the model used, the quality of the input climatology, ρ_c, and the precise form of the averaging operator in (10.5).

The counterpart of the semi-diagnostic method was also introduced. In this case, the high frequency, small scale structures in the model are constrained, but the large-scale circulation is completely free to evolve. We suggest that this method could be used as a means of assimilating high-frequency data (e.g., the altimetric data) or as a technique for nesting models (*Zhai et al.* (2004c) describe the use of the semi-prognostic method as a nesting technique). The semi-diagnostic model can be used to constrain the large-scale structure of the inner (higher-resolution) model, and its counterpart to transfer information

about small scales back to the outer model. We plan to explore these issues in a later paper.

Acknowledgments

We wish to thank Youyu Lu and Jun Zhao for helpful discussions. This project is supported by funding from CFCAS.

Biblilography

Cooper, M., and K. Haines, Altimetric assimilation with water property conservation, *J. Geophys. Res.*, *101*, 1059-1077,1996.

Eden, C., R.J. Greatbatch, and C.W. Böning, Adiabatically correcting an eddy-permitting model using large-scale hydrographic data: Application to the Gulf Stream and the North Atlantic Current, *J. Phys. Oceanogr.*, *34*, 701-719, 2004.

Geshelin, Y., J. Sheng, and R.J. Greatbatch, Monthly mean climatologies of temperature and salinity in the western North Atlantic, Canadian Data Report of Hydrography and Ocean Sciences, 153, 1999.

Gill, A.E., J.S.A. Green, and A.J. Simmons, Energy partition in the large-scale ocean circulation and the production of mid-ocean eddies, *Deep-Sea Res.*, *21*, 499-528, 1974.

Greatbatch, R.J., A model for the inertial recirculation of a gyre, *J. Mar. Res.*, *45*, 601-634, 1987.

Greatbatch, R.J., and Coauthors, The semi-prognostic method, *Cont. Shelf Res.*, *24*, 2149-2165, 2004.

Gregg, M.C., Scaling turbulent dissipation in the thermocline, *J. Geophys. Res.*, *94*, 9686-9698, 1989.

Hogg, N.G., A note on the deep circulation of the western North Atlantic: its nature and causes, *Deep-Sea Res.*, *30*, 945-961, 1983.

Hogg, N.G., R.S. Pickart, R.M. Hendry, and W.J. Smethie, Jr, The northern recirculation gyre of the Gluf Stream, *Deep-Sea Res.*, *33*, 1139-1165, 1986.

Holland, W.R., and L.B. Lin, On the generation of mesoscale eddies and their contribution to the oceanic general circulation. I. A preliminary numerical experiment, *J. Phys. Oceanogr.*, *5*, 642-657, 1975.

Holland, W.R., and P.B. Rhines, An example of eddy-induced ocean circulation, *J. Phys. Oceanogr.*, *10*, 1010-1031, 1980.

Lazier, J.R.N, Observations in the northwest corner of the North-Atlantic Current, *J. Phys. Oceanogr.*, *24*, 1449-1463, 1994.

Ledwell, J.R., A.J. Watson, and C.S. Law, Mixing of a tracer in the pycnocline, *J. Geophys. Res.*, *103*, 21499-21529, 1998.

Philips, N.A., The general circulation of the atmosphere: A numerical experiment, *Quart. J. Roy. Meteor. Soc.*, *82*, 123-164, 1956.

Sarmiento, J.L., and K. Bryan, An ocean transport model for the North Atlantic, *J. Geophys. Res.*, *87*, 394-408, 1982.

Sheng, J., R.J. Greatbatch, and D.G. Wright, Improving the utility of ocean circulation models through adjustment of the momentum balance, *J. Geophys. Res.*, *106*, 16711-16728, 2001.

Wardle, R., and J. Marshall, Representation of eddies in primitive equation models by a PV flux, *J. Phys. Oceanogr.*, 30, 2481-2503, 2000.

Willebrand, J., and Coauthors, Circulation characteristics in three eddy-permitting models of the North Atlantic, *Prog. in Oceanogr.*, 48, 123-161, 2001.

Zhai, X., J. Sheng, and R.J., Greatbatch, A new two-way nested-grid ocean modeling technique applied to the Scotian Shelf and slope, In *Proceedings of the eighth International Conference on Estuarine and Coastal Modeling*, 342-357, 2004.

Zhao, J., and Coauthors, Impact of an adiabatic correction technique on the simulation of CFC-12 in a model of the North Atlantic Ocean, *Geophys. Res. Lett.*, 31, L12309, doi:10.1029/2004GL020206, 2004.

Chapter 11

The Influence of Assimilated Eddies on the Large-Scale Circulation in a Model of the Northwest Atlantic Ocean[1]

In this letter, we apply a novel technique (the "semi-diagnostic method") to assimilate the eddy field from a model with constrained large-scale circulation into a model version with an unconstrained large-scale circulation. Assimilation of the eddies (i) drives an anomalous circulation corresponding to the northern recirculation gyre of the Gulf Stream, but of insufficient strength to appear in the mean field and (ii) leads to a much enhanced circulation in the northwest corner, east of Newfoundland. We argue that the blocking of f/H contours from the east by the mid-Atlantic Ridge is a major influence on the dynamics of the northwest corner, and that the dynamics of the eddy-driven northern recirculation and the northwest corner are fundamentally similar.

[1]**Citation:** Greatbatch, R. J., and X. Zhai, Influence of assimilated eddies on the large-scale circulation in a model of the northwest Atlantic Ocean, *Geophys. Res. Lett.*, *33*, L02614, doi:10.1029/2005GL025139, 2006.

11.1 Introduction

It has long been known that eddies are an essential element in understanding the general circulation of both the atmosphere (e.g., *Philips* (1956)) and the ocean (e.g., *Gill et al.* (1974); *Holland and Lin* (1975)). Of particular interest here are the northwest corner region, east of Newfoundland (*Lazier* (1994)), where the North Atlantic Current turns abruptly eastward towards Europe, and the recirculation gyres associated with the Gulf Stream (e.g. *Worthington* (1976); *Schmitz* (1980);*Hogg* (1983); *Richardson* (1985); *Hogg et al.* (1986)) where forcing by eddies is believed to be important (*Holland and Rhines* (1980); *Hogg and Stommel* (1985); *Marshall and Nurser* (1986); *Greatbatch* (1987)). The northern recirculation of the Gulf Stream is also a feature of diagnostic model studies (e.g. *Mellor et al.* (1982)) where it owes its existence to forcing by the bottom pressure torque (*Greatbatch et al.* (1991)). Recently, *Zhai et al.* (2004b) described what they call the "semi-diagnostic method" (hereafter SDM) and used the method to show that in a model of the northwest Atlantic, the eddies enhance the transport of the northern recirculation by a factor of 2, even though the existence of the recirculation gyre itself is apparent in a diagnostic model calculation. In *Zhai et al.* (2004b), the large scale circulation is constrained by climatological, hydrographic data, whereas the eddies are free to evolve and influence the mean state of the model (we call this version 1 of the SDM). *Zhai et al.* (2004b) also mentioned an alternative version of their method in which the eddies are strongly constrained by the input data, but the large scale is free to evolved in an unconstrained manner (we call this version 2 of the SDM). The latter case is similar to the situation in models that assimilate the eddy field, e.g. from altimeter data, examples being the studies of *Mellor and Ezer* (1991), *Ezer and Mellor* (1997), *Oschlies and Willebrand* (1996) and *Cooper and Haines* (1996). This is because measurement of the large-scale sea surface height (SSH) using satellite altimetry has, until recently, been limited by our knowledge of the geoid, and most assimilation studies have been restricted to assimilating the SSH variability associated with the eddies, and not the large-scale mean state. *Killworth et al.* (2001) note that assimilation of the eddy variability alone is generally not enough to lead to significant improvement in the mean state of a model; large-scale information is usually also required. Here, we use

version 2 of the SDM to illustrate the effect of assimilating the eddy field in a model of the northwest Atlantic similar to that used by *Zhai et al.* (2004b). We are interested in knowing to what extent assimilation of the eddies alone improves the large-scale circulation in the model compared to the prognostic model with no assimilation, and what inferences can be drawn about the dynamics of circulation features in the model from our results.

11.2 Ocean Model and Methods

The model is the same as the northwest Atlantic Ocean model described by *Sheng et al.* (2001), except for the use of higher horizontal resolution. The model domain spans the area between 30°W and 76°W and 35°N and 66°N, and here we use a horizontal resolution of $1/5^o$ in longitude. There are 31 unevenly spaced z levels, as in *Sheng et al.* (2001). The model is initialized with January mean temperature and salinity fields and forced by monthly mean surface heat flux from *da Silva et al.* (1994) and 12-hourly NCEP wind stress starting at the beginning of January 1990. The model sea surface salinity is restored to the monthly mean climatology on a time scale of 15 days. Along the model's open boundaries, temperature and salinity are restored to climatology and the transport is specified as described in *Sheng et al.* (2001).

11.2.1 The Semi-Diagnostic Method (Version 2)

Following *Zhai et al.* (2004b), our starting point is the hydrostatic equation seen by a prognostic model, i.e.,

$$\frac{\partial p}{\partial z} = -g\rho_m \equiv -g\rho_c - (\rho_m - \rho_c)g, \tag{11.1}$$

where p is the pressure variable carried by the model and g is the acceleration due to gravity. Here, $\rho_m = \rho(T, S, p_{ref})$ is the density calculated from the model potential temperature T and salinity S, and p_{ref} is the reference pressure at the center of each z level. ρ_c is the specified input density that is to be "assimilated" into the model and will be associated

with the mesoscale eddy field. By spatially filtering the second term, we get

$$\frac{\partial p}{\partial z} = -g\rho_c - \overline{(\rho_m - \rho_c)}g. \tag{11.2}$$

The filter, denoted by an overbar, passes horizontal scales larger than a specified cut-off scale (here 300 km, as in *Zhai et al.* (2004b)), but effectively eliminates horizontal scales smaller than the cut-off. Since

$$\frac{\partial \overline{p}}{\partial z} = \overline{-g\rho_c - \overline{(\rho_m - \rho_c)}g} = -\overline{\rho_m}g, \tag{11.3}$$

the large-scale flow field of the model is free to evolve. On the other hand, on spatial scales smaller than the cut-off, (11.2) takes the form $\frac{\partial p}{\partial z} = -g\rho_c$, indicating that the mesoscale in the model is strongly constrained by the input hydrography, ρ_c. It should be noted that when data derived from satellites, e.g. altimeter data, is assimilated into a model, it is necessary to associate a subsurface density field, corresponding to ρ_c, with the surface features. Different assimilation schemes use different methods for choosing ρ_c, e.g. correlation analysis *Mellor and Ezer* (1991), *Ezer and Mellor* (1997) or by vertically rearranging the water masses in a model *Cooper and Haines* (1996). Here we take ρ_c from a SDM (version 1) model run using the climatology from *Geshelin et al.* (1999) to constrain the large-scale circulation, as described by *Zhai et al.* (2004b). We then use version 2 of the SDM to assimilate the mesoscale from the version 1 model run into the prognostic version (without assimilation) of the same model set-up. It should be noted that the assimilation takes place only through equation (11.2), and that all other model equations remain as in the prognostic model.

11.3 Model Results

Figure 11.1 shows the annual mean transport streamfunction for Year 5 of the model integrations from the 3 different model versions. Figure 11.1c is from the prognostic model run, without assimilation. As in *Sheng et al.* (2001), it is clear that the prognostic model

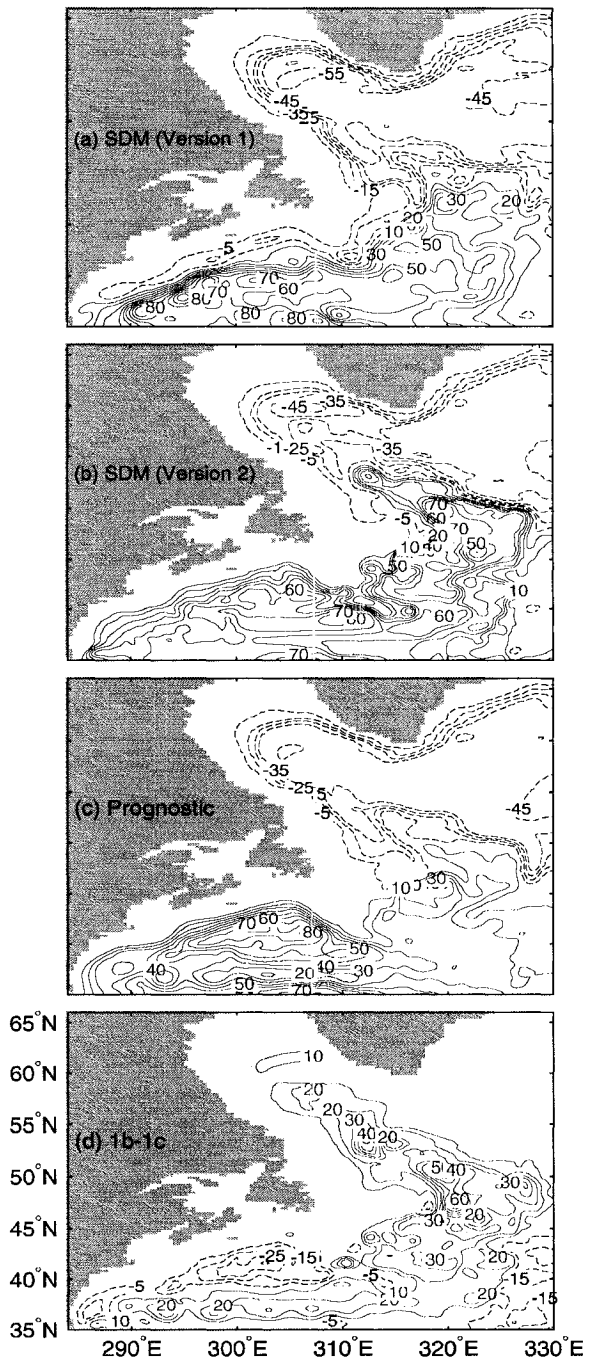

Figure 11.1: Model-calculated annual mean horizontal transport streamfunction in year 5 using the (a) semi-diagnostic version 1, (b) semi-diagnostic version 2, (c) prognostic models and (d) the difference, (b) minus (c). Red contours represent anticyclonic transport and blue contours cyclonic transport. The contour interval is 10 Sv.

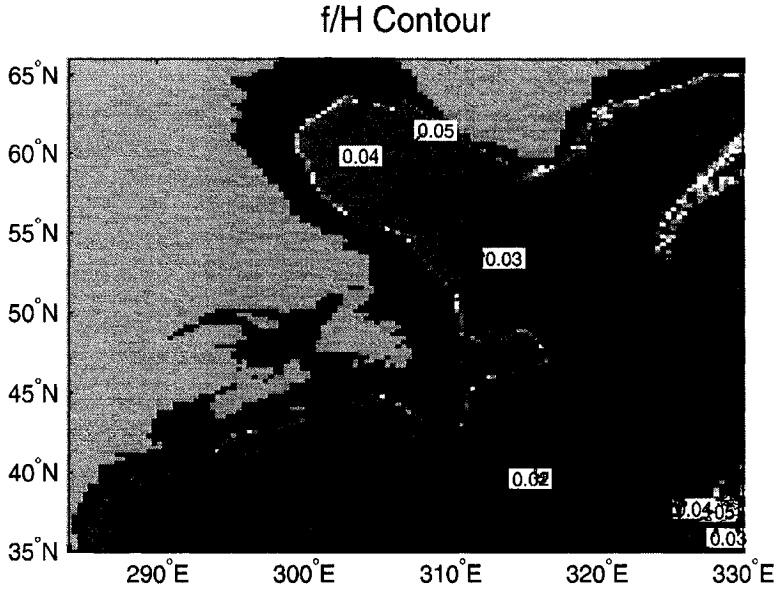

Figure 11.2: The f/H contours in the northwest Atlantic Ocean. The units are $10^{-6}s^{-1}m^{-1}$

lacks the northern recirculation gyre south of Atlantic Canada, the Gulf Stream being too far to the north. Additionally, the circulation in the northwest corner, near 50°N 320°E, is weak. By contrast, when the large scale circulation is strongly constrained, as in the SDM Version 1 case (Fig. 11.1a), both the northern recirculation and the northwest corner are well-developed (*Zhai et al.* (2004b)). To produce Figure 11.1b, the eddies from the SDM Version 1 case (Figure 11.1a) are being assimilated into the prognostic model using Version 2 of the SDM (see Section 2). In Figure 11.1b, the model still lacks a northern recirculation gyre but, on the other hand, has a well-developed northwest corner with even stronger circulation than in Figure 11.1a, and in complete contrast to the weak representation of the northwest corner in Figure 11.1c. In Figure 11.1d, the streamfunction in Figure 11.1b is subtracted from that in Figure 11.1c, revealing the influence of the assimilated eddy field in Figure 11.1b. It is clear that eddies do, indeed, drive a northern recirculation gyre of up to 30 Sv in strength, but clearly, it is not of sufficient strength to show up as a closed gyre in Figure 11.1b. It is also striking how the region of enhanced transport associated with the northwest corner in Figure 11.1b (see also Fig. 11.1d) is bounded roughly by the f/H contour highlighted in Figure 11.2. This particular f/H contour, corresponding to a depth

of around 3700 m at 50°N, connects to the southern boundary of our model domain, and not the eastern boundary, as do the contours with larger values of f/H, the topographic feature that marks this division being the Charlie Gibbs Fracture zone. It is also of interest that the cyclonic circulation associated with the eddy-driven northern recirculation lies to the south of this f/H contour, reminiscent of the theoretical study of *Hogg and Stommel* (1985). Indeed, these results suggest that the dynamics of the northwest corner, and also the eddy-driven part of the northern recirculation shown in Fig. 11.1d, is similar in our model to that described by *Hogg and Stommel* (1985) for the northern recirculation gyre; namely an eddy-driven circulation within potential vorticity contours that are closed on the west, north and east by topography, but on the south by the sloping stratification of the subtropical gyre. In the case of the northwest corner, it is the presence of the mid-Atlantic Ridge, and the blocking to the east of the f/H contours (see Figure 11.2) that makes this possible.

Figure 11.3 compares the corresponding temperature fields in the different model versions at 45 m depth. It should be noted that temperature is not directly assimilated into the model; in fact, the adjustment of the model due to the assimilation takes place entirely in the momentum equations (*Sheng et al.* (2001); *Greatbatch et al.* (2004)), leaving the tracer equations unchanged. We again see the strongly developed northwest corner in the SDM Version 2 case (Figure 11.3b), with even warmer water being found in the northwest corner in this case than in the climatology (Figure 11.3d). Nevertheless, the assimilation used to produce Figure 11.3b has not been successful in improving the temperature field in the Gulf Stream/northern recirculation region, south of Atlantic Canada (compare Figure 11.3b with Figure 11.3c). It seems that in this particular model, assimilation of the large-scale hydrography (used to produce Figure 11.3a) is required to bring the model temperature field south of Atlantic Canada into line with climatology (*Zhai et al.* (2004b)).

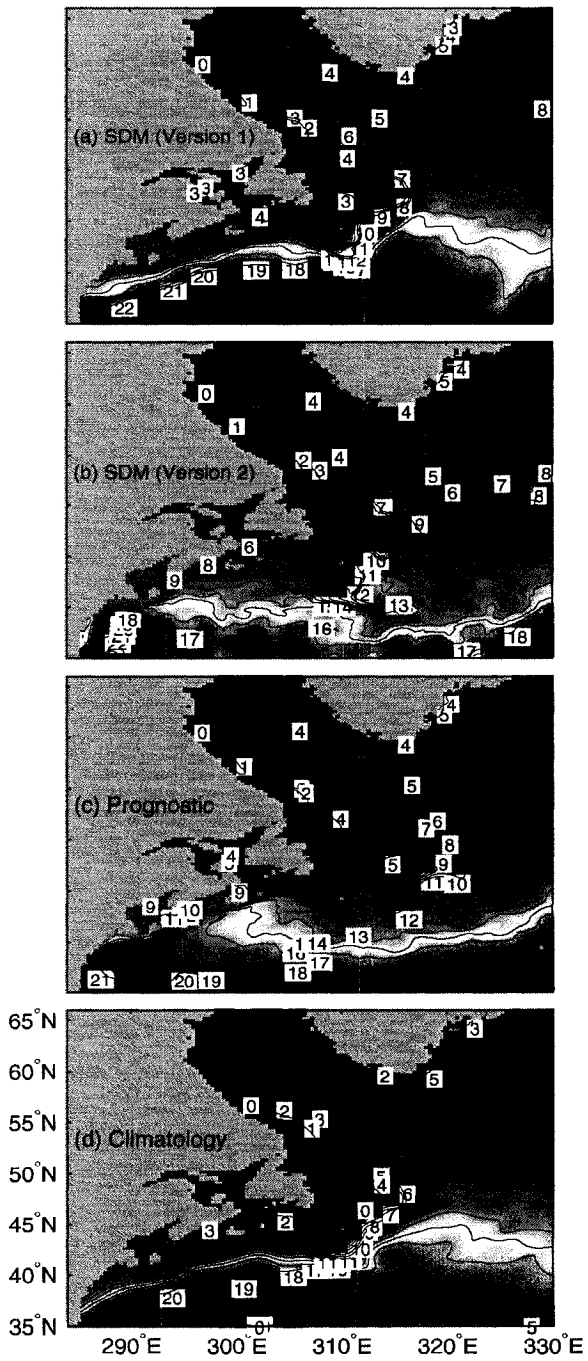

Figure 11.3: Model-calculated annual mean temperature (^{O}C) at 45 m depth in year 5 using the (a) semi-diagnostic version 1, (b) semi-diagnostic version 2, (c) prognostic models and (d) climatological annual mean temperature at the same depth. The contour interval is 1°C.

11.4 Summary and Discussion

In this paper, we have used the counterpart of the semi-diagnostic method (SDM) introduced by *Zhai et al.* (2004b), to examine the impact of assimilating eddies on the large-scale circulation in a model of the northwest Atlantic Ocean. A novel feature of our study is that while the eddy field is strongly constrained by the assimilation procedure, there is no direct constraint on the large-scale circulation in the model. The results support the finding of *Zhai et al.* (2004b) that the existence of the Gulf Stream northern recirculation gyre (*Hogg et al.* (1986)) is owed in the model primarily to bottom pressure torque forcing associated with the large scale hydrography, but that the eddies do contribute to the transport associated with this gyre. In particular, the assimilated eddies in our model do drive a northern recirculation gyre, but not of sufficient strength to appear as a closed gyre in the mean field shown in Figure 11.1b. On the other hand, the northwest corner, east of Newfoundland, is dramatically enhanced in the model run with assimilated eddies compared to the prognostic model run. We argue that this is because f/H contours are blocked to the east by the mid-Atlantic ridge, and that the northward extent of the northwest corner is set by the gap in the mid-Atlantic Ridge due to the Charlie-Gibbs Fracture zone in the model.

Acknowledgments

We wish to thank Jinyu Sheng for his help with the model. This work has been supported by funding from NSERC and CFCAS to the Canadian CLIVAR Research Network.

Bibliography

Cooper, M., and K. Haines (1996), Altimetric assimilation with water property conservation, *J. Geophys. Res.*, *101*, 1059-1077.

Ezer, T., and G.L. Mellor (1997), Data assimilation experiments in the Gulf Stream region: How useful are satellite-derived surface data for nowcasting the subsurface fields? *J. Atmos. Oceanic Tech.*, *14*, 1379-1391.

Geshelin, Y., J. Sheng, and R.J. Greatbatch (1999), Monthly mean climatologies of temperature and salinity in the western North Atlantic, Canadian Data Report of Hydrography and Ocean Sciences, 153pp.

Gill, A.E., J.S.A. Green, and A.J. Simmons (1974), Energy partition in the large-scale ocean circulation and the production of mid-ocean eddies, *Deep-Sea Res.*, *21*, 499-528.

Greatbatch, R.J. (1987), A model for the inertial recirculation of a gyre, *J. Mar. Res.*, *45*, 601-634.

Greatbatch, R.J., et al. (1991), A diagnosis of interpentadal circulation changes in the North Atlantic, *J. Geophys. Res.*, *96*, 22009-22023.

Greatbatch, R.J., et al. (2004), The semi-prognostic method, *Cont. Shelf Res.*, *24/18*, 2149-2165.

Hogg, N.G. (1983), A note on the deep circulation of the western North Atlantic: its nature and causes, *Deep-Sea Res.*, *30*, 945-961.

Hogg, N.G., and H. Stommel (1985), On the relationship between the deep circulation and the Gulf Stream, *Deep-Sea Res.*, *32*, 1181-1193.

Hogg, N.G., R.S. Pickart, R.M. Hendry, and W.J. Smethie, Jr (1986), The northern recirculation gyre of the Gluf Stream, *Deep-Sea Res.*, *33*, 1139-1165.

Holland, W.R., and L.B. Lin (1975), On the generation of mesoscale eddies and their contribution to the oceanic general circulation. I. A preliminary numerical experiment, *J. Phys. Oceanogr.*, *5*, 642-657.

Holland, W.R., and P.B. Rhines (1980), An example of eddy-induced ocean circulation, *J. Phys. Oceanogr.*, *10*, 1010-1031.

Killworth, P.D., C. Dieterich, C. Le Provost, A. Oschlies, and J. Willebrand (2001), Assimilation of altimetric data and mean sea surface height into an eddy-permitting model of the North Atlantic, *Prog. in Oceanography*, *48*, 313-335.

Lazier, J.R.N. (1994), Observations in the northwest corner of the North-Atlantic Current, *J. Phys. Oceanogr.*, *24*, 1449-1463.

Marshall, J., and A.J.G. Nurser (1986), Steady free circulation in a stratified quasi-geostrophic

ocean, *J. Phys.Oceanog.*, *16*, 1799-1813.

Mellor, G.L., C.R. Mechoso, and E. Keto (1982) A diagnostic calculation of the general circulation of the Atlantic Ocean, *Deep-Sea Res.*, *29*, 1171-1192.

Mellor, G.L., and T. Ezer (1991): A Gulf Stream model and an altimetry assimilation scheme, *J. Geophys. Res.*, *96*, 8779-8795.

Oschlies, A., and J. Willebrand (1996) Assimilation of Geosat altimeter data into an eddy-resolving primitive equation model of the North Atlantic Ocean, *J. Geophys. Res.*, *101*, 14175-14190.

Philips, N.A. (1956), The general circulation of the atmosphere: A numerical experiment, *Quart. J. Roy. Meteor. Soc.*, *82*, 123-164.

Richardson, P.L. (1985), Average velocity and transport of the Gulf Stream near 55°W, *J. Mar. Res.*, *43*, 83-111.

Schmitz, W.J. (1980), Weakly-depth-dependent segments of the North Atlantic circulation, *J. Mar. Res.*, *38*, 111-133.

Sheng, J., R.J. Greatbatch, and D.G. Wright (2001), Improving the utility of ocean circulation models through adjustment of the momentum balance, *J. Geophys. Res.*, *106*, 16711-16728.

da Silva, A.M., C.C. Young, and S. Levitus (1994), Atlas of surface marine data 1994, Vol 3., Anomalies of heat and momentum fluxes, NOAA Atlas NESDIS 8, 413pp.

Worthington, L.V. (1976), *On the North Atlantic Circulation.* The Johns Hopkins University Press, 110pp.

Zhai, X., R.J., Greatbatch and J. Sheng (2004), Diagnosing the role of eddies in driving the circulation of the northwest Atlantic Ocean, *Geophys. Res. Lett.*, *31*, L23304, doi:10.1029/2004GL021146.

Chapter 12

Conclusions

In this thesis, several topics have been researched, ranging from wind power input to the ocean and spreading of near-inertial energy, to eddy-induced mixing and its role in ocean heat budget. These topics are closely linked to each other. Here, the research is summarized and the main results discussed. In addition, some speculation is provided on follow-on research that could be carried out in the future.

Wind power input to the ocean is a fundamental problem in oceanography, since it represents one of the two main energy sources for maintaining the circulation. However, recent estimates of wind work on the ocean have ignored the surface motion of the ocean; that is, the parameterized wind stress depends on the 10-m wind alone, instead of considering the relative motion between the atmosphere and the ocean. The consequence of leaving the surface ocean velocity out of the wind stress parameterization is to overestimate the wind power input to the ocean. Consistent with the idealized study by *Duhaut and Straub* (2006), we find (*Zhai and Greatbatch* (2007); see also Chapter 2) that the wind power input is reduced by about 17% when ocean surface currents are included in the wind stress parameterization in a high-resolution model of the northwest Atlantic Ocean. In addition, the modelled eddy kinetic energy decreases by about 10%, in response to direct mechanical damping by the surface stress. We also find that the decrease in wind power input due to including surface ocean velocity in the wind stress is one order of magnitude larger than the energy dissipation associated with bottom friction. This result stresses the importance of

taking account of the ocean velocity dependence in the specification of surface stress if the energetics of the ocean circulation are to be properly represented in models. We note that our model has only been run for 2 years, the second year being used for the analysis, and that model is not fully eddy-resolving. Clearly future work should involve using models of much higher resolution, longer multi-year simulations, and wind forcing with higher time and spatial resolution. The Southern Ocean is one place that is expected to be important for the wind energy input (see *Wunsch* (1998)), since the Antarctic Circumpolar Current (ACC) moves in the same direction as the circumpolar wind. However, the Southern Ocean is also rich in eddies and, hence, we should expect to see a noticable reduction in estimates of the wind power input over the Southern Ocean when the ocean surface velocity dependence of the wind stress is taken into account, a topic for future research.

Wind power input to near-inertial motions at the surface is one of the important energy sources for mixing (*Alford* (2003b)). The traditional view is that the wind-induced near-inertial energy is redistributed by the propagation of inertial-gravity waves to lower latitudes, that is, by the beta-dispersion effect (see *Anderson and Gill* (1979), *Gill* (1984), *Garrett* (2001)). However, the real ocean is not homogeneous, and the background mean currents and mesoscale eddy field can strongly influence the propagation of near-inertial waves. For example, we find (*Zhai et al.* (2004a); see also Chapter 3) that the near-inertial energy induced by Hurricane Juan (2003) is advected into the ocean interior by the Gulf Stream in a model of the northwest Atlantic Ocean, suggesting that geostrophic advection could play a role in redistributing near-inertial energy in the ocean. We also find (*Zhai et al.* (2005a); see also Chapter 4) that inertial oscillations can be advected poleward beyond their turning latitude because of the Doppler shift effect. The inertial oscillations shrink meridionally with latitude during this advection, and could eventually lead mixing through nonlinear interactions. This advection-induced mixing occurs poleward of their source regions. Since a given energy level at higher latitudes causes much more mixing than at lower latitudes (*Gregg et al.* (2003); *Garrett* (2003)), a mechanism for transporting inertial energy to higher latitudes could lead to more efficient mixing than would otherwise be the case. This phenomenon could apply to the North Atlantic Current, the Norwegian

Current, and other poleward currents, even though those are more complicated environments and subject to additional physics than has been considered here. Recently, we point out (*Zhai et al.* (2005b)) that there is a remarkable coincidence between the regions where near-inertial energy is input to the ocean (the atmospheric storm track) and regions of enhanced eddy activity (the oceanic storm track), making it necessary to examine the effect of a mesocale eddy field on the input of near-inertial energy and its subsequent vertical propagation. Using an idealized eddying channel model mimicing the Southern Ocean, we find (*Zhai et al.* (2005b); see also Chapter 5) that the storm-induced near-inertial energy is trapped inside the anticyclonic eddies and drained locally to the deep ocean through the chimney effect (*Lee and Niiler* (1998)). Then, we examined the spreading of near-inertial energy in a realistic $1/12^o$ model of the North Atlantic driven by synoptically varying wind forcing. We find (*Zhai et al.* (2007); see also Chapter 6) that (i) near-inertial energy is strongly influenced by the mesoscale eddy field and appears to be locally drained to the deep ocean, largely by the chimney effect associated with anticyclonic eddies, and (ii) the interior of the subtropical gyre shows very low levels of near-inertial energy, contrary to expectations based on the β-dispersion effect. Enhanced near-inertial energy in warm eddies has been observed to generate turbulence and mixing through shear instability at the critical depth where the vertical group velocity goes to zero (e.g., *Lueck and Osborn* (1986); *Kunze et al.* (1995)). Therefore, strong diapycnal mixing associated with near-inertial wave breaking is expected to occur in the Gulf Stream system and other regions of the world ocean with high levels of eddy kinetic energy (e.g. the Southern Ocean). Furthermore, mesoscale eddies could be efficient in generating mixing at depth, since they can drain the near-inertial energy to depth locally, rather than transferring it to lower latitudes as in the β-dispersion effect (*Gregg et al.* (2003); *Garrett* (2003)). More detailed calculations are necessary to provide accurate estimates of the near-inertial energy input to the ocean in the presence of a mesoscale eddy field, updating *Alford* (2003b), and also to study the fate of near-inertial energy within eddies and the associated mixing, building on the observation work of *Lueck and Osborn* (1986) and *Kunze et al.* (1995). Longer integrations, including the seasonal cycle, and using wind stress forcing with higher temporal and spatial resolution are clearly

required, as well as further relatively short model integrations using even higher model resolution than we have used here. Nevertheless, our results clearly suggest that energy input from the wind to the near-inertial frequency band may well be dissipated, and lead to mixing, locally within mesoscale eddies in the ocean rather than being spread equatorward by β-dispersion. If this result holds up to closer scrutiny, then the diapycnal diffusivity that is specified in the ocean component of climate models will need to be adjusted accordingly, with relatively large values in regions of relatively large eddy kinetic energy in the ocean, complementing recent work by *Hibiya et al.* (2006) on the spatial distribution of the diapycnal diffusivity resulting from tidal forcing.

Eddies can also induce mixing by interaction with the atmosphere. Most state-of-the-art ocean/climate models use the parameterization of *Gent and McWilliams* (1990) (hereafter GM) to parameterize the role of eddies in the large-scale ocean circulation and ocean tracer transport. The GM parameterization assumes the tracer fluxes associated with eddies are completely adiabatic. However, eddies can be strongly modified in the surface mixed layer by interaction with the atmosphere, leading to irreversible mixing and water mass conversion (e.g *Tandon and Garrett* (1996), *Treguier et al.* (1997)), with the implication that eddy fluxes also have a diffusive effect that needs to be taken into account in ocean/climate models. It has been proposed recently that diapycnal eddy fluxes play an important role in the maintenance of the main thermocline (*Marshall et al.* (2002); *Radko and Marshall* (2004)). Using an integral constraint, we point out (*Greatbatch et al.* (2007); see also Chapter 7) the fundamental role played by ocean mixing processes in the ocean heat budget and we argue that eddy-induced mixing in the surface mixed layer due to interaction with the atmosphere can play an important role in closing the ocean heat budget. Meanwhile, we recongize that the error bars associated with the surface heat flux and micro-structure mixing used for estimating our ocean heat budget could be large, and a detailed budget analysis based on a better data set and new measurements is clearly needed. It follows that the lateral mixing applied near the surface in non-eddy resolving ocean/climate models may be required to play an important role in closing the ocean heat budget in these models, and that careful attention should be given to how the lateral mixing in these models is specified. The current

practise is often to simply replace the isopycnal mixing in the ocean interior by horizontal mixing at the surface, with no guarantee that the magnitude and spatial structure of the mixing is appropriate. There is clearly a need to provide estimates of this eddy-induced mixing from observed data or eddy-resolving model output and develop physically-based parameterizations for eddy-induced mixing, especially in the surface mixed layer. We estimate the eddy-induced diffusivity for heat in the surface mixed layer in two ways: (i) directly combining satellite-derived geostrophic velocity and sea surface temperature anomalies from the western North Atlantic Ocean (*Zhai and Greatbatch* (2006a); see also Chapter 8) and (ii) conducting numerical experiments with a high-resolution model of the northwest Atlantic Ocean (*Zhai and Greatbatch* (2006b); see also Chapter 9). The surface eddy-induced diffusivities estimated from these two methods are broadly consistent with each other and show considerable spatial variability with large values to the south of the Gulf Stream and smaller values within the Gulf Stream itself. Finally we note that the eddy-induced diffusivity for different tracers (e.g. salinity, carbon or CFC) depends on the dissipation characteristics for those tracers and is unlikely to be the same as that for heat (see also *Plumb and Mahlman* (1987)), another topic for future research.

Apart from eddy-induced mixing, eddies are also known to play an important role in shaping the large-scale ocean circulation, especially in the western boundary region and in the Southern Ocean (*Danabasoglu et al.* (1994), *Rintoul et al.* (2001)). However, since the flow is highly geostrophic, momentum balances are not a useful way for determining the importance of the eddies; the Reynolds stresses are usually one or two orders of magnitude smaller than the Coriolis and pressure gradient terms (*Holland and Lin* (1975)). We introduce a new method (the semi-diagnostic method) for use with ocean models, which has the advantage that model drift is effectively prevented, while at the same time the meso-scale eddy field is free to evolve (*Zhai et al.* (2004b); see also Chapter 10). This new method is then used to probe the importance of the eddy-driven circulation in the northwest Atlantic Ocean. For the particular model used in this study, we find that the eddies strongly reinforce the eastward Gulf Stream jet and the northern recirculation in the slope region, with over 50% of the total transport of this recirculation being directly eddy-driven. We note,

however, that while these results are broadly consistent with the role we expect eddies to play in this region, the particular diagnosis we have carried out depends on both the model used, the quality of the input climatology, and the precise form of the averaging operator. The counterpart of the semi-diagnostic method is also used to examine the impact of assimilating eddies on the large-scale circulation in a model of the northwest Atlantic Ocean (*Greatbatch and Zhai* (2006); see also Chapter 11). A novel feature of this study is that while the eddy field is strongly constrained by the assimilation procedure, there is no direct constraint on the large-scale circulation in the model. We find assimilation of the eddies (i) drives an anomalous circulation corresponding to the northern recirculation gyre of the Gulf Stream, but of insufficient strength to appear in the mean field and (ii) leads to a much enhanced circulation in the northwest corner, east of Newfoundland. We then argue that the blocking of f/H contours from the east by the mid-Atlantic Ridge is a major influence on the dynamics of the northwest corner, and that the dynamics of the eddy-driven northern recirculation and the northwest corner are fundamentally similar. Since the semi-diagnostic method has been proven to be robust and powerful, it has the potential to be used to address the question of "can eddies make the ocean desert bloom" (e.g., *Oschlies and Garcon* (1998)), another topic for future research.

Bibliography

Alford, M. H., Redistribution of energy available for ocean mixing by long-range propagation of internal waves, *Nature*, *423*, 159–162, 2003a.

Alford, M. H., Improved global maps and 54-years history of wind-work on ocean inertial motions, *Geophys. Res. Lett.*, *1424*, doi:10.1029/2002GL016,614, 2003b.

Anderson, D. L. T., and A. E. Gill, Beta dispersion of inertial waves, *J. Geophys. Res.*, *84*, 1836–1842, 1979.

Bender, M. A., and I. Ginis, Real-case simulations of hurricane-ocean interaction using a high-resolution coupled model: effects on hurricane intensity, *Mon. Wea. Rev.*, *128*, 917–946, 2000.

Boccaletti, G., R. Ferrari, A. Adcroft, D. Ferreira, and J. C. Marshall, The vertical structure of ocean heat transport, *Geophys. Res. Lett.*, *32*, doi:10.1029/2005GL022,474, 2005.

Bretherton, F. P., Ocean climate modeling, *Progress in Oceanogr.*, *11*, 93–129, 1982.

Brink, K. H., Observations of the response of thermocline currents to a hurricane, *J. Phys. Oceanogr.*, *19*, 1017–1022, 1989.

Bryan, K., Measurements of meridional heat transport by ocean currents, *J. Geophys. Res.*, *67*, 3403–3414, 1962.

Bryan, K., Poleward heat transport in the ocean. A review of a hierarchy of models of increasing resolution, *Tellus*, *43*, 104–115, 1991.

Bryan, K., The role of mesoscale eddies in the poleward transport of heat by the oceans: a review, *Physca D*, *98*, 249–257, 1996.

Bryan, K., J. K. Dukowicz, and R. D. Smith, On the mixing coefficient in the parameterization of bolus velocity, *J. Phys. Oceanogr.*, *29*, 2442–2456, 1999.

Chang, S. W., and R. A. Anthes, Numerical simulations of the ocean's nonlinear baroclinic response to translating hurricanes, *J. Phys. Oceanogr.*, *8*, 468–480, 1978.

Chelton, D. B., M. G. Schlax, M. H. Freilich, and R. F. Milliff, Satellite measurements reveal persistent small-scale features in ocean winds, *Science*, *303*, 978–983, 2004.

Chiswell, S. M., Deep equatorward propagation of inertial oscillations, *Geophys. Res. Lett.*, *30*, 1533–1536, 2003.

Cooper, M., and K. Haines, Altimetric assimilation with water property conservation, *J. Geophys. Res.*, *101*, 1059–1077, 1996.

Cornillon, P., and K. A. Park, Warm core ring velocity inferred from NSCAT, *Geophys. Res. Lett.*, *28*, 575–578, 2001.

da Silva, A. M., C. C. Young, and S. Levitus, *Atlas of surface marine data 1994*, vol. 3 of *NOAA Atlas NESDIS 8*, NOAA, Silver Spring, Md, 1994, 413 pp.

Danabasoglu, G., J. C. McWilliams, and P. Gent, The role of mesoscale tracer transport in the global ocean circulation, *Science*, *264*, 1123–1126, 1994.

D'Asaro, E. A., The decay of wind-forced mixed layer inertial oscillations due to the β effect, *J. Geophys. Res.*, *94*, 2045–2056, 1989.

D'Asaro, E. A., Upper-ocean inertial currents forced by a strong storm. Part III: Interaction of inertial currents and mesoscale eddies, *J. Phys. Oceanogr.*, *25*, 2953–2958, 1995.

Davies, A. M., and J. Xing, Influence of coastal fronts on near-inertial internal waves, *Geophys. Res. Lett.*, *29*, 2114–2117, 2002.

Dawe, J. T., and L. Thompson, Effect of ocean surface currents on wind stress, heat flux, and wind power input to the ocean, *Geophys. Res. Lett.*, *33*, doi:10.1029/2006GL025,784, 2006.

Dickey, T., et al., Upper-ocean temperature response to hurricane Felix as measured by the Bermuda tested mooring, *Mon. Wea. Rev.*, *126*, 1195–1201, 1998.

Drijfhout, S., Heat transport by mesoscale eddies in an ocean circulation model, *J. Phys. Oceanogr.*, *24*, 353–369, 1994.

Duhaut, T. H., and D. N. Straub, Wind stress dependence on ocean surface velocity: Implications for mechanical energy input to ocean circulation, *J. Phys. Oceanogr.*, *36*, 202–211, 2006.

Eden, C., and R. J. Greatbatch, A damped decadal oscillation in the North Atlantic climate system, *J. Climate*, *16*, 4043–4060, 2003.

Eden, C., and T. Jung, Wind-driven eddies and plankton blooms in the North Atlantic Ocean, *Technical memorandum 490*, ECMWF, Reading, UK, 2006.

Eden, C., R. J. Greatbatch, and C. W. Böning, Adiabatically correcting an eddy-permitting model of the North Atlantic using large-scale hydrographic data, *J. Phys. Oceanogr.*, *34*, 701–719, 2004.

Eden, C., R. J. Greatbatch, and D. Olbers, Interpreting eddy fluxes, *J. Phys. Oceanogr.*, *37*, 1282–1296, 2007a.

Eden, C., R. J. Greatbatch, and J. Willebrand, A diagnosis of thickness fluxes in an eddy-resolving model, *J. Phys. Oceanogr.*, *37*, 727–742, 2007b.

Ezer, T., and G. L. Mellor, Data assimilation experiments in the Gulf Stream region: How useful are satellite-derived surface data for nowcasting the subsurface fields?, *J. Atmos. Oceanic Tech.*, *14*, 1379–1391, 1997.

Ferrari, R., and J. C. McWilliams, Parameterization of eddy fluxes near oceanic boundaries, *Ocean Modelling*, p. submitted, 2007.

Fu, L. L., Observations and models of inertial waves in the deep ocean, *Rev. Geophys. Space Phys.*, *19*, 141–170, 1981.

Ganachaud, A., and C. Wunsch, Improved estimates of global ocean circulation, heat transport and mixing from hydrological data, *Nature*, *408*, 453–457, 2000.

Garrett, C., What is the "Near-Inertial" band and why is it different from the rest of the internal wave spectrum?, *J. Phys. Oceanogr.*, *31*, 962–971, 2001.

Garrett, C., Mixing with latitude, *Nature*, *422*, 477–478, 2003.

Garrett, C., K. Speer, and E. Tragou, The relationship between water mass formation and the surface buoyancy flux, with application to Phillips's Red Sea model, *J. Phys. Oceanogr.*, *25*, 1696–1705, 1995.

Geisler, J. E., and R. E. Dickinson, The role of variable Coriolis parameter in the propagation of inertia-gravity waves during the process of geostrophic adjustment, *J. Phys. Oceanogr.*, *2*, 263–272, 1972.

Gent, P., and J. C. McWilliams, Isopycnal mixing in ocean circulation models, *J. Phys. Oceanogr.*, *20*, 150–155, 1990.

Gent, P., J. Willebrand, T. J. McDougall, and J. C. McWilliams, Parameterizing eddy-induced tracer transports in ocean circulation models, *J. Phys. Oceanogr.*, *25*, 463–474, 1995.

Geshelin, Y., J. Sheng, and R. J. Greatbatch, Monthly mean climatologies of temperature and salinity in the western North Atlantic, *Tech. rep.*, Fish. and Oceans Can., Ottawa, Ontario, 1999.

Gill, A. E., *Atmosphere-Ocean Dynamics*, vol. 30 of *International Geophysics Series*, Academic Press, 1982, 662 pp.

Gill, A. E., On the behavior of internal waves in the wake of storms, *J. Phys. Oceanogr.*, *14*, 1129–1151, 1984.

Gill, A. E., and J. S. Turner, A comparison of seasonal thermocline models with observation, *Deep-Sea Res.*, *23*, 391–401, 1976.

Gill, A. E., J. S. A. Green, and A. J. Simmons, Energy partition in the large-scale ocean circulation and the production of mid-ocean eddies, *Deep-Sea Res.*, *21*, 499–528, 1974.

Greatbatch, R. J., On the response of the ocean to a moving storm: The nonlinear dynamics, *J. Phys. Oceanogr.*, *13*, 357–367, 1983.

Greatbatch, R. J., On the response of the ocean to a moving storm: Parameters and scales, *J. Phys. Oceanogr.*, *14*, 59–77, 1984.

Greatbatch, R. J., A model for the inertial recirculation of a gyre, *J. Mar. Res.*, *45*, 601–634, 1987.

Greatbatch, R. J., and X. Zhai, The influence of assimilated eddies on the large-scale circulation in a model of the northwest Atlantic Ocean, *Geophys. Res. Lett.*, *33*, doi:10.1029/2005GL025,139, 2006.

Greatbatch, R. J., A. F. Fanning, A. D. Goulding, and S. Levitus, A diagnosis of interpentadal circulation changes in the north atlantic, *J. Geophys. Res.*, *96*, 22,009–22,024, 1991.

Greatbatch, R. J., J. Sheng, C. Eden, L. Tang, X. Zhai, and J. Zhao, The semi-prognostic method, *Continental Shelf Res.*, *24*, 2149–2165, 2004.

Greatbatch, R. J., X. Zhai, C. Eden, and D. Olbers, The possible role in the ocean heat budget of eddy-induced mixing due to air-sea interaction, *Geophys. Res. Lett.*, *34*, doi:10.1029/2007GL029,533, 2007.

Gregg, M. C., Scaling turbulent dissipation in the thermocline, *J. Geophys. Res.*, *94*, 9686–9698, 1989.

Gregg, M. C., T. B. Sanford, and D. P. Winkel, Reduced mixing from the breaking of internal waves in equatorial waters, *Nature*, *422*, 513–515, 2003.

Grist, J. P., and S. A. Josey, Inverse analysis adjustment of the SOC air-sea flux climatology using ocean heat transport constraints, *J. Climate*, *16*, 3274–3295, 2003.

Hall, M. M., and H. L. Bryden, Direct estimates and mechanisms of ocean heat transport, *Deep-Sea Res.*, *29*, 339–359, 1982.

Haney, R. L., Surface thermal boundary condition for ocean circulation models, *J. Phys. Oceanogr.*, *1*, 241–248, 1971.

Hibiya, T., M. Nagasawa, and Y. Niwa, Global mapping of diapycnal diffusivity in the deep ocean based on the results of expendable current profiler (XCP) surveys, *Geophys. Res. Lett.*, *33*, doi:10.1029/2005GL025,218, 2006.

Hogg, N. G., A note on the deep circulation of the western North Atlantic: its nature and causes, *Deep Sea Res.*, *30*, 945–961, 1983.

Hogg, N. G., and H. Stommel, On the relationship between the deep circulation and the Gulf Stream, *Deep Sea Res.*, *32*, 1181–1193, 1985.

Hogg, N. G., R. S. Pickart, R. M. Hendry, and W. J. Smethie, The northern recirculation gyre of the Gluf Stream, *Deep Sea Res.*, *33*, 1139–1165, 1986.

Holland, W. R., and L. B. Lin, On the generation of mesoscale eddies and their contribution to the oceanic general circulation. I. A preliminary numerical experiment, *J. Phys. Oceanogr.*, *5*, 642–657, 1975.

Holland, W. R., and P. B. Rhines, An example of eddy-induced ocean circulation, *J. Phys. Oceanogr.*, *10*, 1010–1031, 1980.

Holloway, G., Estimation of oceanic eddy transports from satellite altimetry, *Nature*, *323*, 243–244, 1986.

Hughes, C. W., An extra dimension to mixing, *Nature*, *16*, 137–139, 2002.

Illari, L., and J. C. Marshall, On the interpretation of eddy fluxes in a blocking episode, *J. Atmos. Sci.*, *40*, 2232–2242, 1983.

Jayne, S. R., and J. Marotzke, The oceaic eddy heat transport, *J. Phys. Oceanogr.*, *32*, 3328–3345, 2002.

Kara, A. B., P. A. Rochford, and H. E. Hurlburt, Mixed layer depth variability over the global ocean, *J. Geophys. Res.*, *108*, doi:10.1029/2000JC000,736, 2003.

Karsten, R., H. Jones, and J. C. Marshall, The role of eddy transfer in setting the stratification and transport of a Circumpolar Current, *J. Phys. Oceanogr.*, *32*, 39–54, 2002.

Keffer, T., and G. Holloway, Estimating Southern Ocean eddy flux of heat and salt from satellite altimetry, *Nature*, *332*, 624–626, 1988.

Kelly, K. A., S. Dickinson, M. J. McPhaden, and G. C. Johnson, Ocean currents evident in satellite wind data, *Geophys. Res. Lett.*, *28*, 2469–2472, 2001.

Killworth, P. D., C. Dieterich, C. L. Provost, A. Oschlies, and J. Willebrand, Assimilation of altimetric data and mean sea surface height into an eddy-permitting model of the North Atlantic, *Prog. in Oceanogr.*, *48*, 313–335, 2001.

Klein, P., and S. G. llewellyn Smith, Horizontal dispersion of near-inertial oscillations in a turbulent mesoscale eddy field, *J. Mar. Res.*, *59*, 697–723, 2001.

Kundu, P. K., and R. E. Thomson, Inertial oscillations due to a moving front, *J. Phys. Oceanogr.*, *15*, 1076–1084, 1985.

Kunze, E., Near-inertial propagation in geostrophic shear, *J. Phys. Oceanogr.*, *15*, 544–565, 1985.

Kunze, E., and T. B. Sanford, Observations of near-inertial waves in a front, *J. Phys. Oceanogr.*, *14*, 566–581, 1984.

Kunze, E., and T. B. Sanford, Near-inertial wave interaction with mean flow and bottom topography near Caryn Seamount, *J. Phys. Oceanogr.*, *16*, 109–120, 1986.

Kunze, E., R. W. Schmitt, and J. M. Toole, The energy balance in a warm-core ring's near-inertial critical layer, *J. Phys. Oceanogr.*, *25*, 942–957, 1995.

Large, W. G., and S. Pond, Open-ocean momentum flux measurements in moderate to strong winds, *J. Phys. Oceanogr.*, *11*, 324–336, 1981.

Lau, N. C., and J. M. Wallace, On the distribution of horizontal transports by transient eddies in the Northern Hemisphere wintering circulation, *J. Atmos. Sci.*, *36*, 1844–1861, 1979.

Lazier, J. R. N., Observations in the northwest corner of the North-Atlantic Current, *J. Phys. Oceanogr.*, *24*, 1449–1463, 1994.

Ledwell, J. R., A. J. Watson, and C. S. Law, Evidence for slow mixing across the pycnocline from an open ocean tracer release experiment, *Nature*, *364*, 701–703, 1993.

Ledwell, J. R., A. J. Watson, and C. S. Law, Mixing of a tracer in the pycnocline, *J. Geophys. Res.*, *103*, 21,499–21,529, 1998.

Ledwell, J. R., E. T. Montgomery, K. L. Polzin, L. C. S. Laurent, R. W. Schmitt, and J. M. Toole, Evidence for enhanced mixing over rough topography in the abyssal ocean, *Nature*, *403*, 179–182, 2000.

Lee, C. M., and C. C. Eriksen, Near-inertial internal wave interactions with mesoscale fronts: Observations and models, *J. Geophys. Res.*, *102*, 3237–3253, 1997.

Lee, D. K., and P. P. Niiler, The inertial chimney: The near-inertial energy drainage from the ocean surface to the deep layer, *J. Geophys. Res.*, *103*, 7579–7591, 1998.

Leipper, D. F., Observed ocean conditions and hurricane Hilda (1964), *J. Atmos. Sci.*, *24*, 182–196, 1967.

LeTraon, P. Y., F. Nadal, and N. Ducet, An improved mapping method of multisatellite altimeter data, *J. Atmos. Oceanic Technol.*, *15*, 522–534, 1998.

Levitus, S., M. E. Conkright, T. P. Boyer, T. O'Brien, J. Antonov, C. Stephens, L. Stathoplos, D. Johnson, and R. Gelfeld, *World Ocean Database 1998*, U.S. Government Printing Office, Washington, DC, 1998.

Lueck, R., and T. Osborn, The dissipation of kinetic energy in a warm-core ring, *J. Geophys. Res.*, *91*, 803–018, 1986.

Luo, J. J., S. Masson, E. Roeckner, G. Madec, and T. Yamagata, Reducing climatology bias in an ocean-atmosphere CGCM with improved coupling physics, *J. Climate*, *18*, 2344–2360, 2005.

Marshall, D. P., Subduction of water masses in an eddying ocean, *J. Marine Res.*, *55*, 201–222, 1997.

Marshall, J. C., and A. J. G. Nurser, Steady free circulation in a stratified quasi-geostrophic ocean, *J. Phys. Oceanogr.*, *16*, 1799–1813, 1986.

Marshall, J. C., and G. J. Shutts, A note on rotational and divergent eddy fluxes, *J. Phys. Oceanogr.*, *11*, 1677–1680, 1981.

Marshall, J. C., H. Jones, R. Karsten, and R. Wardle, Can eddies set ocean stratification?, *J. Phys. Oceanogr.*, *32*, 26–38, 2002.

Marshall, J. C., E. Shuckburgh, H. Jones, and C. Hill, Estimates and implications of surface eddy diffusivity in the southern ocean derived from tracer transport, *J. Phys. Oceanogr.*, *36*, 1806–1821, 2006.

McWilliams, J. C., G. Danabasoglu, and P. R. Gent, Tracer budgets in the warm water sphere, *Tellus*, *48*, 179–192, 1996.

Medvedev, A. S., and R. J. Greatbatch, On advection and diffusion in the mesosphere and lower thermosphere: The role of rotational fluxes, *J. Geophys. Res.*, *109*, doi:10.1029/2003JD003,931, 2004.

Mellor, G. L., and T. Ezer, A gulf stream model and an altimetry assimilation scheme, *J. Geophys. Res.*, *96*, 8779–8795, 1991.

Mellor, G. L., C. R. Mechoso, and E. Keto, A diagnostic model of the general circulation of the Atlantic Ocean, *Deep Sea Res.*, *29*, 1171–1192, 1982.

Mied, R. P., C. Y. Shen, C. L. Trump, and G. J. Lindemann, Internal-inertial waves in a Sargasso Sea front, *J. Phys. Oceanogr.*, *16*, 1751–1762, 1986.

Mooers, C. N. K., Several effects of a baroclinic current on the cross-stream propagation of inertial-internal waves, *Geophys. Fluid Dyn.*, *6*, 245–275, 1975.

Munk, W., and C. Wunsch, Abyssal recipes II, Energetics of tidal and wind mixing, *Deep Sea Res., Part I, 45*, 1977–2010, 1998.

Nagasawa, M., Y. Niwa, and T. Hibiya, Spatial and temporal distribution of the wind-induced internal wave energy available for deep water mixing in the North Pacific, *J. Geophys. Res.*, *105*, 13,933–13,943, 2000.

Niiler, P. P., and J. Stevenson, On the heat budget of tropical warm water pools, *J. Mar. Res.*, *40*, 465–480, 1982.

Olbers, D. J., The propagation of internal waves in a geostrophic current, *J. Phys. Oceanogr.*, *11*, 1224–1233, 1981.

Orvik, K. A., and M. Mork, A case study of Dopper-shifted inertial oscillations in the Norwegian Coastal Current, *Continental Shelf. Res.*, *15*, 1369–1379, 1995.

Oschlies, A., and V. Garcon, Eddy-induced enhancement of primary production in a model of the North Atlantic Ocean, *Nature*, *394*, 266–269, 1998.

Oschlies, A., and J. Willebrand, Assimilation of Geosat altimeter data into an eddy-resolving primitive equation model of the North Atlantic Ocean, *J. Geophys. Res.*, *101*, 14,175–14,190, 1996.

Pacanowski, R. C., Effect of equatorial currents on surface stress, *J. Phys. Oceanogr.*, *17*, 833–838, 1987.

Peterson, K. A., and R. J. Greatbatch, Vorticity fluxes in shallow water ocean models, *Atmos.-Ocean.*, *39(1)*, 1–14, 2001.

Philips, N. A., The general circulation of the atmosphere: A numerical experiment, *Quart. J. Roy. Meteor. Soc.*, *82*, 123–164, 1956.

Plumb, R. A., and J. D. Mahlman, The zonally averaged transport characteristics of the GFDL general circulation/transport model, *J. Atmos. Sci.*, *44*, 298–327, 1987.

Price, J. F., Upper ocean response to a hurricane, *J. Phys. Oceanogr.*, *11*, 153–175, 1981.

Price, J. F., R. A. Weller, and R. Pinkel, Diurnal cycling: Observations and models of the upper ocean response to diurnal heating, cooling, and wind mixing, *J. Geophys. Res.*, *91*, 8411–8427, 1986.

Radko, T., and J. C. Marshall, Eddy-induced diapycnal fluxes and their role in the maintenance of the thermocline, *J. Phys. Oceanogr.*, *34*, 372–383, 2004.

Rahmstorf, S., and J. Willebrand, The role of temperature feedback in stabilizing the thermohaline circulation, *J. Phys. Oceanogr.*, *25*, 787–805, 1995.

Richardson, P. L., Average velocity and transport of the Gulf Stream near 55°W, *J. Mar. Res.*, *43*, 83–111, 1985.

Rintoul, S., C. Hughes, and D. Olbers, The Antarctic Circumpolar Current System, in *Ocean Circulation and Climate: Observing and Modeling the Global Ocean*, pp. 271–302, Academic Press, 2001.

Rix, N., and J. Willebrand, Parameterization of mesoscale eddies as inferred from a high-resolution circulation model, *J. Phys. Oceanogr.*, *26*, 2281–2285, 1996.

Roemmich, D., and C. Wunsch, Two transatlantic sections: meridional circulation and heat flux in the subtropical North Atlantic Ocean, *Deep-Sea Res.*, *32*, 619–664, 1985.

Sarmiento, J. L., and K. Bryan, An ocean transport model for the North Atlantic, *J. Geophys. Res.*, *87*, 394–408, 1982.

Schmitz, W. J., Weakly-depth-dependent segments of the North Atlantic circulation, *J. Mar. Res.*, *38*, 111–133, 1980.

Sheng, J., R. J. Greatbatch, and D. G. Wright, Improving the utility of ocean circulation models through adjustment of the momentum balance, *J. Geophys. Res.*, *106*, 16,711–16,728, 2001.

Speer, K. G., A note on average cross-isopycnal mixing in the North Atlantic ocean, *Deep Sea Res.*, *44*, 1981–1990, 1997.

Stammer, D., On eddy characteristics, eddy transports, and mean flow properties, *J. Phys. Oceanogr.*, *28*, 727–739, 1998.

Stammer, D., and C. Wunsch, Temporal changes in eddy energy of the oceans, *Deep Sea Res.*, *II46*, 77–108, 1999.

Stevens, D. P., On open boundary conditions for three dimensional primitive equation ocean circulation models, *Geophys. Astrophys. Fluid Dyn.*, *51*, 103–133, 1990.

Tandon, A., and C. Garrett, On a recent parameterization of mesoscale eddies, *J. Phys. Oceanogr.*, *26*, 406–411, 1996.

Toggweiler, J. R., and B. Samuels, On the ocean's large scale circulation near the limit of no vertical mixing, *J. Phys. Oceanogr.*, *28*, 1832–1852, 1998.

Treguier, A. M., I. M. Held, and V. D. Larichev, On the parameterization of quasi-geostrophic eddies in primitive equation models, *J. Phys. Oceanogr.*, *27*, 567–580, 1997.

van Meurs, P., Interactions between near-inertial mixed layer currents and the mesoscale: The importance of spatial variabilities in the vorticity field, *J. Phys. Oceanogr.*, *28*, 1363–1388, 1998.

Walin, G., On the relation between sea-surface heat flow and thermal circulation in the ocean, *Tellus*, *34*, 187–195, 1982.

Wardle, R., and J. C. Marshall, Representation of eddies in primitive equation models by a PV flux, *J. Phys. Oceanogr.*, *30*, 2481–2503, 2000.

Watanabe, M., and T. Hibiya, Global estimates of the wind-induced energy flux to inertial motions in the surface mixed layer, *Geophys. Res. Lett*, *29*, doi:10.1029/2001GL014,422, 2002.

Webb, D. J., and N. Suginohara, Vertical mixing in the ocean, *Nature*, *409*, 37–37, 2001.

White, W. B., Dopper shift in the frequency of inertial waves observed in moored spectra, *Deep Sea Res.*, *19*, 595–600, 1972.

Willebrand, J., B. Barnier, C. W. Böning, C. Dieterich, P. Killworth, C. LeProvost, J. Yia, J. M. Molines, and A. L. New, Circulation characteristics in three eddy-permitting models of the North Atlantic, *Prog. in Oceanogr.*, *48*, 123–161, 2001.

Worthington, L. V., *On the North Atlantic Circulation*, The Johns Hopkins University Press, 1976, 110 pp.

Wunsch, C., The work done by the wind on the oceanic general circulation, *J. Phys. Oceanogr.*, *28*, 2332–2340, 1998.

Wunsch, C., What is the thermohaline circulation?, *Science*, *298*, 1179–1181, 2002.

Wunsch, C., The total meridional heat flux and its oceanic and atmosphic patitions, *J. Climate*, *18*, 4374–4380, 2005.

Xing, J., and A. M. Davies, Processes influencing the non-linear interaction between inertial oscillation, near inertial internal waves and internal tides, *Geophys. Res. Lett.*, *29*, 1067–1070, 2002.

Young, W. R., and M. ben Jelloul, Propagation of near-inertial oscillations through a geostrophic flow, *J. Mar. Res.*, *55*, 735–766, 1997.

Zervakis, V., and M. D. Levine, Near-inertial energy propagation from the mixed layer: Theoretical consideration, *J. Phys. Oceanogr.*, *25*, 2872–2889, 1995.

Zhai, X., Studying storm-induced circulation on the Scotian Shelf and slope using a two-way nested-grid model, Master's thesis, Dalhousie University, 2004, 96 pp.

Zhai, X., and R. J. Greatbatch, Inferring the eddy diffusivity for heat in the surface mixed layer using satellite data, *Geophys. Res. Lett.*, *33*, doi:10.1029/2006GL027,875, 2006a.

Zhai, X., and R. J. Greatbatch, The surface eddy diffusivity for heat in a model of the northwest Atlantic Ocean, *Geophys. Res. Lett.*, *33*, doi:10.1029/2006GL028,712, 2006b.

Zhai, X., and R. J. Greatbatch, Wind work in a model of the northwest Atlantic Ocean, *Geophys. Res. Lett.*, *34*, doi:10.1029/2006GL028,907, 2007.

Zhai, X., R. J. Greatbatch, and J. Sheng, Advective spreading of storm-induced inertial oscillations in a model of the northwest Atlantic Ocean, *Geophys. Res. Lett*, *31*, doi:10.1029/2004GL020,084, 2004a.

Zhai, X., R. J. Greatbatch, and J. Sheng, Diagnosing the role of eddies in driving the circulation of the northwest Atlantic Ocean, *Geophys. Res. Lett*, *31*, doi:10.1029/2004GL021,146, 2004b.

Zhai, X., J. Sheng, and R. J. Greatbatch, A new two-way nested-grid ocean modelling technique applied to the Scotian Shelf and slope, in *Proceedings of the eighth International Conference on Estuarine and Coastal Modeling*, pp. 342–357, 2004c.

Zhai, X., R. J. Greatbatch, and J. Sheng, Doppler-shifted inertial oscillations on a beta-plane, *J. Phys. Oceanogr.*, *35*, 1480–1488, 2005a.

Zhai, X., R. J. Greatbatch, and J. Zhao, Enhanced vertical propagation of storm-induced near-inertial energy in an eddying ocean channel model, *Geophys. Res. Lett*, *32*, doi:10.1029/2005GL023,643, 2005b.

Zhai, X., R. J. Greatbatch, and C. Eden, Spreading of near-inertial energy in a 1/12 model of the north atlantic ocean, *Geophys. Res. Lett.*, *34*, doi:10.1029/2007GL029,895, 2007.

Zhao, J., R. J. Greatbatch, J. Sheng, C. Eden, and K. Azetsu-Scott, Impact of an adiabatic correction technique on the simulation of CFC-12 in a model of the North Atlantic Ocean, *Geophys. Res. Lett*, *31*, doi:10.1029/2004GL020,206, 2004.

Zurbas, V., and I. M. Oh, Drifer-derived maps of lateral diffusivity in the Pacific and Atlantic Oceans in relation to surface circulation patterns, *J. Geophys. Res.*, *109*, doi:10.1029/2003JC002,241, 2004.